CLASS VI PERMIT Application Narrative

Gulf Coast Sequestration, LLC (G1037)

Project Minerva, Cameron Parish
Minerva South CCS Well Nos. 001 and 002

EPA Project Id: R06-LA-0002

LDCE Appl Nos: 45031 & 45032

Original: December 2024

Revision 1: December 2025

Revision 2: January 2026

Revision 3: May 2026

Revision 4: May 2026

GEOLOGY CERTIFICATION

Per LAC 43:VII §3603.H.1, the geoscientific aspects of the Narrative have been prepared by or under the supervision of a licensed Professional Geologist authorized to practice by and in good standing with the Louisiana Board of Professional Geoscientists. A separate certification page will be submitted with the Attachments to the Narrative that require certification.

Kaycee M. Garrett LA License No. 1325 *I, Kaycee M. Garrett, certify that I have personally examined and am familiar with the information submitted in this document and the attached documents, and that, based on my inquiry of those individuals immediately responsible for obtaining the information, I believe that the submitted information is true, accurate, and complete.*	 Kaycee Garrett Digitally signed by Kaycee Garrett Date: 2026.06.04 15:36:13 -05'00'
NARRATIVE SECTIONS (Including applicable Tables, Figures, and Appendices) Section 1 Project Background Section 2 Site Characterization	

ENGINEERING CERTIFICATION

Per LAC 43:VII §3603.H.2, the engineering aspects of the Narrative have been prepared by or under the supervision of a licensed Professional Engineer (PE) authorized to practice by and in good standing with the Louisiana Board Professional Engineering and Land Surveying. A separate certification page was submitted with the attachments to the Narrative that require certification.

Peter Erpelding LA License No. 49937 *I, Peter Erpelding, certify that I have personally examined and am familiar with the information submitted in this document and the attached documents, and that, based on my inquiry of those individuals immediately responsible for obtaining the information, I believe that the submitted information is true, accurate, and complete.*	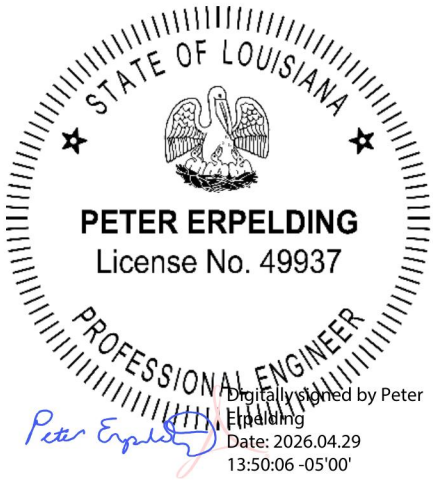

NARRATIVE SECTIONS (Including applicable Tables, Figures, and Appendices)

Section 5 Injection Well Construction

Section 7 Well Operation

Appendix X-1 Drilling Plan for Minerva South CCS No. 001

Appendix X-2 Drilling Plan for Minerva South CCS No. 002

TABLE OF CONTENTS

LIST OF TABLES, FIGURES, AND APPENDICES

TABLES

FIGURES

LIST OF ATTACHMENTS

LIST OF ACRONYMS

2D	Two Dimensional
3D	Three Dimensional
AoR	Area of Review
APSTM	AVO Pre-stack Time Migration
ASL	Above Sea Level
AVO	Amplitude Verses Offset
BSL	Below Sea Level
C&E	Louisiana Department of Conservation and Energy
CCS	Carbon Capture Sequestration
CDR	Carbon Dioxide Removal
CEO	Chief Executive Officer
CEQ	Council on Environmental Quality
CFR	Code of Federal Regulations
CMG	Computer Modeling Group
CSP	Clay Smear Potential
DOE	Department of Energy
DSCA	Differential Strain Curve Analysis
ECFP	Effective Cross-Fault Permeability
ECFT	Effective Cross-Fault Transmissibility
EJ	Environmental Justice
EOR	Enhanced Oil Recovery
EPSTM	Enhanced Pre-stack Time Migrations
FEMA	Federal Emergency Management Agency
FLIGHT	Facility Level Information on Greenhouse Gases Tool
FSP	Fault Slip Potential
GR	Gamma Ray
GCS	Gulf Coast Sequestration, LLC
GEM	General Enhanced Modular
ICW	Intracoastal Waterway
LAC	Louisiana Administrative Code
LDCE	Louisiana Department of Conservation and Energy
LDTOD	Louisiana Department of Transportation and Development
LNG	liquid natural gas
Max	Maximum
Min	Minimum
MD	Measured Depth
MIGNR	Migration with Noise Reduction
MMI	Modified Mercalli Intensity
MMT	Million Metric Tons
MS CCS 1	Minerva South CCS Well No. 001
MS CCS 2	Minerva South CCS Well No. 002
MSL	Mean Sea Level
NAD	North American Datum
NEPA	National Environmental Policy Act
NMR	Nuclear Magnetic Resonance
NRC	Nuclear Regulatory Commission
OBE	Operating Basis Earthquake
P&A	Plugged and Abandoned
PEF	Photoelectric Factor
PISC	Post-Injection Site Characterization
PSTM	Pre-Stack Time Migration
RPSTM	Raw Pre-stack Time Migration
SDC	Seismic Design Category
SDRD	Submitted Drillers Reports Database
SDWA	Safe Drinking Water Act
SGR	Shale Gouge Ratio
SIC	Standard Industrial Classification
SONRIS	Strategic Online Natural Resources Information System
SP	Spontaneous Potential
SWD	Saltwater Disposal
T&M	Testing and Monitoring
TDS	Total Dissolved Solids
TRRC	Texas Railroad Commission
TVDSS	True Vertical Depth Sub Sea
TWDB	Texas Water Development Board
TWT	Two Way Time
UIC	Underground Injection Control
US	United States
USDW	Underground Sources of Drinking Water
USEPA	United States Environmental Protection Agency
USGS	United States Geological Survey
UTC	Universal Time Coordinated
VSP	Vertical Seismic Profile

CHEMICAL/COMPOUNDS

CO_2	carbon dioxide
H_2	hydrogen gas
H_2CO_3	carbonic acid
H_2S	hydrogen sulfide
Hg	mercury
NaCl	sodium chloride
O_2	oxygen
SO_4^{2-}	sulfate
NO_2	nitrogen dioxide

UNITS

%	percent
µm	micrometer
cm	centimeters
ft	feet
g	grams
g/cm^3	grams per cubic centimeter
GPa	gigapascal
lb	pounds
km	kilometers
mi^2	square miles
Mblg	magnitude
mD	millidarcies
mg/L	milligrams per liter
Mgal/d	million gallons per day
MMT	million metric tons
Mpa	megapascal
ppm	parts per million
psi	pounds per square inch
psia	psi absolute

1 PROJECT BACKGROUND AND GENERAL INFORMATION

1.1 PROJECT OVERVIEW

Gulf Coast Sequestration, LLC (GCS) seeks to build and responsibly operate a safe, permanent carbon dioxide (CO_2) sequestration asset for the Louisiana Gulf Coast. Our initial Carbon Capture Sequestration (CCS) development is identified as Project Minerva, located in Cameron Parish in southwest Louisiana. The project will be developed incrementally and will initially include two Class VI CCS injection wells, Minerva South CCS Well No. 001 (MS CCS 1) and Minerva South CCS Well No. 002 (MS CCS 2). The Minerva Facility will be located south of the Intracoastal Waterway and will include the two Class VI injection wells sited on the Minerva South well pad. The two Class VI injection wells were positioned to maximize access to the available pore volume of the upper Frio Formation and to disperse and maximize the flow of CO_2 from the project area. A topographic map showing the location of the proposed injection wells, MS CCS 1 and MS CCS 2, and the delineated Area of Review (AoR) is provided in Figure 1.1-1. The map also identifies wells used to create maps and cross-sections with Map ID numbers, which are keyed to Table 1.1-1. A map and table of landowners within the AoR of Project Minerva are provided at Appendix I.

The Louisiana Department of Conservation and Energy (C&E) has primary permit and enforcement authority (primacy) over Class VI Injection Wells through their Underground Injection Control (UIC) program. The UIC program is administered through the Office of Permitting and Compliance. The primary rule and regulatory priorities are to protect human health and the environment for the State of Louisiana, including the protection of potential Underground Sources of Drinking Water (USDW), surface waters, and the land from endangerment by regulating the subsurface injection of waste such as CO_2 sequestration.

This application is being submitted in compliance with C&E regulations for Class VI Injection Wells, Louisiana Administrative Code (LAC), Title 43, Part XVII, Chapter 36 (LAC 43:XVII §3601-3633). In accordance with Title 40, Chapter I, Subchapter D, Part 146.91 of the Code of Federal Regulations (40 CFR 146.91) and LAC 43:XVII §3629.A.3, the complete application will be submitted to the United States Environmental Protection Agency (USEPA).

1.2 FACILITY/SITE AND GENERAL APPLICATION INFORMATION

Facility Name: Minerva Facility

Facility Contact: David Cook, CEO
(713) 419-6808; dcook@gcscarbon.com

Injection Wells: Minerva South CCS Well No. 001 (MS CCS 1)
Minerva South CCS Well No. 002 (MS CCS 2)

Well Locations: Sec 3, T12S, R13W, Cameron Parish, Louisiana

MS CCS 1 (North American Datum (NAD) 1927)
Surface: 30° 02' 34.10"N, 93° 40' 20.63"W
Bottom-Hole: 30° 02' 34.10"N, 93° 40' 20.63"W
MS CCS 2 (NAD 1927)

Surface:	30° 02' 33.84"N, 93° 40' 20.48"W
Bottom-Hole:	30° 02’ 13.74”N, 93° 40' 42.07"W

Applicant:	Gulf Coast Sequestration, LLC 5599 San Felipe Street, Suite 1450, Houston, Texas 77056 C&E Operator Code: G1037
Ownership Status:	Limited Liability Company (LLC)
Entity Status:	Private
SIC Code:	4953 – Refuse Systems

The Minerva Facility is not located on Federal, Indian, or State lands.

1.3 OWNERSHIP

GCS was established in 2019 with the single purpose of building and operating a world-scale carbon sequestration solution for companies who operate in the southwest Louisiana industrial corridor. GCS is a private entity; its ownership status is a manager-managed LLC.

The company will partner with industrial customers to capture CO_2 and safely contain it underground to help them reduce carbon emissions and achieve their long-term sustainability goals. GCS is comprised of an exceptional management team with more than 15 decades of experience across the core disciplines of energy, finance, operations and subsurface technical that are required to successfully execute one of the first sequestration projects in Louisiana.

GCS has leased land from multiple long-standing, multi-generational landowners in southwestern Louisiana, including the Stream family and other local families with deep historical ties to the region. These landowners have managed and operated land assets for well over a century, and their legacy includes investments in conservation and land stewardship. The Stream family, through affiliated entities, such as Stream Wetland Services, has protected and restored tens of thousands of acres of wetlands and sustainably managed thousands of acres of timber assets, reflecting the broader commitment to responsible land management across the partner landowners.

1.4 CO_2 SOURCE

Project Minerva envisions sourcing CO_2 volumes from multiple sources of CO_2 from industrial facilities in Lake Charles industrial corridor in southwestern Louisiana and Beaumont industrial corridor in southeastern Texas. According to USEPA’s Facility Level Information on Greenhouse Gases Tool (FLIGHT), the total CO_2 emissions from the four counties/parishes adjacent to Project Minerva - Orange County, Beaumont County, Calcasieu Parish, and Cameron Parish - emitted nearly 57 MMT of CO_2 in 2018 (EPA, 2023).

The emissions that are anticipated for Project Minerva in the near term are likely to be higher purity CO_2 that is economically capturable from natural gas processing and other natural gas derived processes including blue Hydrogen (H2) and Liquified Natural Gas (LNG). The Gulf Coast region of Southeast Texas and Southwest Louisiana have a variety of currently

operating or planned facilities for natural gas processing. Such applications can meet the CO_2 specification that GCS has proposed. Further, such specification of CO_2 is consistent with the existing CO_2 pipeline infrastructure in the region.

1.5 PROPOSED INJECTION MASS/VOLUME

Project Minerva is designed to operate for 30 years as a CO_2 sequestration project, operating each injection well, MS CCS 1 and MS CCS 2, at a maximum daily injection rate of 0.002 million metric tons (MMT) per day (MMT/day) and an annual average injection rate ranging from 0.547 to 0.746 MMT/year from combined CO_2 sources. The total injection mass of CO_2 stream, over the life of each well, is anticipated to be at least 9.54 MMT in MS CCS 1 and 9.47 MMT in MS CCS 2. The total injection mass for the project is anticipated to be at least 19.0 MMT.

GCS has also outlined an upside-case scenario that identifies additional storage potential within a separate, discrete reservoir interval. This upside scenario includes the base case mass as well as combined added storage of 2.14 MMT in MS CCS 1 and MS CCS 2. With the additional injection from the upside scenario, the average annual injection rate would increase to 0.587 MMT/year and result in a total injection mass of 21.14 MMT CO_2 stream.

1.6 PROJECT TIMELINE

The total project timeline for Project Minerva is approximately 89 years. This timeline includes a pre-injection timeframe of approximately 4 years, and an injection and post-injection timeline of approximately 85 years.

The pre-injection timeline includes approximately 2 years for permitting and 2 years for construction. Once injection commences, GCS proposes to operate the project for 30 years. During that time, GCS will conduct testing and monitoring (T&M) of the project until the injection wells are plugged and abandoned (P&A), at which time the 50-year Post-Injection Site Care (PISC) period will begin. Though the CO_2 plume does not reach stability until 115 years, GCS can demonstrate non-endangerment of the USDW during the 50-year PISC period. Once the PISC period concludes, GCS will initiate site closure activities and submit the proper demonstrations to C&E, which may take as long as 5 years.

1.7 PERMIT COMPLIANCE

The objective of this permit application is to comply with all conditions of a permit set forth under in the requirements of LAC 43XVII §3609.D. GCS understands appropriate actions are required to prevent the movement of fluids into or between USDWs or into any unauthorized zones consistent with the requirements of LAC 43:XVII §3617.1.a. For purposes of enforcement, compliance with this permit application during its term constitutes compliance with Part C of the Safe Drinking Water Act (SDWA).

In the case GCS is unable to maintain compliance with any conditions of this permit or mitigate any adverse impacts of USDW contamination, GCS understands this constitutes an act of noncompliance and if the C&E Secretary determines that such noncompliance

endangers USDWs can enforce action such as permit termination, revocation and reissuance, or modification, or for denial of a permit renewal application.

1.8 ASSOCIATED PERMITS

Per LAC 43:XVII §3607.B.9, a list of all permits or construction approvals that have been received or applied for that may affect our legal or technical ability to undertake Project Minerva is provided in Table 1.8-1. The Table lists the federal, tribal, state and local permits applicable to Project Minerva; those permits specified in LAC 43:XVII §3607.B.9 are bolded.

1.9 ENVIRONMENTAL ANALYSIS

Louisiana Constitutional Article IX, § 1, of the Louisiana Constitution imposes a duty of environmental protection on all State agencies and officials and requires a balancing process in which environmental costs and benefits must be given careful consideration along with economic, social and other factors.

So that C&E-Office of Conservation can implement a balancing process in their review of Class VI permit applications, they have requested applicants to prepare responses to the following questions:

1. Have the potential and real adverse environmental effects of the proposed project been avoided to the maximum extent possible?
2. Does a cost benefit analysis of the environmental impact costs versus the social and economic benefits of the proposed project demonstrate that the latter outweighs the former?
3. Are there alternative projects which would offer more protection to the environment than the proposed project without unduly curtailing non-environmental benefits?
4. Are there alternative sites which would offer more protection to the environment than the proposed site without unduly curtailing non-environmental benefits?
5. Are there mitigating measures which would offer more protection to the environment than the proposed project without unduly curtailing non-environmental benefits?

GCS has prepared responses to these questions in adequate detail, together with sufficient justification and supporting data, to allow C&E to fulfill their constitutional obligation to perform an environmental analysis for Project Minerva. The Environmental Analysis is provided as Appendix II of this Narrative.

1.10 APPLICATION SUBMISSION

The Class VI Permit Application Narrative for Project Minerva has been submitted via the GCS-LDCE intranet site in Microsoft SharePoint. GCS created the SharePoint site to submit and manage shared permit application documents with LDCE. Once the application is deemed administratively and technically complete by LDCE, the Class VI Permit Application Narrative for Project Minerva will be submitted to USEPA.

2 SITE CHARACTERIZATION

2.1 GEOLOGY AND HYDROGEOLOGY

2.1.1 Regional Geology

The Gulf of Mexico is a relatively small ocean basin covering an area of more than 579,000 square miles (mi^2) (1.5 million kilometers (km)) (National Ocean and Atmospheric Administration, 1985). It began to form via rifting during the Triassic and Jurassic Periods. Sediment input has been particularly voluminous since the start of the Paleogene Period and is responsible for extensive deformation of underlying salt and the resulting abundance of prolific hydrocarbon systems along the Gulf Coast of Texas and Louisiana (Foote, 1984). Project Minerva is comprised of more than 8,000 feet (ft) of regionally extensive clastic strata. A regional geologic stratigraphic column is provided in Figure 2.1.1-1.

The earliest record of sedimentation in the Gulf of Mexico Basin occurred during the Late Triassic to Early Jurassic period, between 160 and 140 million years ago. Repeated cycles of seawater flooding and evaporation resulted in the formation of extensive salt accumulations ranging locally from 10,000 ft to 15,000 ft thick. Subsequently, buoyancy-driven flow created the salt diapirs, pillows and massifs which contribute to the characterization of the Gulf Coast structure present day (Foote, 1984).

The early phases of continental rifting resulted in the deposition of non-marine red bed and deltaic sediments including shales, siltstones, sandstones, and conglomerates of the Eagle Mills Formation in a series of restricted, graben fault-block basins (Figure 2.1.1-2). Following the Eagle Mills Formation, the deposition of thick sequences of anhydrite and salt beds, known as the Werner Anhydrite and Louann Salt, occurred within the major structural basins (Kreitler, et al., 1981). Overlying the Louann Salt, the Norphlet Formation marked the end of the deposition of evaporites with clastic, non-fossiliferous sandstones and conglomerates (Figure 2.1.1-1) (Mancini, Mink, Bearden, & Wilkerson, 1985; Todd & Mitchum, 1977).

Broad carbonate banks composed of limestones, dolomites, and interbedded anhydrites developed along the edges of the Gulf of Mexico Basin, with fine carbonate-muds deposited in deeper water areas. Reef construction and sedimentation kept pace with regional subsidence, which allowed thick carbonate sequences to accumulate (Foote, 1984). These shallow-water carbonates and clastic rocks make up the Smackover, Buckner, Haynesville formations, and the Cotton Valley Group, non-skeletal, carbonate sands and muds which accumulated on a ramp-type shelf with reef buildups developed on subtle basin highs (Baria, Stoudt, Harris, & Crevello, 1982).

During the Upper Cretaceous, a large tectonic uplift formed the Rocky Mountains, while the Gulf of Mexico basin subsided. Large volumes of clastic sediments from the uplift were deposited as wedges into the basin. This effectively shuts off the production of carbonates, except in the Florida and Yucatan regions. Since the Cretaceous, the rate of terrigenous sediment influx has been greater than the rate of basin subsidence, resulting in significant progradation of the continental shelf margin (Figure 2.1.1-3).

Sediment supplies during Cenozoic time overwhelmed the general rate of subsidence, causing the margins to prograde up to 240 miles from the edges of Cretaceous carbonate banks to the current position of the continental slopes off Texas and Louisiana (Foote, 1984). The geometry of Cenozoic deposition in the Gulf Coast Basin was primarily controlled by the interaction of the following factors:

- Changes in the location and rates of sediment input, significantly shifting the areas of maximum sedimentation,
- Changes in the relative position of sea level, developing a series of large-scale depositional cycles throughout Cenozoic time,
- Diapiric intrusion of salt and shale in response to sediment loading, and
- Flexures and growth faults due to sediment loading and gravitational instability.

Early Tertiary sediments are thickest in the Rio Grande Embayment of southern Texas, reflecting the role of the ancestral Rio Grande and Nueces Rivers as sediment sources to the Gulf of Mexico basin (Figure 2.1.1-4). By the Oligocene, deposition had increased to the northeast, suggesting that the ancestral Colorado, Brazos, Sabine, and Mississippi Rivers were increasing in importance. Miocene time is marked by an abrupt decrease in the amount of sediment entering the Rio Grande Embayment, with a coincidence increase in the rate of sediment supply in southeast Texas, Louisiana, and Mississippi. Throughout the Pliocene and Pleistocene Epochs, the maximum depocenters of sedimentation were controlled by the Mississippi River and are located offshore of Louisiana and Texas.

Tertiary sediments accumulated to great thickness where the continental platform began to build toward the Gulf of Mexico, beyond the underlying Mesozoic shelf margin and onto transitional oceanic crust. Rapid loading of sand on water-saturated prodelta and continental slope muds resulted in contemporaneous growth faulting (Loucks, Dodge, & Galloway, 1986). The effect of this syndepositional faulting was a significant expansion of the sedimentary section on the downthrown side of the faults. Sediment loading also led to salt diapirism, with its associated faulting and formation of large salt withdrawal basins (Galloway, Hobday, & Magara, 1982).

Sediments of the Tertiary progradational wedges were deposited in continental, marginal marine, nearshore marine, shelf, and basinal environments and present a complex depositional system along the Texas Gulf Coast.

Overlying the Tertiary progradational wedges along the Texas Gulf Coast are the Pleistocene and Holocene sediments of the Quaternary Period. The voluminous infilling of the Gulf basin during Tertiary time was followed by sediment influx of similar proportions due to the profound effects of continental Pleistocene glaciation (Foote, 1984). Pleistocene sedimentation occurred during a period of complex glacial activity and corresponding sea level changes. As the glaciers made their final retreat, Holocene sediments were deposited under the influence of a fluctuating, but overall rising, sea level. Quaternary sedimentation along the Louisiana Gulf Coast occurred in fluvial, marginal and marine environments.

The formations of interest at Project Minerva are both Oligocene and Miocene stratigraphy. During these periods of time, four sediment-dispersal axes dominated the Gulf margin including (1) the Norma delta, (2) the Norias delta (Rio Grande Embayment), (3) the Houston delta (Houston Embayment), and (4) the central Mississippi delta (Figure 2.1.1-4). The Houston Embayment and central (delta provided a source of coarse-grained sediment for southeast Texas and southwest Louisiana (Swanson & Karlsen, 2009). This coarse-grained sediment consisted of Oligocene and Miocene deposits and were deposited as major progradational wedges along the margin of the Gulf Coast Tertiary basin, a basin comprised of the Houston Embayment and South Louisiana Salt Basin sub-basins (Swanson, Karlsen, & Valentine, 2013).

Major progradational wedges are typically characterized by an up-dip section of interbedded continental and marginal marine sediments underlain by a thick marine section composed of under compacted slope and basin claystone. The instability caused by the direct and rapid loading of water saturated, unconsolidated sediments resulted in the development of large scale, syndepositional, down-to-the-basin faults and intraformational deformation (Galloway, Hobday, & Magara, 1982).

Three major progradational delta complexes, designated the Central Mississippi, Houston and Norias delta systems, identified by (Galloway, Henry, & Smith, 1982), were centered in the South Louisiana Salt Basin, Houston Embayment and Rio Grande Embayment, respectively (Figure 2.1.1-4). Three fluvial systems, the ancestral Mississippi, Chita/Corrigan, the Gueydan, supplied sediment to the delta complexes. The Houston delta system of Texas and southwestern Louisiana is centered in southern Harris County, Texas. The system is composed of several minor, laterally coalescent, and frequently shifting delta lobes. The Chita/Corrigan fluvial systems supplied sediment. Up-dip deltas exhibited wave-dominated, arcuate geometries, while lobate delta geometries characterized episodes of maximum progradation or an area where high subsidence rates were associated with salt withdrawal basins. Due to constant switching of delta lobes, the rate of coastal progradation was slow for the Houston delta system (Galloway, Henry, & Smith, 1982).

A major global sea level rise occurred during the late Cretaceous, creating the Mississippi Embayment and allowing the farthest inland transgression of a shallow epicontinental sea (Vail, Mitchum, & Thompson III, 1977). This embayment is part of the Mississippi Alluvial plain and supplied sediment to the southwestern portion of Louisiana. By the Oligocene, deposition had increased from the northeast, suggesting that the ancestral Colorado, Brazos, Sabine, and Mississippi Rivers were increasing in importance.

2.1.1.1 Regional Stratigraphy

The Gulf Coastal Plain is characterized by rapid subsidence in areas of high sediment loading through multiple cyclic depositional episodes (Figure 2.1.1-5). These cycles represented various transgressive and regressive stages driven by variations in sediment supply and subsidence. Oligocene and Miocene deposits are subdivided according to depositional cycles and paleontological zones (Foote, 1984; Swanson, Karlsen, & Valentine, 2013). These subdivisions are listed below in ascending order:

- Vicksburg Group (early Oligocene). Represents a transgressive phase (mainly shale and some sandstone lenses),
- Frio Formation (middle Oligocene). Split into the lower, middle and upper Frio Formation. Represents a dominantly regressive phase. The upper Frio comprises a mixture of marginal marine and deltaic sandstones and shales, with localized deep marine shales. The lower and middle Frio are dominated by deep marine shales and turbidite sandstones. Downdip equivalent of the continental Catahoula Formation (Swanson, Karlsen, & Valentine, 2013).
- Anahuac Formation (late Oligocene). Represents transgression (marine shales and thin sandstones), and
- Fleming Formation (Miocene). Represents a very high number of alternating regressive and transgressive phases (progradational sandstones and retrogradational shales).

Vicksburg Formation

The Vicksburg Formation lies within the Tertiary depositional wedge of the Gulf Coastal Plain and is regionally extensive across the Gulf Coast of Texas and Louisiana (Coleman & Galloway, 1990). The Vicksburg Formation consists of fluvial-deltaic sandstones, silts, and clays (Swanson, Karlsen, & Valentine, 2013; Delaney, 1963). The Vicksburg sediments were deposited by delta flanks and associated shore-zone, strand plain, and barrier systems (Coleman & Galloway, 1990).

In southeast Texas and southwestern Louisiana, the Vicksburg Formation is comprised of interbedded deltaic, outer-shelf and slope deposits, massive bedded shales, and medium bedded sandstones (Gregory, 1966; Coleman & Galloway, 1990; Swanson, Karlsen, & Valentine, 2013). In the Houston Embayment and the westernmost portion of the South Louisiana Salt Basin of the Gulf Coast Salt Basin, the Vicksburg formation was deposited in a series of stacked delta environments (Figure 2.1.1-3) (Coleman & Galloway, 1990; Swanson, Karlsen, & Valentine, 2013).

During major deltaic progradation in the early Oligocene, the Vicksburg Fault Zone was created in south Texas and northern Mexico, which is a narrow fault zone characterized by vertical displacement of the underlying Frio Formation. The Vicksburg Fault Zone, or flexure, forms the updip limit of significant structural deformation of the Frio Formation. In south Texas, thickening and displacement of Frio sediments are significantly greater in the Frio Fault Zone, downdip of the Vicksburg Fault Zone, than in the Vicksburg Fault Zone. In Louisiana, thickening and displacement of Frio sediments thin spanning across Louisiana from west to east (Swanson & Karlsen, 2009).

Frio Formation

The Frio Formation was deposited during the middle Oligocene and is composed of a thick sequence of mainly regressive sediments that were deposited rapidly in alluvial, lagoonal, marginal marine and deep marine environments, forming a major progradational wedge along the Gulf. The Frio Formation thickness and depth increases southwards, with

localized variations occurring around salt diapirs and major faults. Non-marine sands were deposited in constantly shifting deltas and are interbedded with marine shales, which were deposited during periods of local transgression. In areas between major delta systems such as the central Mississippi delta, shore-face and shallow marine environments deposited broad sandstone units interbedded with marine silts and shales during transgressive periods. The progradational Frio wedge was initiated by a major global fall in sea level, with subsequent Frio sediments deposited under the influence of a slowly rising sea (Galloway, Henry, & Smith, 1982).

The Norias delta system of south Texas constitutes the Frio Formation depocenter in the South Texas Coastal Plain. Typical sand content ranges from 25 percent (%) to 40% for a total Frio Formation section that can be more than 12,000 ft thick. The lateral boundaries of the Norias delta system remained fixed through time, centering on Kennedy County, Texas. Deposition of the system prograded the continental margin more than 60 miles basin ward, primarily during deposition of the lower and middle Frio Formation sections. This major off lapping episode was terminated by the shale-rich Anahuac Formation transgression (Galloway, Henry, & Smith, 1982).

Regionally, the Frio Formation and Catahoula Formation (up-dip equivalent) can be divided into a number of distinct depositional systems. Within Louisiana, the upper Frio Formation transitions into fine-grained, mix-load dominated fluvial sediments up-dip, north of Beauregard Parish, ultimately pinching out in central Louisiana. To the south (offshore Gulf of Mexico) the downdip limit of the upper Frio Formation is defined by large-scale fault-related juxtaposition against thick, fine-grained formations in the overlying Neogene (Swanson, Karlsen, & Valentine, 2013). Local structural highs are the result of salt diapirism, and associated faulting, in combination with the regional structural fabric of major faults dipping dominantly southwards, parallel with the Gulf coastline (Figure 2.1.1-3).

Anahuac Formation

As sea level continued to rise during the late Oligocene, the underlying Frio Formation progradational platform flooded. Wave reworking of sediment along the encroaching shoreline produced thick, time transgressive blanket sands at the top of the Frio Formation and base of the Anahuac Formation section. The transgressive marine shale-rich Anahuac Formation deposited conformably on top of the blanket sands throughout the Texas and Louisiana coastal region. The Anahuac Formation was deposited in an inner-shelf, shallow marine, proximal deltaic, distal deltaic, and slope environments (Swanson, Karlsen, & Valentine, 2013). It is typically composed of calcareous, marine shales with localized, lenticular, micritic limestone units. In western and central parts of Louisiana, including Project Minerva, the interval mostly comprises shales with lesser sandstones. Limestones and calcareous clastics dominate in eastern Louisiana and the eastern Gulf of Mexico, where clastic influx was minimal (Swanson, Karlsen, & Valentine, 2013).

The Anahuac Formation dips towards the Gulf of Mexico and thickens regionally from its inshore margin to nearly 2,000 ft offshore (Galloway, Henry, & Smith, 1982). An erosional unconformity marks the top of the Anahuac Formation, and the start of a regressive period in the basal Miocene interval (Swanson, Karlsen, & Valentine, 2013).

Fleming Group

The thick Miocene strata of the Fleming Group is comprised of more transgressive-regressive cycles than any other epoch. (Rainwater, 1968) has interpreted the middle Miocene as a major delta-forming interval comparable to the present-day Mississippi Delta system. The middle Miocene is representative of much of the entire Miocene interval, with only the site of deposition changing in response to various transgressions and regressions. The result is a complex of interbedded shallow neritic clays; restricted marine clays, silts, sands; and deltaic deposits of sands, silts, and clays. If a composite were made of the thickest Miocene intervals around the Gulf Basin, more than 40,000 ft of accumulated sediment would be obtained, of which about 20,000 ft were deposited in southern Louisiana (Rainwater, 1968).

The two formations in which form the major units of the Fleming Group, in ascending order: (1) the Oakville Formation, and (2) the Lagarto Formation. These formations were deposited in relatively shallow water across a broad, submerged, shelf platform constructed during Frio Formation and Anahuac Formation deposition throughout the Gulf Coast region and are equivalent to the Oakville and Lagarto Formations of East Texas, as well as the Catahoula, Hattiesburg, and Pascagoula Formations of Mississippi (Swanson & Karlsen, 2009). Three major depositional regimes characterize the Fleming Group. Figure 2.1.1-6 shows the distribution of the lower Miocene depositional systems across the Texas Coastal Plain.

Goliad Sand

Conformably overlying the Fleming Group is the Goliad Sand. Similar to the Catahoula Tuff or Sandstone, Willis Sand, and Beaumont Clay, the Goliad Sand is often interchangeably referred to in literature as a formation. The Goliad Sand is comprised of coarse-grained sediments, including localized cobbles, clay balls, and wood fragments at the base of the formation. The Goliad Sand can be distinguished into an upper and lower formation differentiating by sand content (Figure 2.1.1-7). The boundary between the upper and lower Goliad sand class identifies the discrepancy between the base of the Chicot aquifer and the top of the Evangeline aquifer considering the Chicot aquifer is regionally composed of a sandier sedimentary setting (Young, et al., 2006; Chowdhury & Turco, 2006).

The Goliad Sand was deposited during Pliocene time and is similar in character to underlying late Miocene stratigraphic units reflecting a regional depositional transition from fluvial channel and intervening floodplain facies (updip) to a mixture of deltaic and marginal marine environments (downdip) (Young, et al., 2006). The width of the Goliad Sand gradually increases southeastward in Texas toward the Rio Grande Embayment from coastal counties (Baker Jr, 1978). Along the coastal county of Jim Wells, Texas, the Goliad Sand is approximately 400 ft to 600 ft in thickness and yields moderate quantities of fresh to slightly saline water-bearing sands southeastward (Mason, 1963).

Willis Sand

Conformably overlying the Goliad Sands are the Willis Sands. The Willis Sand was deposited in a fluvial-deltaic depositional environment and are comprised of coarsening-upward sequence, commonly indicative of delta-front facies (Young, et al., 2006). In southeast

Texas, the Willis Sand deposits consist of fossiliferous sand and gravelly sand beds and are complexly faulted along the coastal counties. The Willis Sands are locally extensive and grade conformably into the overlying Holocene depositional units consisting of the Lissie Formation and Beaumont Clay (Chowdhury & Turco, 2006). The Willis Sand ranges in thickness up to 80 ft in southeast Texas (Houser & Ryan, 1983).

The Willis Sands were deposited during Pleistocene time under the influence of the complex fluctuations of sea level changes. The changes in sea level influenced the sand and clay content of the Chicot aquifer, which contains the Willis Sand, Bentley Formation, Montgomery Formation, and Beaumont Clay of Pleistocene age and any overlying undifferentiated Holocene alluvium. The Willis Sand comprises the lower part of the Chicot Aquifer yielding the high sand content and yields good quantities of fresh groundwater where the lower part of the Chicot aquifer contains slightly saline groundwater (Baker Jr, 1978; Young, et al., 2006).

Lissie Formation, Beaumont Clay, and Holocene Series

The Lissie Formation and Beaumont Clay are the two dominant subdivisions of the Pleistocene system whereas the Willis Sand represents only a part of the Pleistocene system. The Lissie Formation is unconformably contained between the Goliad Sand and the overlying Beaumont Clay and is comprised of, in ascending order, the Bentley Formation and the Montgomery Formation (Chowdhury & Turco, 2006; Baker Jr, 1978). The Lissie Formation consists of continental deposits laid down on flood plains and partly as delta sands, silts, and mud at the mouth of rivers (Figure 2.1.1-7). Although the Goliad Sand grades into the Lissie Formation and Beaumont Clay, the Lissie contains relatively less conglomerates than the underlying Goliad Sand and is often identified by caliche beds marked at the base of the formation (Chowdhury & Turco, 2006).

The Beaumont Clay is contained between the underlying Lissie Formation and overlying Holocene series. The Beaumont Clay is made up of poorly bedded, marly clay and forms a thin mantle extending eastward. The Beaumont Clay was deposited largely by rivers in the form of natural levees and deltas that coalesced as river mouths shifted along the coast and, to a lesser extent, by marine and lagoonal water in the bays and embayments between stream ridges and delta banks (Figure 2.1.1-7) (Chowdhury & Turco, 2006).

The Holocene series consists of undifferentiated river alluvium and coastal deposits. The Holocene series was deposited in floodplains and point bars with grain sizes ranging from clay to gravel. The Holocene series is the largest surficial outcrop along the Texas and Louisiana Gulf Coast. The Holocene series provides a direct hydraulic connection between the surface water and groundwater systems (Chowdhury & Turco, 2006).

2.1.1.2 Regional Structure

The Gulf of Mexico continental margins and deep ocean basin regions are relatively stable areas (Foote, 1984). The Gulf of Mexico region is characterized by structural dip towards the Gulf Coast, with normal- and growth faults of Miocene/Oligocene age parallel to the contemporaneous shelf edge (Figure 2.1.1-3 and Figure 2.1.1-8) (Jones, Turcan Jr, & Skibitzke, 1954) Tectonism driven in large part by sediment loading and gravity played a key

role in contemporaneous and post-depositional deformation of Tertiary strata (Foote, 1984). Deeper fault zones are present at basement level, mirroring the trend of the shallower Oligocene-level faults, but do not appear to be directly linked (Figure 2.1.1-3).

Salt mobilization led to extensive diapirism across the Texas and Louisiana Gulf Coast. The remobilized salt, originating from the deep Louann Salt Formation, may be present in a number of geometrical forms, including diapirs and pillows. In the area of Project Minerva, salt features typically occur as diapirs, or “salt domes” (Figure 2.1.1-9). Such diapirs buoyantly moved upwards through many thousands of feet of younger strata concurrently with sedimentation during the Oligocene and Miocene. Regional salt features can be rooted deeply in the subsurface, extending vertically several thousand feet deep, where in other cases salt features may have been severed from deeper sources (Swanson, Karlsen, & Valentine, 2013).

Two examples of salt domes are Vinton Salt Dome (Vinton Dome) and Black Bayou Salt Dome (Black Bayou Dome). The Vinton Dome is located in Calcasieu Parish, Louisiana, approximately 7 miles from the bottom-hole location of MS CCS 1 and approximately 7.7 miles from the bottom-hole location of MS CCS 2. Black Bayou Dome is located in Cameron Parish, Louisiana, approximately 2.4 miles east of the bottom-hole location of MS CCS 1 and approximately 2.7 miles east of the bottom-hole location of MS CCS 2 (Figure 2.1.1-10).

Associated faulting is caused either in response to local salt mobilization or evacuation, and on a larger scale where significant volumes of strata have been transported on listric fault surfaces which likely detach along deeper shales and/or salt intervals. Faulting induced by salt evacuation commonly causes an expanded sedimentary section on the downthrown side of the fault (growth fault), usually either down-to-the-coast or down-to-the-basin. Faulting associated with salt movement in the Project Minerva area includes local radial faults emanating from Black Bayou Dome. The influence of salt-dome proximity on permeability is further discussed in Section 2.3 (Faults and Fractures).

A second cause of faulting common to the Texas and Louisiana Gulf Coast is the cause-and-effect relationship between rapid progradation of sediments and slope failure in the vicinity of the shelf edge or outer platform margin. Sediment accumulated in a series of wedges that thicken and dip gulfward. As a result of rapid progradation and sediment loading, large growth-fault systems formed near the downdip edge of each sediment wedge within the area of maximum deposition. Faulting typically aligned parallel with the contemporary shelf edges in the Gulf Coast region. The greatest displacement of faults and thickest accumulations of Oligocene and Miocene sediments occurred in an area known as the Frio Expanded Zone (Figure 2.1.1-3).

The regional structural trends of the upper Frio and Anahuac formations are demonstrated on Figure 2.1.1-8 (Jones, Turcan Jr, & Skibitzke, 1954). Depth increases significantly from north to south and is linked to frequent normal and growth faults striking perpendicular to dip, detaching along deep shale or salt intervals. Such faults are only resolvable with three dimensional (3D) seismic data and appear as noise in lower resolution structural maps generated from regional well data. Localized structural highs are associated with salt diapirism in the regional area of Project Minerva. Synclines within the broad structural

regime result from the interplay of major regional faults with salt domes and the associated counter-regional faulting.

Figure 2.1.1-3 and Figure 2.1.1-8 demonstrate the significant increase in Oligocene strata thickness observed as the “Frio Stable Shelf Fault Zone” (north Orange County and Central Calcasieu Parish, Louisiana) trends southeastwards into the “Frio Expanded Fault Zone” (Figures 2.1.1-3) (Swanson, Karlsen, & J, 2013). While no major growth faulting is observed in the Project Minerva 3D seismic dataset, it is believed that regionally, Oligocene sediments greatly expanded and filled vast amounts of accommodation space created by movement along growth faults within the “Frio Expanded Fault Zone” (Swanson, Karlsen, & J, 2013).

The shallower Oligocene through Holocene section thickens basinward, periodically interrupted by low-relief, broad salt domes and anticlines. Some minor fault displacement occurs as well, particularly where the system overlies deep-seated Eocene or Oligocene growth-fault trends (Galloway, Henry, & Smith, 1982). Structural modification is greatest where the Cenozoic sedimentary section is warped upwards along the margins of salt diapers (Figure 2.1.1-8).

2.1.1.3 Regional Shallow Hydrogeology

The USDW is defined by LAC 43:XVII §3601 as an aquifer or its portion which supplies any public water system or contains a sufficient quantity of ground water to supply a public water system and currently supplies drinking water for human consumption or contains fewer than 10,000 milligrams per liter (mg/L) total dissolved solids (TDS) and which is not an exempted aquifer. The following sections detail regional and local hydrogeology and hydrostratigraphy in the area and are located at Project Minerva.

A hydrogeologic stratigraphic column for southwestern Louisiana is provided as Figure 2.1.1-11. The following sections provide details on the regional expanse and parameters pertaining to the hydrostratigraphy for the defined systems from deepest to shallowest intervals. A regional stratigraphic cross-section (A-A’) parallel to dip from (Baker Jr, 1978) depicting the aquifers in the regional area of southeast Texas is provided as Figure 2.1.1-12 and a local stratigraphic cross-section (A-A’) parallel to dip from (Lindaman M. A., 2023) depicting the aquifers in the local area of southwest Louisiana is provided as Figure 2.1.1-13.

The regional aquifer system is called the Gulf Coast Aquifer System and stretches from Texas, across Louisiana, Mississippi, and Alabama, and includes the westernmost portion of Florida. Miocene and younger formations contain water from <3,000 mg/L TDS to >10,000 mg/L TDS. These aquifer systems regionally crop out in bands parallel to the coast and consist of units that dip and thicken towards the southeast. (Baker Jr, 1978) describes four major hydrogeologic units that comprise the Gulf Coast Aquifer System in the Texas and Louisiana region. In ascending order, the four units are:

- Jasper aquifer
- Burkeville confining system
- Evangeline aquifer

— Chicot aquifer

The Burkeville confining system hydrologically separates the Evangeline aquifer from the underlying Jasper aquifer. However, the Chicot and Evangeline aquifers are thought to be hydrologically connected.

Regional Hydrostratigraphy

Jasper Aquifer

The Jasper aquifer is a hydrostratigraphic unit contained within the Miocene sands in the southwestern portion of Louisiana and Texas. The base of the aquifer coincides with the stratigraphic lower boundary of the Fleming Formation. In parts of Texas, this also includes the Oakville Sandstone. However, in the area of Project Minerva, this geological interval is not present. The Jasper aquifer is separated from the deeper saline formation waters of the upper Frio Formation by the shale-rich Anahuac Formation and is a confined system overlain by the Burkeville confining unit (Figure 2.1.1-12). The system is laterally extensive throughout the southern portion of Louisiana and along Texas and Louisiana Gulf Coast of Texas. Regionally, the Jasper aquifer system dips southwards and becomes deeper increasing in salinity towards the Gulf of Mexico.

In Louisiana, the Jasper Aquifer System is only used as a freshwater source north of Project Minerva in Vernon, Beauregard, Rapides and Allen Parishes. In the area of Project Minerva, the Jasper aquifer contains saline waters, ranges in thickness from 50 ft to 2,400 ft thick regionally and is comprised of medium- to fine-grained sands. It is geologically isolated from other aquifers by laterally extensive overlying and underlying clay strata with recharge to the system northward (up-dip) of Project Minerva (Baker Jr, 1986).

Burkeville Confining System

The Burkeville confining system separates the Jasper and Evangeline aquifers and retards the interchange of water between the two aquifers. The Burkeville confining system is comprised of compacted clays and fine-grained silts, with occasional lenses of sands. This system is shown to be an effective confining unit due to the differing hydrostatic pressures within the underlying Jasper aquifer and overlying Evangeline aquifer. The thickness of the Burkeville confining system is 300 ft along the Gulf Coast of Texas (Baker Jr, 1978). However, the unit thickness can vary from 100 ft to 1,000 ft within the Gulf Coast region. The Burkeville confining system's clay fraction varies across the Gulf Coast, from greater than 0.8 in southwest Texas to less than 0.3 in southeast Texas and southwestern Louisiana. The areas of low clay fraction are indicated by an increase in sand layers, containing fresh to slightly saline water, but because of the unit's relatively large percentage of silt and clay, when compared to the Jasper aquifer and Evangeline aquifer, the Burkeville confining system functions strictly as a confining unit (Baker, 1979).

Figure 2.1.1-12 identifies and depicts the confining system dipping down toward the Gulf Coast of Texas, and although the geological units of the Gulf Coast Aquifer System are stratigraphically correlated across the Texas-Louisiana border, the stratigraphic charts of Louisiana (Figure 2.1.1-11) do not identify the confining unit as the "Burkeville confining

unit," but instead inferred as the "Castor Creek confining unit" (Louisiana Geological Survey, 2000). Figure 2.1.1-14 is a hydrogeologic cross-section (Section-1) from the Texas Water Development Board (TWDB) study of the Gulf Coast Aquifer; the study extended from southeast Texas to southwest Louisiana (Young, Ewing, Hamlin, Baker, & Lupton, 2012). Both Figure 2.1.1-12 and Figure 2.1.1-14 demonstrate a confining clay separating the Jasper aquifer and Evangeline aquifer, and although assigned a different name in the Louisiana stratigraphic nomenclature (Castor Creek confining unit), this confining unit can be traced across neighboring state lines and are hydrogeologically the same.

Evangeline Aquifer

The Evangeline aquifer consists of Pliocene and late Miocene deposits ranging from loosely consolidated sands to gravels, with interbeds of silts and clays. The sands of the Evangeline aquifer are moderately well- to well-sorted and fine- to medium-grained with interbedded coarse sand, silt, and clay. The Evangeline aquifer includes the Goliad Sand and the upper unit of the Lagarto Formation, a member of the Miocene Fleming Group (DEQ of Louisiana, 2009). In southwest Louisiana, the Evangeline aquifer includes, in ascending order, the Castor Creek confining unit, Blounts Creek Member, and the lower units of the Pliocene Upland Allogroup (Lindaman, 2023).

The Evangeline aquifer underlies the Chicot aquifer and is separated from the Jasper aquifer by a Castor Creek confining unit. The upper portion of the Evangeline aquifer is separated from the Chicot aquifer by thin clay beds, although in some areas, the confining beds do not exist, and the upper sands of the Evangeline aquifer are in direct contact with the basal sands of the Chicot aquifer (DEQ of Louisiana, 2009).

In southwest Louisiana, recharge to the Evangeline aquifer occurs via rainfall inland from the Gulf of Mexico, and minimally, by leakage downwards from other shallow aquifers. The hydraulic conductivity of the Evangeline aquifer varies between 20 ft to 100 ft/day. The maximum depths of the Evangeline aquifer fresh water range from 150 ft above sea level (ASL) to 2,250 ft below sea level (BSL), and the freshwater interval thickness ranges from 50 ft to 1,900 ft deep (DEQ of Louisiana, 2009).

Chicot Aquifer System

The Chicot aquifer system consists of Pleistocene and Holocene deposits ranging from unconsolidated to loosely consolidated gravels and coarse graded sands. The Chicot aquifer system includes the Pleistocene Willis Sand, Lissie Formation, and Beaumont Formation, as well as the Holocene undifferentiated alluvial sediments (Lindaman M. A., 2023).

The Chicot aquifer system and the Evangeline aquifer have similar hydraulic frameworks, but the Chicot aquifer system is largely comprised of one major undifferentiated sand whereas the Evangeline aquifer contains interbedded silts and clays. In central and western Calcasieu and Cameron Parishes, the Chicot aquifer system includes the "200-," "500-," and "700-foot" sands (White & Griffith, 2020; Nyman, 1984). These sands are discussed in detail in Section 2.1.2.3 (Local Hydrogeology). The uppermost sand of the Chicot aquifer system contains freshwater underlain by saltwater in Cameron Parish (Nyman, 1984),

except along the southeastern coast where no freshwater is present (Smoot, 1988). Freshwater to saline water interface is driven northwards from the coast by water production for public supply, rice irrigation, and aquaculture. The southern limit of freshwater in the upper aquifer occurs near the coastline (Nyman, 1984). The Chicot aquifer system is the main regional aquifer system that provides usable groundwater for southwestern Louisiana (White & Griffith, 2020).

In southwestern Louisiana, the recharge to the Chicot aquifer system occurs where the Chicot outcrops in southern Rapides and Vernon Parishes, and in northern Allen, Beauregard, and Evangeline Parishes. There is also minimal recharge to the aquifer system via vertical leakage from the shallow overlying alluvial deposits. The aquifer system thickens and deepens to the south at a rate of about 30 ft/mile (Nyman, 1984).

Regional Groundwater Usage

The most recent Louisiana groundwater withdrawals from aquifers are reported by (Collier & Sargent, 2018) and summarize water withdrawals by 13 aquifer or aquifer system in on Appendix IV – Water-use by Aquifer Summaries. The Chicot aquifer system, Chicot equivalent aquifer system (southeastern Louisiana), Evangeline aquifer, Evangeline equivalent aquifer system (southeastern Louisiana), Jasper aquifer system, Jasper equivalent aquifer system (southeastern Louisiana) are all represented in Appendix IV – Water-use by Aquifer Summaries for the period 1980 – 2015.

The United States Geological Survey (USGS), in partnership with the Louisiana Department of Transportation and Development (LDOTD), has conducted a water-withdrawal and water-use inventory on a five-year basis since 1960. In *Water Use in Louisiana, 2015*, is to date the most recent Louisiana water use inventory report (Collier & Sargent, 2018; Purpera, 2020).

According to *Water Use in Louisiana, 2015,* the Jasper aquifer system is not a major source for regional freshwater use along the Louisiana Gulf Coast, except in Beauregard, Rapides and Vernon Parishes (Collier & Sargent, 2018). The Jasper aquifer contains freshwater for varying distances downdip regionally toward the gulf coast beyond which the aquifer contains saltwater. The increase in salinity is less commercially ideal to produce in comparison to the overlying Chicot and Evangeline aquifers as both are prolific water-yielding groundwater reservoirs in southern Louisiana. Precipitation on the outcrop of the Jasper aquifer is the source of recharge to the aquifer (Baker Jr, 1986). The aquifer's primary uses are for public water supply and industry with groundwater withdrawals in Louisiana at 47.95 million gallons per day (Mgal/d) (Collier & Sargent, 2018).

According to *Water Use in Louisiana, 2015,* groundwater withdrawal from the Evangeline aquifer in Louisiana is 28.56 Mgal/d, approximately half of that from the Jasper aquifer system. The Evangeline aquifer is used primarily in Evangeline, Allen, Avoyelles, and Beauregard Parishes for public supply and industry (Collier & Sargent, 2018).

The Chicot aquifer system yields the highest amount of groundwater withdrawals in Louisiana at 849.90 Mgal/d. The Chicot aquifer system is used primarily in Acadia, Calcasieu, Cameron, and Jefferson Davis Parishes (Collier & Sargent, 2018). Although prolific aquifers, because of both the Chicot and Evangeline aquifers shallower positions

and downdip edge of the aquifer's outcrop toward the coast, only the upper portion of the aquifer is used as a source of groundwater (Baker Jr, 1986). The largest contributor for withdrawal is rice irrigation and aquaculture, specifically water used for crawfish ponds. According to the *Water Use in Louisiana, 2015,* in southwestern Louisiana, the Chicot aquifer system is the major source of groundwater, providing 95.60 Mgal/d of groundwater used for public supply (Collier & Sargent, 2018).

According to *Water Use in Louisiana, 2015,* from 1980 to 2015 (i.e., the most recent reported Louisiana groundwater withdrawals from aquifers), total groundwater withdrawals decreased by 1.8% (Collier & Sargent, 2018). Unregulated groundwater withdrawals from aquifers can cause groundwater levels to decline especially if the water is withdrawn from the ground at a faster rate than it is replenished, resulting in seawater intrusion, land subsidence, streamflow depletion, and wells running dry. As groundwater is withdrawn, it lowers the water level near any proximity well and can result in a "cone of depression" around the well. Therefore, with a decrease in groundwater withdrawal, the less influence there is on water level in the aquifer, the less risk there is associated with the injection wells or injection operations. GCS will monitor and measure groundwater levels at Project Minerva to ensure the injection well and injection operations are stable and safe, as well as provide protection to the USDW.

Regional Groundwater Flow

Groundwater moves through aquifer systems from areas of high hydraulic head to areas of lower hydraulic head (Woessner & Poeter, 2020). In some areas, contributors of withdrawal, such as industry and the public water system usage, can alter flow directions of groundwater in aquifers (Lovelace, Fontenot, & Frederick, 2004).

The Chicot aquifer system is the primary source of fresh groundwater in southwestern Louisiana. Project Minerva and Lake Charles are located within the boundary of fresh groundwater of the Chicot aquifer system (Figure 2.1.1-15). Rice irrigation and aquaculture are the largest contributors of withdrawal for the Chicot aquifer system; therefore, seasonal pumping of these water uses have altered flow directions and induced lateral or upward movement of saltwater (Lovelace, Fontenot, & Frederick, 2004). Figure 2.1.1-16 shows the potentiometric surface and the direction of groundwater flow of the Chicot aquifer system in southwestern Louisiana.

As pumping continues, wells in southwestern Louisiana could draw an increase proportion of water from lower, more saline parts of the aquifer. This occurrence is known as saltwater coning, or more formerly, "upconing." To reduce the potential for upconing saltwater in wells, decreasing the rate or duration of pumping and screening high-capacity wells as far above the base of freshwater could substantially recover the declining seasonal water levels and stop saltwater encroachment in agricultural activities (Lovelace, Fontenot, & Frederick, 2004). Figure 2.1.1-17 shows saltwater encroachment of the Chicot aquifer system on two local cross-sections extending across Calcasieu and Cameron Parishes in southwestern Louisiana. Project Minerva is located in the divot, south- to southwest in the boundary of fresh groundwater of the Chicot aquifer system, and less than the interpreted 20 ft potentiometric contour where water-level declines occur due to seasonal ground-water

withdrawals (Lovelace, Fontenot, & Frederick, 2004; White & Griffith, 2020). This indicates that the shallow aquifer systems at Project Minerva are less impacted by the increase in groundwater withdrawals and saltwater encroachment.

2.1.1.4 Regional Deep Hydrogeology

A hydrogeologic stratigraphic column for southwestern Louisiana is provided as Figure 2.1.1-11. The Frio Formation is the downdip equivalent of the continental Catahoula Formation. These formations comprise a mixture of marginal marine and deltaic sandstones and shales, with localized deep marine shales and turbidite sandstones (Teeple, Becher, Walton-Day, Humberson, & Gallegos, 2022; Griffith, 2003). The Catahoula Formation (and down-dip Frio Formation equivalent) is known to contain only saltwater due to its greater depths compared to other shallower hydrogeologic units. The top of the Catahoula Formation is Anahuac Formation (late Oligocene), a regionally extensive transgressive marine shale unit. Aquifers underlying the Catahoula aquifer are known to contain only saltwater in southern Louisiana.

Regional Deep Aquifer Fluid Flow

Many of the studies for flow rates in deep saline aquifers come from the search for subsurface waste disposal sites. These studies show slow circulation to nearly static conditions in the deep subsurface (Bethke, Altaner, Harrison, & Upson, 1988). Flow rates in the deep saline aquifers (Clark, 1981), were found generally to be in the order of "centimeters per year in the Gulf Coast Plain" and less than those for shallower freshwater aquifers. In general, groundwater flow in the deeper saline aquifers, such as the middle Frio Formation, is a function of lower permeability of the sand units rather than hydraulic gradients. Studies conducted by the federal government in search of subsurface waste disposal sites indicate that deeper units have less porosity and permeability and have higher salinity content. Background velocities in the deep subsurface, in general, and in the Frio Formation in particular, are generally less than 1.0 ft/year (Clark, 1988).

A south-southeastern (down-dip/basinward) direction of regional flow assumed for the Frio Formation is consistent with the theory of deep basin flows and the physical mechanisms (topographic relief near outcrops and deep basin compaction) identified as contributing to natural formation drift (Bethke, Altaner, Harrison, & Upson, 1988; Kreitler, et al., 1981). Work by (Griffith, 2003) also indicates that the saline waters in the Injection Zone flow downdip toward the modern coastline.

Fluid flow in the Injection Zone (upper Frio Formation) is assumed to be very slow (less than 1.0 ft/year) in a basinward direction. This assumption will be tested/validated via the periodic history matching of the simulation model.

2.1.2 Local Geology

The structural geology and stratigraphy beneath Project Minerva were developed from a series of structure maps, stratigraphic maps, and cross-sections prepared from the publicly available well-control data / information locally. Figure 2.1.2-1 is a basemap showing an entire view of both Figure 2.1.2-2 (N-SW cross-section) and Figure 2.1.2-3 (W-E cross-

section). Figure 2.1.2-2 and Figure 2.1.2-3 are detailed cross-sections across Project Minerva. Data logs used in the cross-sectional Figures are provided in Appendix V.

The analysis of regional and local geology near Project Minerva demonstrates that the subsurface is geologically ideal for injection. The middle Oligocene massive sandstones of the upper Frio Formation serve as effective injection reservoirs for the Injection Zone, in terms of their lateral extent, mineralogical composition, and petrophysical characteristics.

Initial studies show that the Injection Zone has effective permeability, porosity, thickness, and lateral continuity to accept and contain injected fluid. Shales of the overlying late Oligocene-age Anahuac Formation possess the necessary criteria to serve as the Upper Confining Zone and provide effective barriers to upward movement. Significant separation exists between the Upper Confining Zone and the base of the lowermost USDW (Figure 2.1.2-2 and Figure 2.1.2-3).

The following sections provide a detailed assessment of the local geology as it pertains to Project Minerva.

2.1.2.1 Local Stratigraphy

At Project Minerva, the stratigraphic units of interest, in descending order, include:

- Quaternary interval (i.e., glacial sediments and regional potable water aquifers) - the Lowermost USDW
- Late Oligocene, Anahuac Formation - Upper Confining Zone
- Middle Oligocene, upper Frio Formation - Injection Zone
- Middle Oligocene, upper Frio Formation - Lower Confining Zone

The stratigraphic units of interest have been correlated across Project Minerva by constructing north-south and west-east cross-section lines, centered on the proposed injection well locations and extending at least two miles beyond the extent of the proposed AoR (Figure 2.1.2-1). Figure 2.1.2-2 shows the north-southwest oriented cross-section line (A-A') that is approximately parallel to strike, and Figure 2.1.2-3 shows the west-east oriented cross-section line (B-B') that is approximately parallel to dip.

2.1.2.2 Local Structure

The local structure at Project Minerva is the result of subsidence along deep-seated normal faults in combination with salt diapir movement at Black Bayou Dome to the east and Vinton Salt Dome to the north. The two proposed Class VI injection wells, MS CCS 1 and MS CCS 2, are strategically located so that CO_2 drainage is predicted to move dominantly up-dip to the west (Figure 2.1.2-3) and southwest (Figure 2.1.2-2).

The structure of the project area is presented in Section 2.2.3 (Structure Maps) and structural interpretation is discussed in Section 2.4.2 (Description of the Injection Zone and Confining Zone System). The following subsections discuss the influence of salt dome development and faulting on the local structure.

Local Salt Dome

Project Minerva is located westward from the Black Bayou Salt Dome (Black Bayou Dome) in Cameron Parish, Louisiana, approximately 2.4-miles east of the bottom-hole locations of MS CCS 1 and MS CCS 2 (Figure 2.1.1-10). Black Bayou Dome is a southwestern Louisiana salt dome where the salt is relatively near the surface. The Louisiana Gulf Coast is approximately 19-miles south of the dome and the Intracoastal Waterway (ICW) is 2-miles north. Black Bayou Dome underlies a marsh that is crisscrossed by a canal and bayou network. Black Bayou, which crosses over the center of the dome, is a large bayou extending from Sabine Lake, and is connected to the ICW by the Black Bayou Cutoff Canal.

Black Bayou Dome has a shallow piercement structure with steep, nearly vertical sides, circular horizontal cross-section, and generally flat top. The approximate depth to caprock is 881 ft to a maximum of 1,369 ft, and the approximate depth to the shallowest salt is 1,035 ft BSL and the deepest salt is 8,553 ft BSL on the northeast periphery of the dome. The caprock is composed of 76.3 ft of calcite, 66 ft of gypsum, and 800 ft of anhydrite (DOE, 1978).

The base of freshwater in the area of Black Bayou Dome is approximately 500 ft below MSL. Slightly saline groundwater occurs in the approximate depth interval of 500 ft to 900 ft below MSL (DOE, 1978).

The Black Bayou Dome is a productive salt dome producing petroleum from the cap rock of the reservoir. Drilling for sizable deposits of Sulphur have been produced as a result of drilling for oil (Beckman & Williamson, 1990).

Local Faulting

In the area of Project Minerva, the direction of majority faulting is parallel to the edge of the Louisiana Gulf Coast. Local faulting connected to the growth and presence of numerous salt features originating from Black Bayou Dome to the east of Project Minerva adds complexity to structural architecture. Faults located further from Black Bayou Dome tend strike between 70° and 90°, although, radial faults originating from Black Bayou Dome have a wide variation in strike due to the complex structural regime associated with diapiric salt structures regionally. Section 2.3.1.4 summarizes the local faulting and structures at Project Minerva.

2.1.2.3 Local Hydrogeology

As discussed in Section 2.1.1.3 (Regional Shallow Hydrogeology), the four major hydrogeologic units that comprise the Gulf Coast Aquifer System in the Texas and Louisiana region include, in ascending order, the Jasper aquifer, the Burkeville confining system, the Evangeline aquifer, and the Chicot aquifer.

In the area of Project Minerva, the top of the Jasper aquifer strikes (east to west) at approximately 4,080 ft MSL and dips (north to south) at approximately 5,080 ft MSL toward the Gulf Coast of Louisiana. The approximate average thickness of the Jasper aquifer ranges from 1,601 ft to 2,400 ft thick (Intera, Frontera-Exploration, Hamlin, & Baker, 2012).

Locally, the Burkeville confining system, recognized by the stratigraphic charts of Louisiana as the "Castor Creek confining unit," separates the underlying Jasper aquifer and the overlying Evangeline aquifer (Louisiana Geological Survey, 2000). In the area of Project Minerva, the confining unit is located in the middle of the Lagarto Formation of early Miocene time with the top of confining unit at a strike (east to west) of approximately 4,020 ft MSL and a dip (north to south) of approximately 5,010 ft MSL toward the Gulf Coast of Louisiana. The approximate average thickness of the confining unit ranges from 201 ft to 400 ft thick (Intera, Frontera-Exploration, Hamlin, & Baker, 2012).

In the area of Project Minerva, the top of the Evangeline aquifer strikes (east to west) at approximately 1,040 ft MSL and dips (north to south) at approximately 1,070 ft MSL toward the Gulf Coast of Louisiana. The approximate average thickness of the Evangeline aquifer ranges from 2,401 ft to 3,200 ft thick (Intera, Frontera-Exploration, Hamlin, & Baker, 2012).

In the Project Minerva area, the Chicot aquifer's approximate average thickness ranges up to 1,070 ft thick (Intera, Frontera-Exploration, Hamlin, & Baker, 2012). Project Minerva is located in Cameron Parish, Louisiana within the boundary of fresh groundwater of the Chicot aquifer system. The Chicot aquifer system is used primarily in Cameron Parish, Louisiana, however, the Chicot and Evangeline aquifers are thought to be hydrologically connected in southwestern Louisiana (Baker Jr, 1978). The lowermost USDW is located approximately at the base of the Chicot aquifer's 700-Foot Sand or the uppermost portion of the Evangeline aquifer. The following sections provide details on the local hydrostratigraphic units for the defined aquifer systems from deepest to shallowest intervals.

Local Hydrostratigraphy

The two main aquifers of local interest, in ascending order, include:

- The Chicot aquifer (Pleistocene), and
- the Evangeline aquifer (Pliocene).

The geologic units that make up these two hydrogeologic units, in ascending order, include:

- Fleming Formation / Lagarto Clay (Miocene),
- Goliad Sand (Pliocene),
- Willis Sand (Pleistocene),
- Lissie Formation (subdivided into the Montgomery and Bentley formations) (Pleistocene),
- Beaumont Formation (Pleistocene), and
- Holocene Alluvial sediments.

Most of the information provided below is derived from Calcasieu Parish, directly north of Cameron Parish where Project Minerva is located. Project Minerva is located in a specific area in Cameron Parish where freshwater exists.

Evangeline Aquifer

In the area of Project Minerva, the Evangeline aquifer predominantly contains saline groundwater (greater than 10,000 mg/l TDS). Upper and lower boundaries to the Evangeline include the Goliad Formation and the upper part of the Fleming Formation, respectively. The Evangeline and Chicot aquifers are usually separated by thin layers of confining clay that comprise the top of the Goliad Formation. However, when this clay is absent, the geologic boundary between the two aquifers is indistinguishable with the Goliad grading into the Willis Formation. In general, the Evangeline aquifer tends to have greater sand to clay ratio with individual sand beds up to several tens of feet thick.

Figure 2.1.2-4 is a Piper diagram demonstrating a graphical representation of the chemistry of water samples in the Lake Charles area to best represent the water chemistry at Project Minerva. This water chemistry data helps in understanding the sources of the dissolved constituent salts in water samples taken from each of the local aquifers. According to Figure 2.1.2-4, the Evangeline aquifer of Lake Charles area contains a sodium-potassium bicarbonate type of water chemistry with an ionic composition of sodium and potassium cations and bicarbonate type anions. The hydrochemical facies of the Evangeline aquifer is predominately sodium bicarbonate waters.

Because the Evangeline aquifer is mostly saline within the Project Minerva area, it is not considered USDW and is not used for groundwater in Cameron Parish.

Chicot Aquifer

In the area of Project Minerva, the major aquifer system is the Chicot aquifer. The Chicot aquifer is divided into distinct, shallow alluvial sands: (1) the “200-foot” sand, (2) the “500-foot” sand, and (3) the “700-foot” sand, named after their depths of occurrence, in the Lake Charles area (Figure 2.1.2-5). The eastern most side of Calcasieu Parish, and northeast into Cameron Parish in Louisiana, the Chicot aquifer is divided into the “upper sand” (i.e., “200-foot” sand), the “lower sand” (i.e., “700-foot” sand), and the “500-foot sand” being largely isolated between the two sands. The sands are separated by confining layers except where the “500-foot” sand merges with the “700-foot” sand further north of Calcasieu Parish, Louisiana (DEQ of Louisiana, 2017).

Salt water occurs within the Chicot aquifer near the coast and in isolated bodies north of the modern coastline (DEQ of Louisiana, 2017). In the area of Project Minerva, the “200-foot sand,” “500-foot sand,” and “700-foot sand” contain freshwater although saltwater encroachment does occur southward toward the Louisiana Gulf Coast (Milner & Fish, 2009).

According to Figure 2.1.2-4, the Chicot aquifer of Lake Charles area contains a mixed type of water chemistry with an ionic composition of sodium and potassium cations and bicarbonate-chloride type anions. The hydrochemical facies of the Chicot aquifer is predominately sodium bicarbonate-chloride waters.

200-Foot Sand

The “200-foot sand” is stratigraphically equivalent to, and continuous with, the “upper sand” of the Chicot aquifer. It is a shallow aquifer sand, with the sand grading from fine to

medium sand in the uppermost portion to coarse sand or gravel at the base. The "200-foot sand" is used mainly to supply water for irrigation and domestic purposes. In the western part of Calcasieu Parish, the Chicot aquifer is thin, providing water strictly for domestic purposes, and in the central part of the parish, it provides water for industrial purposes (Harder, 1960).

The "200-foot sand" has a chloride content generally less than 100 parts per million (ppm), whereas in the eastern part of Calcasieu Parish, it increases up to approximately 300 ppm and the dissolved solids increase up to approximately 700 ppm. The "200-foot sand" contains the lowest TDS concentration waters in the Chicot aquifer. According to Figure 2.1.2-4, the "200-foot sand" of Lake Charles area contains a mixed type of water chemistry with an ionic composition of sodium and potassium cations and bicarbonate type anions. The hydrochemical facies of the "200-foot-sand" is predominately sodium bicarbonate waters.

The top of the "200-foot sand" dips southward (from the aquifer's recharge outcrop in Beauregard Parish, Louisiana) at a rate of 4 ft/mile to 10 ft/mile: however, variance in thickness locally may change the dip to vary considerably, as in the southwestern part of Calcasieu Parish where it increases to 50 ft/mile (Harder, 1960).

500-Foot Sand

The "500-foot sand" is the most well-developed aquifer portion and the principal aquifer of Calcasieu Parish, Louisiana. The "500-foot sand" is composed of gray to brownish sand ranging from fine sand in the uppermost portion to coarse sand and gravel near the base. The "500-foot sand" is used in about all industries and supplies water to many irrigation wells. The "500-foot sand" is not utilized largely as a source of supply in the southeastern part of Calcasieu Parish, where the sand is relatively thin and consists of mainly fine sand (Harder, 1960).

The average dissolved solids content is 302 ppm, and the chloride content is generally low in the northern and central parts of Calcasieu Parish, where the average well supplies 30 ppm. According to Figure 2.1.2-4, the "500-foot sand" of Lake Charles area contains a mixed type of water chemistry with an ionic composition of sodium and potassium cations and bicarbonate type anions. The hydrochemical facies of the "500-foot-sand" is predominately calcium-sodium bicarbonate waters.

The dissolved solids increase up to more than 600 ppm, where the "500-foot sand" directly overlays salt dome structures (i.e. Vinton Dome). At Vinton Salt Dome, the "500-foot sand" is between depths of 410 ft and 600 ft and contains a clay unit between 470 ft and 500 ft. The "500-foot sand" dips southward (from the aquifer's outcrop area in central Beauregard and Alien Parishes, Louisiana) at an average rate of 18 ft/mile (Harder, 1960).

700-Foot Sand

The "700-foot sand" is thick and continuous throughout Calcasieu Parish. Clay units divide the Chicot aquifer into two or three separate layers; however, because the clay layers are not continuous, the sands are hydrologically connected. The "700-foot sand" is tan to

grayish sands grading from fine in the uppermost portion to coarse at the base. The “700-foot sand” supplies water to industries and irrigators and is the source for public water supply in the area of Lake Charles, Louisiana.

The chloride content of water in the "700-foot sand” is greater than that in the "200-foot sand" and "500-foot sand." According to Figure 2.1.2-4, the "700-foot sand" of Lake Charles area contains a mixed type of water chemistry with an ionic composition of strictly sodium and potassium cations and bicarbonate-chloride type anions. The hydrochemical facies of the "700-foot-sand" is predominately sodium chloride-bicarbonate waters.

The regional dip of the sand is generally southward at about 10 ft/mile (Harder, 1960).

2.2 MAPS AND CROSS-SECTIONS OF THE AOR

The following sections discuss the data collection efforts employed by GCS to interpret the subsurface and the workflows followed to integrate the data into a geostatistical model for simulation and mapping.

2.2.1 Subsurface Interpretation and Integration

Continual peer review and critical assessment of model inputs, outputs and assumptions by the GCS technical team and GCS senior advisors ensures reasonable results and ongoing model refinement.

The following steps provide an overview of the full-cycle GCS data, model, and simulation workflow:

— **A comprehensive data collection** effort was undertaken, drawing primarily from TGS Well Dataset services, C&E Strategic Natural Resources Information System (SONRIS), Texas Railroad Commission (TRRC), and Stream Family Office Archives. “Stream Family Office Archives” refers to data contributed by the Stream Family, whose history in Southwest Louisiana spans decades of oil and gas development. As long-standing stewards of the land, the Stream Family has accumulated extensive well records and seismic datasets through a variety of lease and working-interest agreements. Their archive encompasses a wide range of subsurface and operational data including well files, LAS and raster logs, directional surveys, pressure and production test results, completion and stimulation reports, and daily drilling records, all derived from operator and working-interest documentation. While much of this data overlaps with the public domain, e.g. SONRIS database, some of it exists only as private, hard-copy records retained by the family. Some examples of these exclusive datasets include high-resolution dipmeter logs, formation and mud logs, cement bond logs, lithologic descriptions, dual-induction sonic logs, shale-density and gas-analysis logs, segmented bond logs, and thermal time-decay logs. In addition, the Stream Family's archives include historical operator maps, well-location plats, geologic cross-sections, and other available interpretations. Where possible, these records were digitized and integrated into the broader GCS analysis.

  All well header information, digitized well logs, raster well logs, core data, and formation tops were compiled and integrated into a centralized Petrel database to

support geologic and reservoir modeling. Additional regional context was incorporated from publicly available datasets, including published literature and shapefiles representing geologic trends, regional fault systems, and cultural mapping data. A significant portion of the work involved digitizing static well logs and standardizing disparate data formats to ensure a consistent, high-quality dataset suitable for subsurface interpretation and simulation workflows.

- **Regional stratigraphic and structural evaluation** across east Texas and southwestern Louisiana were evaluated. More than 1,700 regional legacy oil and gas wells were analyzed to generate an in-depth understanding of the structural and thickness trends of the late Oligocene and Miocene intervals overburden. A detailed analysis of structural closures and migration pathways. Injection Zone and Confining Zone were defined, and the location of Project Minerva was narrowed down to Cameron, Louisiana.
- **Detailed geological and petrophysical characterization** completed on more than 470 wells with available log and core data, centered around Project Minerva. The upper Frio Formation within the Injection Zone is subdivided into 11 intervals based on sequence stratigraphic interpretation of maximum flooding surfaces. A detailed property (i.e., shale content, facies, porosity, permeability) modeling was also performed for all layers.
- **Analysis of local legacy oil and gas wells and historical production** to confirm depletion of the upper Frio Formation is not an issue for CO_2 injection and containment.
- **3D seismic data imported and interpreted** to provide the seismically derived framework of the geostatistical model. Structural formation tops and resulting surfaces generated in Petrel, a software platform by Schlumberger Information Solutions, from log data combined with seismic horizons to extend the regional geostatistical model beyond the available seismic data. Detailed structural interpretation completed throughout available 3D seismic coverage.
- **Petrophysical analysis and facies modeled combined with the structural model** generates the static geo-model. Probabilistic property distribution is used to reduce data uncertainty.
- **Model outputs are used to apply a rigorous set of subsurface constraints** on the controlled acreage to identify the optimal location for CO_2 injection.
- **Geo-model upscaled and imported to modeling software** to create the “reservoir simulation model” (See Section 2.10.5). A full suite of engineering data and assumptions were used to build and iterate a robust simulation model to simulate pressure and CO_2 plume.
- **Based on the results and key learnings from the simulation runs, the inputs were then optimized, and the model is rerun.** This process commenced initially on a regional scale, and then ultimately allowed the geological characterization to focus

on the areas that are of higher interest to injection. These iterations, which now number more than 700, have been key to GCS's understanding of the key parameters and mechanisms and have ultimately allowed GCS to accurately define how CO_2 injections will occur.

2.2.1.1 Available Data Sets

History of Subsurface Data Development

The state of Louisiana was the 9th largest producer of crude oil and 4th largest producer of natural gas in the U.S. in 2018 (U.S. Energy Information Administration (EIA), 2020). The Frio Formation, including the Anahuac Formation, is the largest producer of hydrocarbons from the Paleogene in the Gulf of Mexico. Project Minerva is located in a highly productive and extensively developed Frio Formation (including the Anahuac Formation) "play" (i.e., a geological reservoir group) where millions of barrels of oil (MMBO) have been produced along the Texas and Louisiana Gulf Coast (Swanson, Karlsen, & Valentine, 2013).

As such, the project benefits from a substantial dataset including geophysical well logs, core samples, production data, regional studies, and seismic surveys.

History of exploration at Project Minerva includes the following:

- In the 1920's, early wells targeted the crest and flanks of the Vinton Dome and Black Bayou Domes in which included relatively few shallow Miocene wells drilled.
- From the 1930's to the 1950's, there was a big increase in drilling (hundreds of wells, targeted salt dome flanks with wildcat wells extending further afield; large, less structurally complex fault block traps were targeted in the Miocene reservoir.
- From the 1960's to the 1980's, there was an increase of two dimensional (2D) seismic use which encouraged the expansion of drilling into deeper reservoirs (Miocene and Frio Formation) and more structurally complex areas of the salt dome flanks (e.g. southern flank of Vinton Dome). The peak of Miocene reservoir drilling took place during the 1970's just before decreasing in the 1980's.
- In the early 1990's, there was a dramatic drop in drilling before the advent of 3D seismic in the late 1990's. This allowed imaging of deeper Hackberry sandstone reservoirs and better understanding in the development of structural traps. A new phase of drilling deeper, over pressurized wells occurred.

The drilling of deeper, over pressurized wells is important to Project Minerva as it provides a modern, analogous data set for the project area (i.e., the upper Frio and Anahuac Formations).

- In the Early 2000's, there was a great increase in Miocene and Oligocene drilling across the flanks of Vinton Dome and Black Bayou Dome. Deep well targeted the Hackberry sandstone channels away from salt dome structures, notably in the structural low targeted by Project Minerva. The deeper wells targeting the Hackberry were enabled by the extensive 3D seismic (90's-early 2000's). Modern well logs

suites were acquired in these wells providing a critical data source for the Project Minerva analysis.

— From the mid-2000's to the present day, the more recent drilling has continued at a much-reduced rate, mainly targeting previously overlooked accumulations in fault blocks around Vinton Dome, Black Bayou Dome and Phoenix Lake Field with vertical and directional wells.

Historic subsurface development has provided a wealth of information and knowledge about the Injection Zone and Confining Zone. Adjacent production has predominately been from the shallower Miocene or deeper mid Frio Formation (known as the "Hackberry Trend" in the project area). Within the Project Minerva AoR, there are no productive intervals within the proposed Injection Zone (upper Frio Formation).

Well Data

A substantial amount of time was dedicated to building a comprehensive regional wells and subsurface database that integrates multiple data sources across Louisiana and Texas. Well logs and records were compiled from TGS Well Dataset Services, C&E SONRIS, the Texas Railroad Commission (TRRC), Cambe Well Services, and Stream Family Office archives, supplemented by back-office data retrieval from the TRRC District Office, and the Lafayette and Baton Rouge District Offices.

The data-mining process included digitizing hard-copy well logs and merging duplicate or conflicting well entries through a Master Data Management workflow to establish a single authoritative source of truth. Each well was validated through a spatial QC process in ArcGIS and attributes cross-checks against public datasets.

This regional database serves as the foundation for geologic and reservoir modeling efforts. ArcGIS was extensively used for spatial integration, mapping, and validation of wells, while Petrel supported well interpretation, seismic interpretation and geostatistical modeling.

Geomechanics

See Section 2.5.1 (Geomechanical Information) for detailed discussion of geomechanical data available.

Because site-specific mechanical measurements are not yet available, analogous data were compiled from published studies of the upper and lower Frio Formation.

- Frio Formation CO_2 injection Pilot Project (Hovorka, et al., 2005), providing porosity, permeability, grain-size distributions, and elastic properties.
- Lower Frio in-situ stress testing (Ramos, Katahara, Keck, & Batzle, 1994), providing stress gradients, elastic moduli, and strength parameters.

These studies constrain the likely stress state and mechanical response of Frio sandstones and shales and establish the uncertainty ranges expected for Project Minerva's fracture-pressure and fault-stability evaluations.

Core

Available core data in the project area is sourced from wells surrounding the Vinton Dome. Side-wall core samples have been evaluated for permeability and porosity from the Injection Zone (upper Frio Formation) and from the Upper Confining Zone (Anahuac Formation). Section 2.5.2.1 (Data Sources) discusses available core data in detail.

Formation Fluid

Analog data was combined with a petrophysical study of 12 wells in the area to estimate salinity. The CECOS Project was used as an analog for detailed fluid chemistry, as detailed in Section 2.8.1 (Geochemical Study) of this document and in Sections 1.5.9 and 1.6.4.4 of the AoR and Corrective Action Plan (Attachment A).

Seismic Data

GCS has access to over 422 mi^2 of proprietary and licensed 3D seismic. The available seismic data extends from southeast Texas to Lake Calcasieu River, across Project Minerva. The dataset was collected in the late 1990's and has since been used in the entire seismic database as set forth below. In the mid-2010's, the inventory and digitization exercise of the historical 3D seismic survey began, which has since been upgraded from analog to digital to enable the full realizations of data volubility. All surveys merged were used to assess different degrees in response to the complexity of the geology overall. The surveys include:

- Big Island 3D Survey,
- Black Bayou 3D Survey,
- Vinton Dome 3D Survey, and
- Alligator Cove 3D Survey.

The seismic surveys were permitted, along with *Black Bayou 3D Survey*, in August of 1998 by Seitel Inc. The seismic survey was conducted by Seitel Inc., and the data was processed by Vector Seismic Data Processing. Data delivery under the permit occurred in March, April and July of 1999.

Big Island 3-Dimensional Survey

The *Big Island 3D Survey* was conducted in Calcasieu Parish, Louisiana, primarily in Township 10 and 11 South and covers a combined total live seismic area of approximately 55.26 mi^2. The seismic dataset contains both gathered field data and processed data. GCS utilizes the Pre-Stack Time Migration (PSTM) processed data set. The PSTM data file for the survey has a data record length of 5.996 seconds with 4 millisecond sample intervals, and a bin size of 110 ft by 110 ft. Although located in adjacent parish, Calcasieu Parish, the seismic lines from the *Big Island 3D Survey* were not used in the permit application for Project Minerva. The header for the PSTM is set forth in Figure 2.2.1-1.

Black Bayou Dome 3-Dimensional Survey

The *Black Bayou 3D Survey* was conducted in Calcasieu Parish, Township 11 South and Cameron, Parish, Louisiana Township 12 and 13 South covering a combined total live

seismic area of 82.99 mi^2. The seismic survey contains one field data set and two processed data sets. GCS utilizes the PSTM processed data set. The PSTM data set is a Stacked Migration with Noise Reduction (MIGNR) and has a data record length of 8.5000 seconds with four millisecond sample intervals, and a bin size of 110 ft by 110 ft. The *Black Bayou 3D Survey* is the only seismic survey used in evaluating Project Minerva as the seismic lines cover the entirety of the AoR. The header for the MIGNR processed data set is set forth in Figure 2.2.1-2.

Vinton Dome 3D Survey

The *Vinton Dome 3D Survey* is a radial seismic survey acquired with receivers placed along radial-lines and sources on concentric arcs. A Vertical Seismic Profile (VSP) was available in 'Well G-23' located on the northwestern flank of the Vinton Dome. Concentric circles approximate source locations, with shot spacing being 165 ft along the arc. The seismic source consisted of 5.5 lb. pentolite charges set off at 60 ft depth. The receiver line interval on the surface is variable, ranging from approximately 900 ft to 1,200 ft, with alternating long and short line segments spaced at 5 increments. The receiver station spacing was 165 ft along a receiver line segment.

Alligator Cove 3D Survey

The *Alligator Cove 3D Survey* was conducted in Calcasieu Parish, Louisiana covering approximately 50 mi^2 of Stream Family Office property with a total live seismic area of 260.63 mi^2. The *Alligator Cove 3D Survey* is a merger of the following projects:

- *Big Island 3D Survey*,
- *Vinton Dome 3D Survey,*
- *Garter 3D Survey,*
- *Sulphur 3D Survey*,
- *Gillis 3D Survey,*
- *Houston River 3D Survey, and*
- *Pine Ridge 3D Survey* (which includes Calcasieu River, South Sulphur, and South Lake Charles 3D seismic surveys).

The project contains two gathered data sets and seven stacked data sets, and deliverables including three data type products:

- Raw Pre-stack Time Migration (RPSTM),
- Enhanced Pre-stack Time Migrations (EPSTM),
- Enhanced 1,
- Enhanced 2, and
- Amplitude Verses Offset (AVO) Pre-stack Time Migration (APSTM).

The APSTM included three angle sub-stacks (near, mid and far), and a Velocity model in SEG-Y format. The *Alligator Cove 3D Survey* has a record length of 7.988 seconds with two milliseconds sample intervals. The bins for all data sets are 110 ft by 110 ft. Data delivery for reprocessing occurred in July of 2019.

Limitations and Assumptions of the 3-Dimensional Datasets

As with any seismic reflection survey, the datasets utilized in Project Minerva have inherent limitations related to their differing differences in acquisition vintage, survey design and processing and reprocessing workflows. These factors collectively influence the effective seismic resolution and, consequently, the ability of the data to detect and distinguish subsurface features of interest, including those associated with CO_2 plume evolution.

Seismic resolution can be broadly divided into two components: (1) vertical resolution and (2) horizontal (lateral) resolution. Vertical resolution refers to the ability to distinguish closely spaced reflectors in time/depth and therefore controls the minimum bed thickness that can be resolved as separated events. Horizontal resolution refers to the ability to distinguish laterally separated features, and is influenced by factors such as seismic wavelength, acquisition geometry, and migration. In the context of CO_2 monitoring, these resolution limits directly impact the detectability and delineation of plume boundaries and internal heterogeneities. As per industry standards, GCS uses an approximation of the vertical resolution using Rayleigh's criterion, whereby two reflectors are considered resolvable when separated by approximately a quarter to half of the dominant seismic wavelength, commonly expressed as the tuning thickness).

To solve for thickness:

$$\Delta h \geq \frac{\lambda}{4}$$

Where h corresponds to the thickness and λ to the wavelength. The vertical resolution can be calculated from the length of the propagation wave and the layer thickness below $\frac{\lambda}{4}$ for resolving limits of beds. It is possible to detect layers down to $\frac{1}{32\lambda}$, and hence why in some cases in the presence of faults, the reflections are not completely disassociated but seem more continuous with unexplained changes in their dipping angles.

Vertical seismic resolution varies, normally decreasing with depth as the earth works as a filter rapidly attenuating high frequency. As high frequencies play a key role in defining the vertical seismic resolution, the low frequencies play a role in penetration. Therefore, the importance of seismic surveys in having a broad frequency spectrum.

Utilizing Rayleigh's Limit of Resolution, an average vertical seismic resolution at reservoir depth level has been calculated for the seismic surveys as follows:

Big Island 3D Survey

$$\frac{\lambda}{4} \cong 82\ ft$$

Equation 2.2-1

Black Bayou 3D Survey	$\frac{\lambda}{4} \cong 85\ ft$	Equation 2.2-2
Vinton Dome 3D Survey	$\frac{\lambda}{4} \cong 90\ ft$	Equation 2.2-3
Alligator Cove "merged" 3D Survey	$\frac{\lambda}{4} \cong 90\ ft$	Equation 2.2-4

These $\frac{\lambda}{4}$ values represent average estimates derived from frequency spectra generated using both statistical and deterministic wavelets at multiple well locations, based on zero-offset synthetic seismograms used for seismic-to-well ties. Seismic resolution is expected to decrease in areas of steeply dipping reflectors, such as around the Black Bayou Dome, where fault illumination is reduced, and with increasing depth due to the attenuation of higher frequencies.

Differences in vertical seismic resolution between the available surveys are minimal and not expected to materially impact interpretation. As such, datasets can be used in combination, including the Alligator Cove 3D Survey, without introducing significant inconsistencies.

Although vertical seismic resolution was evaluated for all available surveys, the primary datasets used for Project Minerva are the Black Bayou and the Alligator Cove. No additional seismic data are required, as the only overlapping survey (Big Island) provides limited coverage, restricted to a small area near the Calcasieu-Cameron parish boundary (Figure 2.2.1-3).

2.2.1.2 Seismic Interpretation Workflow

Petrel, a software platform by Schlumberger Information Solutions, was used throughout the subsurface workflow for data integration, interpretation, and analysis, providing a consistent technical framework to support reservoir characterization and informed decision making. The seismic interpretation workflow applied in this study is summarized below.

Reconnaissance Viewing of Data

This stage consists of a rapid screening of the available seismic datasets with the following objectives:

1. Seismic data quality assessment survey selection: A visual quality control of the available seismic surveys was performed to evaluate their suitability for interpretation and to define their respective roles within the workflow. The seismic surveys considered exhibit comparable vertical resolution at reservoir level. Differences are primarily observed in fault illumination, which is slightly improved in the Big Island and Black Bayou surveys due to their relatively higher high-frequency content. Within the Vinton Dome area, the Vinton Dome radial 3D survey provides superior fault definition, and as a result, it was used for detailed structural mapping,

with results integrated into the regional interpretation. Based on this assessment, the Big Island and Black Bayou surveys were selected for regional horizon and fault mapping, while the Alligator Cove survey was used to extend coverage in the eastern portion of the study area where the other datasets are absent.

2. Structural framework familiarization: This stage also involves familiarization with the structural styles present in the area including fault geometry (strike and dip), vertical displacement, and the heave (horizontal displacement of geological horizons across faults), as well as other geological features such as the salt domes. The study area is dominated by extensional (normal) faulting, with no evidence of fault inversion to date. Fault displacement varies significantly, ranging from values close to the limit of seismic detectability to well-resolved offsets observable in the data (Figure 2.2.1-4).
3. Horizon continuity and stratigraphic characterization: The interpreter is also familiarized with the continuity and character of key stratigraphic intervals. The upper Frio Formation (Injection Zone and Lower Confining Zone) is generally characterized by laterally continuous reflectors, locally disrupted by normal faulting, and is not expected to present significant challenges for mapping. In contrast, the Anahuac Formation (Upper Confining Zone), representing an unconformity, is typically expressed as a trough and locally as a zero crossing. As is common for unconformities with variable underlying lithologies, this horizon is less straightforward to interpret and required careful picking.

Synthetic Seismogram Generation for Seismic-To-Well Tie

Wavelet estimation and seismic-to-well ties are fundamental components of the seismic interpretation workflow, providing the link between seismic reflections and subsurface stratigraphy and rock properties. Wavelet estimation is typically performed to enable seismic deconvolution, calibrate well logs to seismic data, and support inversion workflows. In this study, wavelets were primarily used for seismic calibration and quality assessment of the available datasets.

The seismic wavelet is generally not known and is commonly assumed to be broadband and zero phase, i.e., symmetric with a maximum amplitude at time zero. To improve robustness, two complementary approaches were applied for wavelet estimation: (1) a statistical method, derived directly from the seismic data, and (2) a deterministic method, based on well log data.

Wavelets were estimated at selected wells distributed across the study area. These were used to generate zero-offset synthetic seismograms, which form the basis for tying well data to seismic reflections and for correlating geological markers with seismic events across the different surveys.

Generation of synthetic seismograms required both a p-wave sonic (DT) and a density logs. In the study area, most wells were drilled for deeper targets, and density logs are often limited or absent within the interval of interest. To address this limitation, pseudo-density logs were generated for selected wells using the Gardner's equation (equation 2.2-5). See Table 2.2.1-1 and Figure 2.2.1-5 for Minerva's specific wells with seismic ties.

$$\rho = \alpha V p \beta \qquad \text{Equation 2.2-5}$$

Where ρ is bulk density in (g/cm3) Vp is P-wave sonic (ft/s), and α and β are empirical constants. Standard industry values of α= 1.74 and β = 0.25, were applied, resulting in:

$$\rho = 1.74 V p^{0.25} \qquad \text{Equation 2.2-6}$$

The use of Gardner-derived density logs is standard industry practice for synthetic seismogram generation. This approach primarily affects amplitude scaling and does not impact event timing or reflector positioning. Density estimated were used exclusively for synthetic construction and were not incorporated into velocity modeling or time-to-depth conversion, which were constrained by seismic velocities and calibrated with available well control. In intervals lacking density data, constant density values were also tested to validate the robustness of the seismic tie.

Although the number of wells with sonic data was limited, their spatial distribution provides adequate coverage to support reliable seismic calibration (Figure 2.2.1-5). All sonic logs were quality-controlled and conditioned, when necessary, all prior to being used in the synthetic generation process.

Calibration results indicate that the best seismic-to-well ties were achieved using the deterministic wavelets, with correlation coefficients of approximately 75% at reservoir level within a 600ms window. This level of correlation is consistent with accepted industry standards, where coefficients in the range of 70-80% are considered indicative of a good to strong seismic-to-well tie.

The seismic-to-well tie was used to define the polarity and onset character of key stratigraphic markers, Following the SEG polarity convention, where a peak represents an increase in acoustic impedance (+) and a trough a decrease (-), the principal markers are interpreted as follows:

- Upper Confining Zone: Trough (decrease in acoustic impedance), and in some areas a zero crossing (±),
- Injection Zone: Trough (decrease in acoustic impedance), and
- Lower Confining Zone: Trough (decrease in acoustic impedance).

Horizon Interpretation

Horizon interpretation was initiated at well locations where reliable seismic-to-well ties were established, providing the primary control (“ground truth”) for stratigraphic correlation. From these control points, horizons were propagated across the seismic datasets, with additional well ties incorporated as needed to reduce uncertainty in areas of lower data quality or increased structural complexity.

The three key horizons of interest (as defined above) were interpreted on a regular grid of every 8 inlines and crosslines across the full extent of the surveys. In areas of structural complexity, such as zones of dense faulting, or where seismic data quality is reduced, the interpretation grid was refined to a higher resolution (typically every 4 inlines and crosslines) to improve horizon continuity and accuracy.

Given the prevalence of normal faulting within the study area, horizon and fault interpretation were carried out iteratively in a cyclic workflow. Faults were interpreted in conjunction with horizon picking to ensure consistent correlation across fault blocks, including both footwall and hanging wall compartments. In areas with smaller-scale faulting, interpretation density was further increased locally to capture subtle displacements and maintain structural consistency.

Fault Interpretation (Including Fault Polygon Generation)

Fault interpretation was initially conducted on a regular grid of every 8 inlines and/or crosslines. To ensure adequate characterization of smaller-scale faults, interpretation density was increased to every 4 inlines and/or crosslines where required. In addition, random lines of varying orientations were used to better constrain fault geometry, vertical displacement, and kinematic relationships.

Interpretation of the fault framework within the dome area was performed in multiple stages. An initial mapping pass was carried out using the Big Island, Black Bayou and Alligator Cove merged 3D surveys to establish the regional structural framework. This was followed by a refinement stage using the Vinton Dome radial 3D survey, which provides improved imaging of complex fault geometries. This higher-resolution dataset enabled a more detailed characterization of the structural style, including counter-regional faulting, multiple peripheral fault sets, and a sub-seismic scale polygonal fault system distributed across the dome.

Polygonal fault systems similar to those observed in the Vinton Dome have been documented in other basins, including the Central North Sea and the Alberta Basin, and are commonly interpreted as the result of dewatering and compaction processes. The presence of comparable features in the Vinton Dome suggests a similar origin, potentially influenced by deformation associated with salt movement (Dewhurst et al., 1999; Haskell et al., 1999).

Creation of Structural Time Maps

The interpreted horizons were gridded in Petrel and constrained by the mapped fault framework to ensure structural consistency across fault blocks. In areas where seismic coverage was limited or data quality was insufficient, well top data were incorporated to guide the gridding process and maintain continuity of the interpreted surfaces. This integrated approach ensures that the resulting structural maps are consistent with both seismic interpretation and available well control.

Velocity Model Generation & Time-To-Depth Conversion

A layer-cake velocity model was constructed using interval velocities derived from stacking velocities of the Alligator Cove merged 3D survey, in combination with time-to-depth relationships (TDRs) established from seismic-to-well ties and interpreted horizons in two-way time (TWT). This approach assumes laterally consistent velocities within each stratigraphic layer, providing a simplified but effective framework for regional depth conversion.

The resulting velocity model was implemented in Petrel to perform depth conversion of the time-domain structural maps. Subsequent calibration was carried out at well locations to reduce uncertainty associated with resolution differences between well data and seismic data, ensuring improved consistency between seismic-derived depths and well control.

2.2.1.3 Petrophysical Workflow

The following outlines the steps taken in the initial petrophysical workflow focused on the upper Frio Formation (Injection Zone):

- Raw log data collated for the Project Minerva area
  - Digital logs and scanned raster images where available. Data collected from log header data to understand the well logging parameters.
  - Where only a scanned or paper image existed, the log data was digitized to enable petrophysical calculations.
  - Data loaded and organized into an interpretation software tool (Petrel)
- Log data quality checked and normalized/conditioned
  - Based on the regional understanding, baseline adjustments were used to calibrate the data. This is typically done using zones that are consistent, for example using a clean sand interval within the upper Frio Formation, or a shale baseline from the Anahuac Formation and/or mid Frio (Hackberry Trend). Data points and wells with results that were outliers were re-examined and discarded if not believed to be representative of the zone.
  - Issues such as log splicing identified and/or corrected; logs with poor data (e.g. run through casing) eliminated from the data set.
- Shale volume (Vshale) analysis was calculated primarily using SP logs, with Gamma Ray logs used where SP logs were unavailable. The SP curve was normalized and conditioned to account for depth-related variations and compaction trends. Reference intervals from blocky sands within the upper Frio Formation and shales of the Anahuac Formation were used to define clean sand and 100% shale baselines (Figure 2.2.1-6).

  The baseline shift was applied by:
  - Identifying clean sand and shale reference points, where clean sand corresponds to the maximum negative SP deflection and shales exhibit a near-zero response.
  - Adjusting for regional variations in formation water resistivity, compensating for mud-related baseline shifts associated with drilling fluid changes.
  - Correcting for anomalous readings caused by borehole conditions or tool calibration drift.

- The SP logs presented in the figures utilize a standard industry color gradient to illustrate variations in rock type based on SP values ranging from +50 mV to −150 mV. This gradient represents the transition from sand-dominated to shale-dominated intervals and is subdivided into four color bands corresponding to 0, −20, −40, and −150 mV. An SP value of −40 mV is applied as the lithology cutoff, with values less than −40 mV interpreted as higher-quality sand for facies classification purposes. The cross sections are displayed with a vertical exaggeration of 2.4, based on a horizontal scale of 12 feet per inch and a vertical (depth) scale of 5 feet per inch.
- Porosity and sonic logs were corrected for compaction effects. This is a standard approach using Wylie equation that applies a compaction correction factor (Cp), calculated as shale slowness divided by 100, when the shale slowness exceeds 100 µs/ft.
  - A compaction correction is applied to the interpreted sonic porosity in intervals where shale slowness exceeds 100 µs/ft and sonic porosity is used.
  - The purpose of this correction is to prevent unrealistically high porosity values in zones with uncompacted shales, where the sonic travel time is excessively slow.
  - The Cp value reduces porosity estimates, accordingly, ensuring more reliable porosity interpretation in these intervals.

Wylie Equation:

$$\phi = \frac{Dt - Dtma - Vcl \times (Dtcl - Dtma)}{(Dftl \times Sxo + Dthy \times (1 - Sxo) - Dtma) \times Cp}$$ Equation 2.2-7

Where:

Dt	Sonic input curve	*Dthy*	Sonic hydrocarbon
Dtma	Sonic matrix value	*Vcl*	Wet clay volume
Dtcl	Sonic clay value	*Sxo*	Flushed zone water saturation
Dtfl	Sonic filtrate value	*Cp*	Compaction factor

- Vshale used to correct porosity log
  - Vshale (Vsh) was primarily estimated from SP logs, with gamma ray logs used in intervals where SP was unavailable. This correction accounts for the porosity contribution of shale, which typically contains bound water and does not contribute to effective pore space (Figure 2.2.1-6).

The normalized SP value is defined as:

$$\mathrm{SP_{norm}} = \frac{\mathrm{SP_{log}} - \mathrm{SP_{shale}}}{\mathrm{SP_{sand}} - \mathrm{SP_{shale}}}$$ Equation 2.2-8

Where:

- SP_{log}= measured SP value
- SP_{sand}= maximum negative deflection (clean sand line)
- SP_{shale}= shale baseline (near-zero response)

and shale volume is estimated as:

$$V_{sh} = 1 - SP_{norm}$$ Equation 2.2-9

— Effective porosity (PHIE) generated across upper Frio Formation interval

- Incorporated into the facies classification, where High-Quality Sand (HQSand) was defined where SP < –40 mV and PHIE > 0.10, while lower-porosity values were assigned as Shaley Interbedded Facies. The 10% porosity cutoff and its associated permeability (~0.5mD) relationship were applied to distinguish net reservoir from non-net zones, providing a more reliable correlation between porosity and flow potential (Figure 2.2.1-7).
- A Net-to-Gross (NTG) property was also derived by assigning a value of 1 to cells with PHIE > 0.005 and 0 to those below. This approach captures low-permeability facies, such as Shaley Interbedded facies, which, though limited in flow capacity, can still influence pressure propagation within the AoR.
- Total porosity was calculated using sonic logs (DT) and then corrected for shale content to derive effective porosity (PHIE). The correction used the standard equation:

Sonic Log Correction for Effective Porosity:

$$PHIE = PHIT - Vsh * (Total\ porosity\ of\ clay\ fraction)$$ Equation 2.2-10

Where:

PHIT Total porosity from the sonic log and/or density log
Vsh Volume of shale

2.2.1.4 Geostatistical Model Workflow

To accurately represent the subsurface over the wider context, GCS has developed a regional mapping workflow. The steps of the workflow are as follows:

— The upper Frio Formation has been divided into 11 regionally correlated, geological sequences, Frio 0, Frio 0.5, Frio 1 through 9 (Figure 2.2.1-8 and Figure 2.2.1-9). The shallower upper Frio sandstones represent thicker more proximal depositional units in the NW of the mapping area, with these units thinning towards the SE across the main injection area. The deeper upper Frio sandstone layers thicken in the NW of the mapping area and extend across the AoR, transitioning into more shale-rich deposits toward the offshore SE portion of the basin. Table 2.2.1-2 summarizes the geologic sequences according to the name and depths of the geostatistical model and the

associated simulation layer and correlates the layers to the respective regulatory zones.

- Outputs from the seismic interpretation workflow in Section 2.2.1.2 (Seismic Interpretation Workflow) were integrated with well log data. Key outputs: depth-converted surfaces (middle Frio, upper Frio, and Anahuac Formations) and a fault model.
- A litho-facies scheme was created in wells that penetrate the upper Frio Formation and have log data. Two litho-facies types were interpreted in the upper Frio depositional system using a spontaneous potential log or calculated sonic porosity log: “High Quality Sandstone” units, generally displaying effective porosities greater than 10% and “Shaley-Interbedded” units that are generally more shale dominated with thin interbedded sands having less than 10% effective porosity (Figure 2.2.1-10).
- Effective porosity (PHIE) was calculated by using Vshale logs (calculated from spontaneous potential and/or gamma ray logs) to correct density, sonic and neutron porosity logs for shale content. The input to the modeling workflow is effective porosity (Figure 2.2.1-11).
- Using all the available data points along with facies proportion mapped trends (Figure 2.2.1-12), sequential and gaussian simulation is used to calculate facies (Figure 2.2.1-13) and porosity maps (Figure 2.2.1-14).
- Horizontal and vertical permeabilities are calculated from the porosity-permeability relationships identified in the core samples (Figure 2.2.1-15).

The porosity and permeabilities calculated represent the averages in the geostatistical model:

- Anahuac Formation (all lithologies) – 4.8% porosity, 0.18 millidarcies (mD) horizontal permeability, 0.0184 mD vertical permeability (porosity values from log calculation and permeability from core derived porosity to permeability transform)
- Upper Frio Formation (High Quality Sandstone) – 19.6% porosity, 392 mD horizontal permeability, 243 mD vertical permeability.
- Upper Frio Formation (Shaley Interbedded) – 1.9% porosity, 0.14 mD horizontal permeability, 0.014 mD vertical permeability.

To balance model size and maintain sufficient detail, properties from the geostatistical model were vertically upscaled from a fine grid (~ 3 ft average) to a coarser simulation grid (~24 ft average) (Table 2.2.1-3). This process preserves grid fidelity, structural integrity, and property relationships, ensuring consistency between the static and dynamic models. The resulting upscaled grid and property models form the basis of the reservoir simulation and maintain geological continuity throughout the workflow.

2.2.1.5 Reservoir Simulation Model Workflow

A comprehensive overview of the reservoir simulation model is set forth in a separate document, AoR and Corrective Action Plan (Attachment A). The following is a high-level summary of the full workflow and output.

The reservoir simulation model was used in two phases; the first was a regional, coarse-gridded study to find potential injection sites; and the second incorporating a refined grid around the chosen injection sites modeled the fine-scale behavior of the CO_2 and pressure plumes.

GCS began using a large-scale regional grid with coarse cells based on an interpretation of proprietary seismic and petrophysical data to find potential injection sites. The CO_2 plume exhibited an up-dip migration from buoyancy away from the injection site along higher permeability paths, so a combination of structure and permeability determined the direction and speed of dispersal. GCS sought to avoid areas such as the Vinton Dome, which might increase the risk to successful containment. The initial search tested eight separate injection sites. GCS discovered two Primary sites, now referred to as the North and South injection sites.

Over a series of simulations, GCS optimized the grid (extending it to ensure the best representation of the boundary conditions, centralizing it around the injection sites and added grids to represent the overlying Anahuac Formation. The simulation results were used to determine improvements to the geostatistical model in a combined active and continuous iteration workflow. The simulation results drove the development of the geostatistical model, and, in turn, the geostatistical model l drove the reservoir simulation model.

GCS decided to use two injection wells at each of the two sites to provide the project with sufficient injectivity and redundancy.

The choice of injection site was predicated on a set of constraints. The constraints are:

- Sufficient horizontal permeability to ensure injection pressures stayed well below fracturing pressure at the required injection rates.
- Injection depth greater than approximately 9,000 ft true vertical depth subsea (TVDSS) to ensure a large vertical distance between the injection point and the confining Anahuac Formation, and to utilize the high pressure to ensure efficient use of the storage volume.
- Sufficient distance between neighboring injection wells to avoid interference and hence reduced injectivity
- A fault stability analysis was conducted to determine fault reactivation risk, as part of the site selection process (see Section 2.3.3)
- That local dip directs the CO_2 plume away from areas which may compromise containment, such as the Black Bayou Dome

The reservoir simulation model uses a structured grid consisting of 125 hexahedral cells in the X-direction, 87 cells in the Y-direction, and 63 cells in the Z-direction. This results in a total of approximately 685,125 cells, of which 476,812 are active in the simulation domain.

The simulation software uses feet for grid dimensions and degrees Fahrenheit for temperature units.

The grid is 58,080 ft (approximately 11 miles) in the X-direction and 42,240 ft (approximately 8 miles) in the Y-direction. The grid cells are 500 x 500 ft in both X- and Y-directions across the entire model domain. Vertically, the cell thickness varies as a proportion of the mapped gross geological thickness for each zone divided by the number of grid layers in each zone. This approach preserves stratigraphic resolution while maintaining numerical stability for flow simulation (Table 2.2.1-4).

The model uses a uniform horizontal grid of 500 × 500 ft for simplicity and computational efficiency, while applying variable vertical layering to capture critical geological features. Vertical resolution is highest in the Injection Zone to accurately simulate CO_2 plume migration and pressure changes, and coarser in the confining zone where less detail is needed. This approach balances accuracy in key areas with overall computational efficiency.

The upper Frio Formation (Injection Zone) and Anahuac Formation (Upper Confining Zone) are modeled. The top of the Confining Zone is modeled using a pressure versus depth correlation, representing a constant pressure boundary. Infinite analytical aquifers are applied at the base of the deepest sands in the Injection Zone (to account for the behavior of the Lower Confining Zone). These infinite analytical aquifers are also applied along the edges of the model to account for the hypothetical lateral continuation of the Injection Zone. The area of review (AoR) is delineated using simulation outputs in combination with a depth grid of the lowermost USDW.

The trapping mechanisms are buoyant trapping of CO_2 against local and regional shales, capillary trapping of CO_2 and dissolution of CO_2 within reservoir brine. No communication with the USDW is evidenced in the reservoir simulation model.

The simulation time period was designed to capture the full operational and post-injection evolution of the storage system. Simulation timing is 475 years, which includes the 30-year operational period, the subsequent 50-year post-injection site care (PISC) period and an extended 395-year simulation horizon to evaluate the long-term stabilization of pressure and plume behavior.

The pressure front shrinks rapidly after injection ceases. Simulation results demonstrate rapid pressure relaxation in the target zones, as the pressure front successfully dissipates to sub-threshold levels within 6 months post-injection. GCS can demonstrate non-endangerment of the USDW during the 50-year PISC period; however, the CO_2 plume reaches “Near Steady-State” stability at 75 years and reaches “Numerical Steady-State” stability at 115 years. Stabilization logic can be found in Section 4.2 of the AoR and Corrective Action Plan (Attachment A).

2.2.2 Cross-Sections

The cross-sections for Project Minerva represent two-dimensional views of three-dimensional geological features below ground. The geological cross-sections are constructed from data collected from publicly available data sources and online databases. The cross-sections are centered north-south and west-east on the area of Project Minerva. The cross-sections fully illustrate the subsurface structural features below ground and are referenced to TVDSS. Subsurface structural features include faults, formation tops and estimated thicknesses, USDW, and zones of interest. Dashed lines are used when well data log coverage is insufficient, and formations are interpreted.

The following geological intervals are defined by the following:

- **Base of the Lowermost USDW**

  The base of the lowermost USDW was selected using the deep induction curve of an open-hole as described in Section 2.7.2 (USDW within the AoR).

- **Upper Confining Zone**

  The Upper Confining Zone is the Anahuac Formation of late Oligocene age. This stratigraphic unit is identified by an interval of consistent, uniform high frequencies in SP, GR, and resistivity well logs. The consistent high frequencies can be interpreted as dominantly shale-rich intervals containing minimal sand intervals, primarily at the base of the formation. The regional continuity of sand intervals is not clearly interpreted from well log data used.

  The top of the Confining Zone is identified as distinct by a sharp drop in well-log values and an increase in log variability (serrated log character); indicative of a regional unconformity related to a drop in sea level and a transition to a period of frequent transgression and regression.

- **Injection Zone**

  The Injection Zone is the upper Frio Formation of late Oligocene age. This stratigraphic unit is identified as an interval with frequent fluctuations between high and low values on SP, GR, and resistivity logs. Intervals of low resistivity, GR and SP are interpreted to be sand-rich units. The interval thickness is very variable and may be up to 100 ft thick or less than 5 ft. Intervals of higher resistivity, GR and SP are interpreted to be shale-rich units. Transition between sand-rich and shale-rich intervals may be sharp, creating blocky well log character, gradual, with fining or coarsening upwards trends, or a combination.

  The top of the Injection Zone is marked variably by a sharp or gradational increase in SP, GR and resistivity and a transition to more uniform well log character.

- **Lower Confining Zone**

  The Lower Confining Zone corresponds to the upper Frio Formation of late Oligocene age. It is defined by a laterally continuous shale interval at the base of the formation, located at the deepest sands of interest within the Minerva Project area.

Well logs (SP, GR, and resistivity) display consistent high-frequency responses, indicating a shale-dominated unit with minimal sand content, primarily near the middle of the interval. Regionally, sand bodies within this unit thin and terminate southeastward, with local thickening in the northwest. The zone's thickness is highly variable, ranging from less than 60 ft to about 140 ft.

The top of the Lower Confining Zone is marked by a sharp or gradational decrease in SP, GR, and resistivity, transitioning to a more uniform log character that reflects the onset of the confining shale interval.

Figure 2.1.2-1 shows the local cross-sections for Project Minerva, with Figure 2.1.2-2 showing north-southwest oriented cross-section that is approximately parallel to strike and Figure 2.1.2-3 showing west-east oriented cross-section that is approximately parallel to dip. All data logs used in cross-sectional Figures are provided in Appendix V.

2.2.2.1 North-Southwest Cross-Sections

Figure 2.1.2-2 provides a regional dip-line view through Project Minerva, from North (proximal/continental platform) to the Southwest (distal/Gulf of Mexico Basin):

- The Injection and Confining Zones are demonstrably regionally continuous from north to southwest across Project Minerva.
- Some variability in interval log character from up-dip (proximal) to downdip (distal) depositional areas – zones are typically thinner and more coarse-grained in the north and thicker, with high interpreted shale content in the south, towards the deeper water setting.

2.2.2.2 West-East Cross-Section

Figure 2.1.2-3 provides a regional strike-line view through the Project Minerva area, from West to East:

- The Injection and Confining Zones are demonstrably regionally continuous from west to east across Project Minerva.
- Relatively uniform log character in each defined interval along strike. Depositional environment interpreted to vary most strongly North-South.
- The upper Frio Formation thickens into the syncline structure at Project Minerva. Likely linked to accommodation space creation by syndepositional fault movement and early Jurassic salt movement beneath, creating bathymetric changes on the paleo sea floor. Sediment may also have been preferentially deposited or redeposited off surrounding highs to east and west.

2.2.3 Structure Maps

The structure maps displaying the elevation of the formations of interest for Project Minerva are provided as:

- Figure 2.2.3-1 Top of Anahuac Formation (Upper Confining Zone)

- Figure 2.2.3-2 Top of Upper Frio Formation (Injection Zone)
- Figure 2.2.3-3 Top of Upper Frio Shale Interval underlying deepest sand (Lower Confining Zone)

Faults, shear zones, unconformities, or any other geological features are illustrated on the structure maps. Dashed lines are used when well data log coverage is insufficient, and formations are interpreted. Structural interpretation of the formations and regulatory zones is described in Section 2.4.2 (Description of the Injection Zone and Confining Zone System).

All structure maps are constructed from data collected from all publicly available data sources and online databases. This data is the most up-to-date subsurface data available. Section 2.2.1.1 (Available Datasets) provides a detailed discussion of the data used to construct the structure maps, including boreholes, wells, and seismic data. Table 1.1-1 lists all wells and well data used to construct the maps. Table 1.1-1 includes, for each well, the operator's name, well name, well number, state serial number, total depth (TVD and MD if directional), and reference elevation.

2.2.4 Isopach Maps

The isopach maps for Project Minerva displaying the variation in thickness of the formations of interest for Project Minerva are provided as:

- Figure 2.2.4-1 Anahuac Formation (Upper Confining Zone)
- Figure 2.2.4-2 Upper Frio Formation (Injection Zone)
- Figure 2.2.4-3 Upper Frio Formation Shale Interval underlying deepest sand (Lower Confining Zone)

All faults, shear zones, unconformities, or any other geological features are illustrated on the structure maps. Dashed lines are used when well data log coverage is insufficient, and formations are interpreted. Discussion of the gross thickness and lateral continuity of the formations of interest and regulatory zones is provided in Section 2.4.2 (Description of the Injection Zone and Confining Zone System).

The isopach maps are constructed from data collected from all publicly available data sources and online databases. This data is the most up-to-date subsurface data available. Section 2.2.1.1 (Available Datasets) provides a detailed discussion of the data used to construct the isopach maps, including boreholes, wells, and seismic data. Table 1.1-1 lists all wells and well data used to construct the isopach maps, and includes the operator's name, well name, well number, state serial number, total depth (TVD and MD if directional), and reference elevation for each well.

2.3 FAULTS AND FRACTURES

2.3.1 Presence of Faults and Fractures

2.3.1.1 Sources of Data

The faults identified and interpreted throughout the area of Project Minerva on the 3D seismic datasets have been mapped and modeled with detail. The seismic horizons and faults were used to construct a structural framework within the geologic model.

Faults were initially interpreted in the time domain across multiple seismic surveys, ensuring a consistent structural framework. These fault sticks were then depth converted using the same multi-layered velocity model as the horizons, maintaining alignment between fault geometries and stratigraphic surfaces.

All 3D seismic data is represented in the following figures:

Figure 2.3.1-1	Figure 2.3.1-2	Figure 2.3.1-3	Figure 2.3.1-4	Figure 2.3.1-5
Figure 2.3.1-6	Figure 2.3.1-7	Figure 2.3.1-8	Figure 2.3.1-9	Figure 2.3.1-10
Figure 2.3.1-11	Figure 2.3.1-12	Figure 2.3.1-13	Figure 2.3.1-14	Figure 2.3.1-15
Figure 2.3.1-16	Figure 2.3.1-17	Figure 2.3.1-18	Figure 2.3.1-19	

Based on the detailed seismic mapping, the final depth-converted fault interpretations and horizon grids were incorporated into the static geomodel, ensuring that the complex fault network was accurately represented. This integrated approach preserved the structural integrity of the model, ensuring that fault geometries and stratigraphic relationships were accurately represented (Figure 2.3.1-20).

All structural features, including faults from the upper Frio Formation and Anahuac Formation, are provided in the following Figures:

- Figure 2.2.3-1 (Top of Anahuac Formation (Upper Confining Zone))
- Figure 2.2.3-2 (Top of upper Frio Formation (Injection Zone)), and
- Figure 2.2.3-3 (Top of upper Frio Formation shale interval (Lower Confining Zone)).

Any faults or fractures below seismic resolution in the Injection and Confining Zones will be identified and characterized using data collected during the Preoperational Logging and Testing Program (Attachment C). See Section 2.3.4 for a description of the data that will be acquired to address uncertainties in the current model.

Additionally, during injection, micro-seismic monitoring will be implemented in Minerva South In-Zone Well No. 001 (MS IZ 1). This data will be used to characterize any injection-related hydraulic stimulation of existing or new fractures. See Section 9.1, Testing and Monitoring Plan (Attachment D), for additional details.

2.3.1.2 Description of Faulting

Regional Faulting Summary

The dominant direction of the faulting is parallel to the edge of the Louisiana Gulf Coast. This is approximately 54° (+/-20°) at Project Minerva. The faulting is a result of deposition of large quantities of sand and mud along the margins of the Gulf of Mexico resulting in rapid sedimentation creating large growth fault systems near the downdip edge of each sediment wedge within the area of maximum deposition. This growth faulting and rapid subsidence of Cenozoic shelf margins in the northwest Gulf of Mexico is also related to large-scale, deep-seated gravity sliding of the continental slope (Swanson, Karlsen, & J, 2013). Decoupling of listic faults typically occurs along deeper intervals of Jurassic and Upper Cretaceous age shale- and salt-rich facies, significantly below the Project Minerva Injection Zone. (Swanson, Karlsen, & J, 2013) discusses deeper, thick Jurassic salt mobilized by the weight of the overburden into a series of ridges and troughs. Examples of this geologic process are the Black Bayou (salt) Dome and Vinton (salt) Dome.

Local Faulting Summary

All faults interpreted throughout the area of Project Minerva are normal faults—steeply dipping features that accommodate differential subsidence as thick sand and mud packages compact and shift. Figures 2.3.1-1 to 2.3.1-19 display the fault geometries mapped in 3D seismic data (see Section 2.3.1.1). These normal faults are characteristic of an extensional tectonic regime and are expressed on seismic data as relatively planar structures that bound downthrown blocks, creating accommodation space and thickened stratigraphy within the Frio Formation depocenters.

No surface representation of fault movement has been mapped in the project area by (USGS, 2024) and, consequently, all faults are determined to be inactive at the present day. According to (USGS, 2024), the gulf-margin normal faults in Louisiana are assigned as ‘Class B’ structures because of their low seismicity and because they may be decoupled from underlying crust making it unclear if they can generate significant seismic ruptures causing damaging ground motion.

Within the AoR, no growth or listric faults have been interpreted in 3D seismic data (see Section 2.3.1.1). Regionally, such faults typically flatten into detachments within overpressured shales or Jurassic salt. Figures 2.3.1-1 to 2.3.1-19 demonstrate that there are no listric faults that intersect the Lower Confining Zone, Injection Zone or Upper Confining Zone.

Radial faults associated with Black Bayou Dome, 2.4 miles east of Project Minerva, add complexity to structural architecture. Interpretation of the Black Bayou and Alligator Cove 3D seismic datasets shows that the salt-related deformation halo does not extend into the project area, and both the Injection Zone and Confining Zone remain structurally continuous between the dome margin and the AoR (Figure 2.3.1-21).

Radial faults adjacent to the dome are localized features and do not impact the Confining Zone. Fault permeability in these intervals is expected to be low due to clay smear and shale

gouge, consistent with Gulf Coast analogs where dome-related radial faults act as hydraulic seals (Anderson, R.E, Eargle, D.G, & Davis, B., 1973) (Anderson, R. E. 1973).

For a detailed discussion on seismic events associated with faulting, see Section 2.6 (Seismic History).

2.3.1.3 Description of Fractures

Fractures are not evident in available site data. Within the AoR, natural fractures may coincide with the three major faults identified in 3D seismic data (Figure 2.3.1-22). The AoR was designed to avoid the Black Bayou Salt Dome and any localized natural fractures associated with this structural feature.

Data will be acquired as part of the Preoperational Testing Program (Attachment C) to characterize any fractures present in the AoR. Additionally, the following monitoring data will be collected to characterize fractures, as part of the Testing and Monitoring Plan (Attachment D):

1. In-situ pressure and indirect CO_2 measurements will be collected at the in-zone monitoring well, MS IZ 1. This well will provide information about how pressure and CO_2 interact with Fault F02.
2. Multiple 4D seismic lines (multi-azimuthal walkaway vertical seismic profiles and 2D) will intersect all three AoR faults and provide information about CO_2 plume interaction with any fractures.

2.3.1.4 Summary of Mapped Faults and Fractures within the AOR

The faults mapped in the Project Minerva static geomodel were analyzed as part of the fault seal capacity study to better understand seal capacity and juxtaposition in the region. Information from this study was then applied to the AoR extent, focusing on the faults intersected by the CO_2 plume. Within the AoR, the plume intersects three faults. An additional three faults outside the AoR near the Black Bayou Dome were also included to provide additional control, given their potential influence on the CO_2 plume and AoR pressure.

These are normal faults and are generally moderately transmissive where sand-on-sand juxtaposition occurs. A fault transmissibility factor was applied to the AoR faults accordingly.

Figure 2.3.1-22 illustrates all the faults identified in Project Minerva, with the three AoR-related faults and three additional control faults highlighted for emphasis. These include Fault F01, Fault F02, Fault 3, Fault 11, Fault 13, and Fault F16.

No fractures are evident in current data. Presence of fractures will be verified upon collection and analysis of site-specific data.

2.3.2 Fault Sealing Capacity

2.3.2.1 Fault Juxtaposition and Caprock Integrity

Lateral fault seal can occur through two primary mechanisms:

1. **Juxtaposition** of porous, permeable reservoir rock against low-permeability or sealing lithologies.
2. **Development of fault rock** with sufficiently high capillary entry pressure to restrict fluid flow.

While Downey (1984) suggested that fault planes themselves may not inherently act as seals, they can juxtapose reservoir intervals against sealing units, thereby creating effective traps that impede fluid migration.

Fault Juxtaposition

In the Gulf Coast region, the Tertiary fault rock seals are utilized greatly for their outstanding trapping capabilities to prevent the upward migration of hydrocarbons. The sand and shales are very thick, and the juxtaposition of shale-to-shale or sand-to-shale beds across a fault form a vertical rock barrier (i.e., seal) for fluid flow due to their low-permeability (Downey, 1984).

In Project Minerva, fault juxtaposition mapping was performed using the 3D facies model (Figure 2.2.1-10), which distinguishes two lithofacies types: “High Quality Sandstone” and “Shaley-Interbedded” units. Results indicate that the Upper Frio faulting places Injection Zone sandstones against extensive interbedded shales and the overlying top seal (~750 ft thick). These shale–shale and shale–sand juxtapositions provide robust barriers to vertical fluid migration.

Model outputs illustrated in Figures 2.3.2-1 and 2.3.2-2 show:

- Shale-on-shale juxtapositions: ~60%
- Shale-on-sand juxtapositions: ~32%
- Sand-on-sand juxtapositions: ~8%

This distribution strongly supports the presence of effective vertical seals, with shale-to-shale contacts dominating along the fault planes.

Caprock Integrity

Faults within the Project Minerva are not expected to allow vertical fluid migration due to multiple internal shale layers and an overlying sealing Confining Zone. Although faults with low SGR and CSP may have moderate transmissibility, a thick sequence of low permeability Confining Zone rock further prevents upward flow acting as a sealing barrier. Instead, the high net-to-gross nature of the Injection Zone promotes horizontal flow across faults without acting as barriers to pressure or CO_2 plume migration.

The shales at Project Minerva are ductile at the depths of the intervals of interest, and the juxtaposition of shale beds or sand-to-shale beds across a fault form a vertical barrier (seal) to fluid flow, due to their very low vertical permeability. This property of viscoelastic deformation behavior will cause any fractures and faults to close very rapidly in response to the in-situ compressive stresses, like squeezing into the fault plane from both sides. This well-known ductile, or plastic, behavior of the Gulf Coast shales is demonstrated by the presence of shale diapir structures and the natural closure of uncased boreholes with time

(Gray, Darley, & Rogers, 1980; Johnston & Greene, 1979; Warner, 1988; Warner & Syed, 1986).

An example of a worse-case scenario presented to the EPA is in 1991, the E.I. Du Pont de Nemours and Company (DuPont) Sabine River Works Plant, located approximately 3 miles west of Project Minerva, conducted a borehole closure test demonstrating that the plastic nature of the Gulf Coast shales and the rapidity of shale movement can seal off openings in the subsurface. The test demonstrates that the Miocene shales of the Gulf Coast will flow and seal off an open area in the subsurface relatively quickly. The test duration was one-week, during which time the formation pressure achieved equilibrium. The conclusive evidence resulted in, even under worse-case scenario, no fluid flow migrates, and the borehole closes naturally (Clark, Papadeas, Sparks, & McGowen, 1991).

The vertical sealing nature of shale-to-shale or sand-to-shale juxtaposed lithologies across the Gulf Coast region having fault traps where both the top and the lateral seals are provided by shale beds (Figure 2.3.2-3). Due to the very plastic nature, the natural sealing capabilities, and the potential deformation of shales faults can seal based on the juxtaposition of like and unlike lithology across the fault plane. The deeper underlying geologic sequence of predominately shales provide extensive shale-to-shale contacts along the fault plane which will prevent CO_2 migration from the Injection Zone.

2.3.2.2 Lithology and Fault Gouge Composition

Fault sealing capacity within the Injection Zone (upper Frio Formation), the Lower Confining Zone (upper Frio Formation), and the overlying Confining Zone (Anahuac Formation) is primarily controlled by lithology. Their high shale content present in both zones generally causes faults to act as barriers or baffles to fluid flow rather than conduits. Model analysis indicates that cross-fault flow is only possible when:

1. Sand content is high (high net-to-gross)
2. Sand bodies are directly juxtaposed (sand-on-sand)

Low-displacement faults, where offset is less than formation thickness, may permit limited horizontal flow under these conditions.

Fault seal analysis was conducted on faults using Shale Gouge Ratio (Yielding, 2002) and Clay Smear Potential (Lehner, 1997) (CSP; Lehner & Pilaar, 1997), derived from the VShale property (Figure 2.3.2-4) in the 3D geomodel.

$$SGR = \left(\frac{\Sigma \, (V_{shale} \text{ x T})}{\text{Total Throw}} \right) \text{x } 100 \qquad \text{Equation 2.3-1}$$

Where:

V_{shale}	Volume fraction of shale in each stratigraphic unit
T	Thickness of each unit
Total Throw	Total fault displacement

$$CSP = \frac{t_{sh}^2}{d} \qquad \text{Equation 2.3-2}$$

Where:

t_{sh} Thickness of the source shale bed

d Smear distance, typically the fault throw or displacement

The SGR and CSP calculations provide insight into the fault seal behavior for the following juxtaposition scenarios:

- Shale-on-shale: Very high SGR (81%) and CSP (91%), negligible permeability, and zero transmissibility. These contacts represent excellent vertical seals.
- Sand-on-shale: High SGR (69%) and CSP (91%), with negligible permeability and zero transmissibility. Strong sealing behavior prevents fault-related flow.
- Sand-on-sand: Lower SGR (39%) and CSP (53%), with higher estimated fault permeability (129 mD) and transmissibility (1.08). These intervals represent localized zones of potential lateral flow.

Results show SGR values in shale-to-shale or sand-to-shale consistently (> 60 %) and CSP values (> 90 %) (Figure 2.3.2-5), both of which exceed commonly accepted thresholds for effective sealing (Lindsay, 1993). These findings indicate that faults within Project Minerva are not likely to permit vertical fluid migration.

Although sand-on-sand contacts show reduced sealing capacity, their limited extent (8%) (Figure 2.3.2-1) and the dominance of shale–shale and shale–sand contacts confirm that overall sealing behavior is strong (Table 2.3.2-1).

2.3.2.3 Fault Plane Transmissibility Assessment

Fault planes significantly influence fluid migration depending on depth, stress regime, and fault zone properties. For example, shallow near-surface faults in tensional settings often behave as transmissive features (Secor Jr., 1965), whereas deeper faults in compressional regimes can act as either barriers or conduits depending on sealing capacity (Sibson, 2000).

In CCUS applications, where long-term CO_2 containment is critical, fault zones must be evaluated through a two-tiered fault seal analysis:

- **First-order analysis:** identification of reservoir juxtaposition across fault surfaces using structural mapping.
- **Second-order analysis:** evaluation of whether juxtaposed contacts can sustain pressure differences, considering fault zone properties such as clay smear potential, shale gouge ratio (SGR), and diagenetic modification.

In the static geomodel, the following fault sealing mechanisms are recognized:

- **Juxtaposition Seal**

  When a permeable reservoir is faulted against a sealing lithology (e.g., shale or evaporite), the fault acts as a lateral barrier to flow. This first-order control on fault seal potential is assessed in our model through facies juxtaposition mapping (Figure 2.3.2-6).

— **Fault Rock Seal (Capillary Seal)**

Fault movement may create low-permeability rocks such as gouge, smear, or cataclasite. These fault rocks exhibit high capillary entry pressures that restrict cross-fault flow, particularly in cases where reservoir is juxtaposed against reservoir (Figure 2.3.2-7).

— **Clay Smear and Shale Gouge**

In interbedded sand–shale successions, clay smear or shale gouge can form continuous sealing layers along the fault plane. The Shale Gouge Ratio (SGR) quantifies this effect, with values >20–30% typically associated with effective seals.

Our sand-sand model indicates an SGR of 39%, classifying the fault zone as a *phyllosilicate-frame rock seal* (Zhu, 2016):

- Cataclastic rock seal: <15% shale/phyllosilicate
- Phyllosilicate-frame rock seal: 15–40%
- Clay smear seal: >40%

With 39% SGR and 53% CSP, the fault zone likely exhibits phyllosilicate-frame sealing behavior, significantly reducing lateral transmissibility and strengthening caprock integrity for CO_2 storage.

— **Cementation and Diagenesis**

Over geological time, mineral precipitation (e.g., calcite, quartz) within fault zones may reduce permeability, enhance sealing capacity, or eliminate porosity entirely, forming an effective hydraulic seal (Knipe, 1989; Nicol et al., 2016).

Based on these established fault sealing mechanisms, the following indicators are used to assess whether faults are likely to be laterally sealing or transmissive. These indicators collectively provide a diagnostic framework for predicting fault behavior in CO_2 storage scenarios, supporting the identification of laterally transmissive versus sealed fault zones within the AoR at Project Minerva (Table 2.3.2-2).

- **Clay Smear Potential:** In faulted sections where shale beds constitute ≥25% of the stratigraphy (Yielding, 2002), clay or shale can be smeared along the fault plane during fault growth. This smear can significantly impede lateral fluid flow. In our model, the CSP of 91% suggests the fault rock is largely impermeable, indicating strong sealing potential.
- **Sand–Shale Juxtaposition:** Faults are likely to be laterally sealing when the injection interval (sandstone) is juxtaposed against low-permeability layers such as clay or shale. Our SGR of 69% for sand-on-shale zones supports effective sealing behavior, consistent with phyllosilicate-frame fault rock classification (Zhu & Gong, 2016).

- **Sand–Sand Juxtaposition:** Faults may be laterally transmissive where sandstone intervals are juxtaposed against other sandstones, especially in the absence of interbedded shale (Knipe, 1997; Smith, 1966; Nicol et al., 2016). In our model, sand-on-sand zones with an SGR of 39% may exhibit partial or limited sealing, depending on fault rock development and stress conditions.

Transmissibility Multiplier

Fault permeability was estimated using Fault Clay Prediction (Shale Gouge Ratio, SGR) and calculated following the methodology of (Sperrevik, 2002), incorporating an estimated depth at deformation ~3,280 ft (~1000 m) and maximum reservoir burial ~9,843 ft (~3000 m).

The Sperrevik Equation:

$$k_f = a((SGR)^b)(Depth)^c \qquad \text{Equation 2.3-3}$$

Where:

k_f	fault rock permeability (mD)
SGR	Shale Gouge Ratio (fraction of shale)
Depth	Maximum burial depth (m) or depth at deformation,
a	Empirical scaling factor. Sets the base permeability
b	Exponent controlling the influence of SGR on fault permeability.
c	Exponent controlling the influence of depth on fault permeability

The transmissibility multiplier (TM) was then derived by integrating the calculated fault permeability with fault rock thickness and the 3D permeability model from the geomodel. The resulting average transmissibility multiplier was applied across the model.

These transmissibility values were applied in the AoR simulation model to assess the effect of faults on fluid movement. The indication of the fluid flow observed is summarized here:

- Sand-on-sand juxtaposition shows moderate sealing, with low SGR and clay smear values, resulting in higher fault permeability and effective cross-fault permeability (ECFP). The average transmissibility multiplier of ~0.48 indicates partial sealing with significant leakage potential (Table 2.3.2-1).
- Sand-on-shale juxtaposition shows strong sealing, with high SGR and clay smear and negligible cross-fault flow, acting as an effective barrier (Table 2.3.2-1).
- Shale-on-shale juxtaposition represents the most sealed condition, with very high SGR, minimal fault permeability, and no effective cross-fault transmissibility (ECFT) (Table 2.3.2-1).

The Upper Confining Zone (Anahuac Formation) and Lower Confining Zone (upper Frio Formation) show no transmissibility due to its high shale content. This ensures containment and prevents upward and downward migration of CO_2 from the Injection Zone. In contrast, transmissibility within the Injection zone (Upper Frio Formation) varies because of interbedded sands and shales. Thicker, more porous sands show higher transmissibility,

while thinner or shalier intervals show lower values, averaging ~0.48 overall. Shale layers act as vertical flow barriers that compartmentalize and control CO_2 movement, while high net-to-gross sand intervals with low SGR and higher fault permeability display lower sealing capacity and enable lateral fluid migration across faults (Table 2.3.2-3).

Impact of Fault Transmissibility on AoR Delineation

The simulation model evaluated the effect of fault transmissibility on CO_2 plume and pressure behavior within the AoR for the applied transmissibility multiplier (TM = 0.48) and compared with the Project Minerva sensitivity cases provided in Section 5.1.2 (Discussion of Sensitivity Analyses) of AoR and Corrective Action Plan (Attachment A).

In the TM = 0 case (fully sealing faults), the pressure front expands significantly, and the CO_2 plume shows increased lateral spread due to compartmentalization and pressure buildup.

In the TM = 1 case (fully open faults), the pressure front is smaller and dissipates more efficiently, and the plume distributes uniformly across the compartment.

The applied TM = 0.48 produces behavior similar to the TM = 1 case, indicating that sand-on-sand juxtapositions remain transmissive. Under this scenario, the pressure front is reduced and the CO_2 plume extends broadly within the Injection Zone.

Across all transmissibility scenarios, the dominant migration direction for both pressure and CO_2 remain consistently up-dip to the west, demonstrating that regional reservoir structure, not fault behavior controls overall flow dynamics. (Figure 2.3.2-8).

2.3.3 Fault Stability Analysis

2.3.3.1 Overview of the Fault Slip Potential Tool

A fault slip potential study was carried out using the Fault Slip Potential (FSP) tool. The FSP tool is an open-source tool to screen existing faults in contact with a reservoir undergoing a change in pore-pressure (ΔPp), providing a quick and cost-effective method for assessing uncertainty based on relative influence of key factors (Walsh, et al., 2016-2018). Originally developed by ExxonMobil and the Stanford Center for Induced and Triggered Seismicity, it is now overseen by the University of Texas Bureau of Economic Geology and Center for Injection and Seismicity Research.

The FSP tool quantifies the potential for pore fluids inducing fault slip via Morh-Coulomb unclamping and addresses uncertainty by using Quantitative Risk Assessment (QRA) to evaluate the possibility of fault slip, adopting a Monte-Carlo method to evaluate the probability of an uncertain outcome. The resulting output is a Cumulative Distribution Function (CDF) describing the cumulative probability of fault slip as a function of pore pressure added to the fault.

The purpose of the tool is to screen and highlight faults that may need additional study and attention in future work; it cannot predict the probability of a felt earthquake being produced by injection activity or fault slip. The probabilistic values output by the tool, and discussed in this section, represent the chance of a fault experiencing a change in pressure that would

be required to reactive at fault, the values do not represent the direct probability that a fault will reactivate.

Appendix VI provides a full overview of the complete Fault Slip Potential study along with all model outputs.

FSP Data Inputs

Before utilizing the FSP tool, faults within the AoR must be identified. Three faults intersect the AoR and were included in the FSP study: Fault F02, Fault 3, and Fault 13 (Figure 2.3.3-1).

Data pertaining to fault geometries and change in pore-pressure (ΔPp) must be extracted, transformed to be compatible with the FSP tool, and then loaded for analysis. ΔPp data is sourced directly from the simulation model output and then uploaded into the static geomodel to be spatially tied to fault geometries. It is at this point data pertaining to the fault geometries, including reference depth, fault strike angle, fault dip angle, and X/Y coordinates are also sourced. Over 3,500 data points in total were utilized across the three faults included in the FSP study.

A series of python scripts are used to format the data to be compatible with the FSP tool standards. Faults are divided into fault segments based on similar fault geometries and spatial characteristics to more accurately represent the faults in the tool (Figure 2.3.3-2). Each fault segment is assigned a unique fault strike angle, fault dip angle, length (km), and centroid X/Y coordinates (Table 2.3.3-1).

To best represent fault segment geometry, strike and dip angles are averaged across all data points associated with a given fault segment. As each fault segment requires unique fault strike and fault dip values, averaging segment specific values based on similar fault geometries provides the most representative input for the FSP tool. Additionally, the FSP tool uses a probabilistic Monte-Carlo simulation which deploys repeated random sampling to model the probability of different outcomes in a complex system. These Monte-Carlo based iterations are designed to address uncertainty in variables, including fault strike and dip, and highlight high risk areas.

A hydrologic model was developed using ΔPp data derived from the simulation model and formatted as an input for the FSP tool to specify the ΔPp at each fault segment across all modeled timesteps (Table 2.3.3-2). Although the current version of the tool (FSP 2.0) does not have capability to consider poroelastic stress changes if utilizing the built-in hydrologic model, the custom simulation model derived hydrologic model utilized in this study adequately captures these changes. As a conservative approach, each fault segment was assigned the absolute maximum ΔPp value at each modeled timestep to document the largest possible impact of reservoir pressure on fault planes.

The FSP tool requires a singular reference depth value to be specified for an entire fault and is not capable of dynamically referencing depth for each fault segment, meaning all fault segments associated with a given fault will use the same depth value. Depth data was sourced directly from the static Geomodel and averaged across all data points associated with a fault. This provides the most representative depth value possible given the

constraints of the tool. The following reference depth values were used for the faults analyzed in this study:

- Fault F02: 9,556 ft
- Fault 3: 9,758 ft
- Fault 13: 8,835 ft

Regional Stress Field Characterization

Regional stress is modeled in the FSP tool using a series of specified variables. This section discusses the variables, specific values, and ranges of uncertainty used.

Maximum Horizontal Stress Direction (54.1° ± 20°)

In the absence of site-specific data, a series of regional published literature values were used to understand principal stress orientations. (Trevino & Meckel, 2017) calculated the average fault strike for 297 faults or fault segments to be 54.1° and aligns with values found by (Zoback & Zoback, 1980). A conservative uncertainty range of ± 20° was applied to capture a wide range of possible values. This value range is consistent with the fault orientations mapped in 3D seismic data at Project Minerva.

Pressure Gradient (0.458 psi/ft ± 0.02 psi/ft)

The most-likely value derived from the base case of the simulation model as described in Section 1.6.3 (Initial Pressure Gradient) of the AoR and Corrective Action Plan (Attachment A).

Friction Coefficient (0.72 ± 0.10)

Based on the midpoint of value ranges documented in published literature:

- (Engelder, 1974): 0.68-0.72
- (Byerlee, 1978): 0.6-0.85
- (Trevino & Meckel, 2017): 0.6

An uncertainty range of ± 0.10 was used to capture the full range of published values.

Vertical Stress Gradient (1.0 psi/ft ± 0.1 psi/ft)

Based on ranges documented in published literature:

- (Nicholson, 2012): 1.0 psi/ft
- (Trevino & Meckel, 2017): 1.0 psi/ft
- (Ramos, Katahara, Keck, & Batzle, 1994): 0.9 psi/ft
- (Eaton, 1969) predicts approximately 0.93 to 0.95 psi/ft for Gulf Coast strata at Project Minerva depths

Given the ranges, estimated error in the total vertical stress gradient to be approximately ± 0.1 psi/ft.

A-Phi Parameter (0.6 ± 0.05)

Based on published literature from (Simpson, 1997) (Table 2.3.3-3) and spatial data obtained from (Lundstern & Zoback, 2020).

Fault Strike Angle and Fault Dip Angle (Values Vary ± 5°)

The fault dip, dip direction and strike are computed directly from the modeled fault surfaces in the 3D structural framework, ensuring that these outputs represent the true geometric properties of each fault plane. The extracted dip-direction data show consistent orientations along each surface (Table 2.3.3-4); therefore, averaging dip values within each fault segment provides the most representative input for the FSP Tool. Where minor changes in dip orientation occur, they are captured as discrete fault segments (Figure 2.3.3-2), and the segment-level averaged dips incorporate these variations appropriately.

The uncertainty analysis within the AoR shows variability consistently below ±5°, and dip angle variations across individual fault segments remain small. Specifically, the uncertainty ranges are:

- Fault F02 (Segments 1–6): ±1.31° to ±4.46°
- Fault 13 (Segments 1–5): ±0.18° to ±1.21°
- Fault 3 (Segments 1–3): ±0.47° to ±1.45°

Averaging the dip does not mask potential high-risk areas because the Project Minerva 3D geomodel shows uniformly low-angle dips across the region. These narrow uncertainty ranges demonstrate that dip measurements are consistent and do not display the variability typically associated with elevated slip or leakage risk. Additionally, structural gradients within the AoR range from approximately 3° to 9°, corroborating that the structural setting is overall low-relief (Figure 2.3.3-3). Together, these observations justify the averaging approach and confirm that no steeply dipping fault zones are present within the modeled area.

An uncertainty range of ± 5° captures the full range of fault strike and fault dip angle values associated with each fault segment.

2.3.3.2 FSP Methodology

After loading the fault geometry and hydrologic data into the FSP tool, and specifying all input variables along with uncertainty ranges, the tool works through three modules to analyze slip potential:

- **Deterministic Geomechanics Module:** A singular geomechanical model of stress and pore-pressure conditions to allow for a basic exploration of the model without Monte-Carlo iteration. A singular Mohr-Coulomb ΔPp required to slip is calculated for each fault segment (Table 2.3.3-5) but contains large uncertainties often present in relevant geomechanical parameters. The singular value is a product of fault geometry data, hydrologic model data, and stress variable inputs.

- **Probabilistic Geomechanics Module:** A similar model to the deterministic geomechanics module, except as a Monte-Carlo simulation iterating through ranges of scenarios allowing uncertainties in each input parameter to be sampled randomly. The Monte-Carlo approach propagates the relevant uncertainties through the model, producing a distribution of ΔPp values required to slip for each fault segment.
- **Integrated Fault Slip Potential Simulation Model:** A combination of the results of the probabilistic geomechanics module with the hydrologic (ΔPp) model derived from the simulation model, providing an FSP value for each fault segment at every modeled timestep. The calculated FSP value represents the probability of a fault segment experiencing ΔPp that would be needed to cause slip, after accounting for all uncertainties, it does not represent the direct probability that a fault will reactivate.

2.3.3.3 Results of FSP Analysis

Key findings are discussed in this section based on the deterministic, probabilistic and integrated module results. A full presentation of FSP results and model outputs can be found in Appendix VI – Fault Slip. Table 2.3.3-6 documents the calculated FSP values for all fault segments at every modeled timestep and Figure 2.3.3-4 plots these values over time.

While there is no standardized framework to interpret FSP values, Table 2.3.3-7 presents a general risk-matrix compiled from various literature sources to help provide context to the FSP values discussed in this section (Walsh & Zoback, 2016; Hennings et al., 2019; Hennings et al., 2021; Dvory & Zoback, 2025).

Deterministic Geomechanics Module

- Across all faults, the lowest ΔPp to slip (227 psi) is observed in the eastern-most segment of Fault 13 (Segment #5). The maximum ΔPp applied to Fault 13 Segment #5 is 65 psi.
- The lowest ΔPp to slip in Fault F02 (420 psi) is observed in the eastern-most fault segment (Segment #1), and 276 psi in the central fault segment of Fault 3 (Segment #2). The maximum pressure observed across the entire hydrologic model is 110 psi.
- This shows that no fault segments are predicted to experience ΔPp required to slip at any point of the project

Probabilistic and Integrated Geomechanics Modules

- The highest FSP value recorded was 15% in the eastern-most segment of Fault 13 (Segment #5) at year 30 (end of injection).
- The second highest FSP value recorded was 10% in the central segment of Fault 3 (Segment #2) at year 20.
- All other fault segments, including all segments in Fault F02, have FSP values ≤ 5% throughout the entire life of the project.

Range of Uncertainty and Future Considerations

- The FSP values documented in this analysis are intended to be used as a screening tool to identify areas of additional study using site-specific data.
- The highest uncertainty emerges from the maximum horizontal stress direction, fault strike angle, and fault dip angle.
- Pre-operational data acquisition will focus on refining geomechanical analysis including structural and stratigraphic features (formation dip, faults, and fractures, if any), and core analyses focused on rock strength, ductility, and principal stresses.

Based on these key findings, the overall probability of fault slip throughout the life of Project Minerva is low, with most fault segments having a FSP value ≤ 5%.

2.3.4 Addressing Uncertainties

GCS will address the uncertainties associated with the faults and fractures within the AoR and the impact on modeled reservoir performance by implementing the baseline geomechanical and reservoir testing proposed in Pre-Operational Testing Plan (Attachment C) and monitoring activities outlined in the Testing and Monitoring Plan (Attachment D).

2.3.4.1 Pre-Operational Testing

The Pre-Operational Testing Plan (Attachment C) outlines how GCS plans to verify the geologic characteristics of the Injection Zone as required by C&E (LAC 43:XVII §3617.B.5). The following section outlines how analyses and testing recommended in the Pre-Operational Testing Plan can address geomechanical and reservoir uncertainties prior to operation of the proposed injection wells.

Logging

Section 2.2.1 (Open Hole Logging and Testing Plan) of the Pre-Operational Testing Plan outlines the open hole logging that will be conducted from the Confining and Injection Zones. The following logs provide essential information that helps mitigate fault uncertainties through comprehensive analysis of borehole geometry, stress distributions, and structural features.

- Caliper log measures borehole diameter and is used to assess the shape of the borehole. The data from caliper log is used for geo-mechanical analysis and determination of maximum and minimum horizontal stress.
- Borehole Image log provides an acoustic image or resistivity image of the borehole based on sonic waves or resistivity measured from multiple caliper arms and/or pads. Resistivity based image is more applicable with conductive drilling fluid, while the acoustic image is preferred in oil-based mud. The information from the borehole images is analyzed to assess stratigraphic and structural features including but not limited to structural dips, presence and orientation of faults and/or fractures, and formation stress.

- Acoustic (compressional and shear) log provides a measure of rock strength and brittleness. Elastic properties are determined for geomechanical analysis. Provides a stress analysis and determines if the rock is fractured.

Core sampling and analyses

Section 2.3.3 (Core Analyses) of the Pre-Operational Testing Plan outlines the geo-mechanical analyses that will be performed on the whole cores collected from the Confining and Injection Zones. These analyses will allow GCS to determine the stress orientation, fault geometry, rock strength and elastic properties, and fracture network.

- Stress Orientation
  - Identifying the maximum horizontal stress direction helps predict how injected CO_2 might propagate.
  - Breakouts and drilling-induced tensile fractures (DITFs) in core or image logs reveal stress anisotropy, guiding GCS on the safe storage of CO_2 in the Injection Zone.
- Fault and Fracture Geometry
  - Core-scale fault gouge and microfractures will indicate proximity to faults and their mechanical behavior.
  - Mineralized veins or healed fractures can show past fluid migration, hinting at fault permeability.
- Rock Strength & Elastic Properties
  - Lab tests on core samples (triaxial compression, tensile strength) can help model fracture propagation and fault slip potential under injection scenarios.
- Fracture Networks
  - Mapping natural fractures will help assess fluid pathways and seal integrity.

Reservoir Tests

The reservoir tests described in Section 2.6 (Hydrogeologic Testing) of the Pre-Operational Testing Plan will measure transmissibility, skin effects due to well construction and near borehole effect, injectivity of the formation, injection flowing and static pressures of the formation, and determine Maximum Surface Injection Pressures (MSIP) for the wells. These tests will provide a baseline for well and reservoir performance over time; specifically, the proposed pressure fall-off and injectivity tests, which can provide insights into the impact of local faults on the proposed reservoir.

Pressure Fall-Off Test

Pressure fall-off tests are conducted to monitor how pressure declines over time after injection stops. GCS will perform a baseline test described in Section 2.6.2 (Pressure Fall-Off Test) of the Pre-Operational Testing Plan to establish the rate and pattern of pressure decline in the reservoir. This data can indicate reservoir boundaries, barriers, or

connectivity. The test can also suggest if fluid is escaping through a fault, or if the fault is acting as seal, trapping pressure within the Injection Zone. They can also identify if the fault behaves as a no-flow boundary or a transmissive feature.

Injectivity Tests

Injectivity test access how easily fluids can be injected into a formation. GCS will use the baseline test described in Section 2.6.3 (Step Rate Injectivity Test) of the Pre-Operational Testing Plan to demonstrate the reservoir permeability, as well as to assess if anomalous injectivity behavior is attributed to fluid migration along a fault or facture.

2.3.4.2 Additional Testing and Monitoring

The Testing and Monitoring Plan (Attachment D) commits GCS to perform regular monitoring of the faults over the lifetime of the project. The proposed monitoring program is described in Section 10 (Fault Characterization and Monitoring) and provides a comprehensive description of the tests and surveys that will further characterize the faults and monitor fault-stability during injection operations.

Reservoir Testing

After injection commences, a pressure fall-off test will be performed at least once every 5 years during the operational period as required by LAC 43.XVII §3625.A.6. Pressure fall-off tests monitor how pressure declines over time after injection stops. The rate and pattern of pressure decline can indicate reservoir boundaries, barriers, or connectivity. Along with monitoring the operational health of the injection interval, the test can determine if fluid is escaping through a fault, or if the fault is acting as a seal, trapping pressure within the Injection Zone. The test will also indicate if the fault behaves as a no-flow boundary or a transmissive feature.

Seismic Surveillance

GCS will employ advanced microseismic surveying and seismic monitoring techniques to assess and manage fault activity associated with Project Minerva. By establishing a comprehensive baseline through initial microseismic surveys and subsequently monitoring any induced seismicity during the injection phase, GCS aims to detect pre-existing faults or fractures and understand natural seismicity patterns. These combined efforts will facilitate informed decision-making and proactive risk management throughout the life of the CCS project.

Microseismic Surveying

GCS will conduct microseismic surveys prior to injection to establish a baseline for natural seismic activity. Once injection commences, GCS will continue to collect data to monitor for evidence of induced seismicity due to CO_2 injection. GCS will utilize distributed acoustic sensing (DAS) technology installed on MS CCS 1 and downhole geophones and/or accelerometers installed strategically at various depths within an offset monitoring well, Minerva South In-Zone Well No. 001 (MS IZ 1).

In-direct Seismic Monitoring

GCS will employ seismic technologies, such as Vertical Seismic Profiling (VSP), Walk Away VSP, and 2D seismic surveys, to monitor plume movement throughout the Injection Zone. VSP and 2D seismic surveys will be performed as a baseline examination to acquire high-resolution images of the subsurface structures, including faults. This data will be used to validate the dip and strike angles interpreted from existing 3D seismic data. This detailed imaging allows for the identification and characterization of fault lines before and during CO_2 injection.

Walk-Away VSP and 2D seismic surveys will be performed during the injection phase. By creating a profile of the subsurface using seismic wave data collected along a linear survey line, GCS will gather valuable insights into the broader geological framework, including regional fault systems and sedimentary structures afield from the injection site. Collecting surveys before and after CCS activities allow for the assessment of any alterations or deformations in the fault structure, ensuring proactive management of potential risks.

2.4 INJECTION ZONE AND CONFINING ZONE SYSTEM DETAILS

The Injection Zone is defined as the zone capable of accepting fluids and of sufficient areal extent, thickness, porosity, and permeability to receive carbon dioxide through a well(s). Additionally, an adequate Injection Zone must be confined by formations that prevent the migration of fluids from the zone.

A sufficient Confining Zone System must provide upper and lower containment of the Injection Zone. The Confining Zone System consists of the Lower Confining Zone and Upper Confining Zone.

Figure 2.4.1-1 illustrates a cross-section of the geostatistical model layers intersecting MS CCS 1 and MS CCS 2 and identifies the regulatory zones, the respective proposed depths, and the associated formations. Table 2.2.1-2 summarizes the information presented in Figure 2.4.1-1 by correlating the regulatory zones to the geostatistical model formation top depths and the simulation layers.

2.4.1 Geologic Summary

At Project Minerva, the regional and local geology demonstrates ideal geologic conditions for CO_2 injection and storage. The massive, fluvial-deltaic sandstones of the upper Frio Formation offer effective injection reservoirs in terms of the lateral extent, mineralogical composition, and petrophysical characteristics of the formation. This formation has the permeability, porosity, thickness, and lateral continuity to serve as the Injection Zone.

The Anahuac Formation will serve as Upper Confining Zone and will provide an effective barrier to prevent upward fluid migration from the proposed Injection Zone. The Lower Confining Zone consists of a shale interval underlying the deepest sand of the upper Frio Formation. These layers are thick, impermeable, and have lateral continuity to confine the injected fluids in the Injection Zone. The Upper and Lower Confining Zones are regionally extensive and are significantly less permeable than the Injection Zone, as demonstrated in the following sections.

Between the lowermost USDW and the Upper Confining Zone, there are nearly 5,000 ft of interbedded sand-shale layers within the Miocene formation that provide an additional level of safety as a containment interval. This interval could capture and retain any fluids that might migrate vertically through an undetected potential breach in the Injection Zone and Upper Confining Zone.

2.4.2 Description of the Injection Zone and Confining Zone System

At Project Minerva, the Injection Zone has the permeability, porosity, thickness, and lateral continuity to accept injected materials. Both the Upper and Lower Confining Zones are impermeable units with sufficient thickness and low permeability necessary to meet the confining criteria to be an effective barrier for upward fluid migration. A description of the Injection Zone and the injection intervals, as well as the Upper and Lower Confining Zones are discussed below in detail.

2.4.2.1 Injection Zone

The Injection Zone at Project Minerva is delineated in the upper Frio Formation. The Frio Formation is comprised of three intervals, informally referred to, in ascending order, as: (1) the lower Frio Formation, (2) the middle Frio Formation, and (3) the upper Frio Formation.

The upper Frio Formation consists of an extensive shoreface and fluvial–deltaic sandstone sequence with favorable mineralogy and petrophysical characteristics. It is a prolific hydrocarbon producer and, consequently, is the interval most frequently sampled during well logging. While the upper Frio Formation has been extensively developed in southwest Louisiana, it is water-wet at Project Minerva and sparsely penetrated by historic wells that targeted the middle Frio Formation.

The Injection Zone extends from the Anahuac–Frio contact defined by the base of the confining shale interval and the top of the sand down to the top of a shale interval underlying the deepest sand of interest, as shown in Figures 2.1.2-2 and 2.1.2-3. Gross thickness within Project Minerva's AoR ranges from approximately 1,150 ft to 1,450 ft. Gross thickness trends are shown in Figure 2.2.4-2.

The upper Frio Formation is a well-defined seismic reflector mappable in 3D seismic data across Project Minerva's AoR. Seismic sections within the AoR are represented in the following figures:

Figure 2.3.1-1	Figure 2.3.1-2	Figure 2.3.1-3	Figure 2.3.1-4	Figure 2.3.1-5
Figure 2.3.1-6	Figure 2.3.1-7	Figure 2.3.1-8	Figure 2.3.1-9	Figure 2.3.1-10
Figure 2.3.1-11	Figure 2.3.1-12	Figure 2.3.1-13	Figure 2.3.1-14	Figure 2.3.1-15
Figure 2.3.1-16	Figure 2.3.1-17	Figure 2.3.1-18	Figure 2.3.1-19	

Some variability in interval log character from up-dip (proximal) to downdip (distal) depositional areas – zones are typically thinner and more coarse-grained in the north and thicker, with high interpreted shale content in the south, towards the deeper. Depth varies from 8,000 ft TVDSS to 10,200 ft TVDSS at Project Minerva. Figure 2.2.3-1, Figure 2.2.3-2, and

Figure 2.2.3-3 demonstrate the local structure at Project Minerva. The structure maps were generated using high quality 3D seismic data in conjunction with logs/formation tops to create a depth surface. Modeled structural dip is variable and derived primarily from 3D seismic.

Log data within the Injection Zone indicate individual or stacked sand-rich beds alternating with shale-rich intervals and/or siltstones:

1. Sand-rich intervals
    - Interpreted as a negative deflection in spontaneous potential, resistivity, and gamma ray log value,
    - Multiple feet to >100 ft thick,
    - May appear as induvial beds or amalgamated/stacked,
    - Variably sharp or gradational upper- and lower-unit boundaries give log curves a blocky or serrated character, and
    - May be correlated laterally at the scale of the AoR and are therefore interpreted to be laterally extensive shoreface sandstones.
2. Fine grained/shale-rich intervals
    - Interpreted as a positive deflection in spontaneous potential, resistivity, and gamma ray log values, and
    - Multiple feet to hundreds of feet thick.

This interpretation conforms with published analysis of Oligocene Gulf Coast depositional environments: the middle Oligocene Frio Formation is described as a thick sequence of mainly regressive sand-rich sediments interbedded with silts/shales, deposited rapidly in alluvial, lagoonal, marginal marine and deep marine environments, forming a major progradational wedge along the Gulf (Swanson, Karlsen, & Valentine, 2013).

Sand-rich beds correlated across the AoR are relative pay intervals and are likely to have very good lateral communication and variable vertical communication through intra-Frio shales/siltstones.

Petrophysical interpretations were conducted on 14 wells selected where Sonic (DT) and Density (RHOB) logs were available. These wells served as calibration points for estimating porosity and lithology variations, defining effective porosity distributions, and establishing core-to-log porosity–permeability relationships.

Log analysis indicates that sand-rich units range from 14% to 20% porosity, with an average porosity of approximately 17% (Table 2.4.2-1, Figure 2.4.2-1). These values form the basis for characterizing reservoir quality across the study area.

Relatively limited sidewall core data were available from offset wells located north of Vinton Dome (Table 2.4.2-2 and Figure 2.4.2-2). These cores provided porosity and horizontal

permeability measurements, which were used to develop a porosity–permeability transforms for the upper Frio and Anahuac Formations.

This transform was applied to the effective porosity model built in Petrel, enabling permeability estimates to be generated across the field. Based on this approach, sand-rich units exhibit permeabilities ranging from 65 mD to 551 mD, with an average permeability of 275 mD (Table 2.4.2-1 and Figure 2.4.2-1).

X-ray diffraction analysis is available in the upper Frio Formation in the M Gray G Well. 85 (API: 17019216270000). Data indicates that the upper Frio Formation sand-rich intervals typically comprise 69-80% quartz 6-11% clay minerals, with the rest consisting of 5-7% feldspar and 3-4% calcite (Table 2.4.2-3 and Table 2.4.2-4). Site-specific data will be collected in pre-operational data testing prior to commencement of injection to verify this data.

The top of the Frio Formation is a well-defined seismic reflector that is mappable across the 3D seismic dataset. As can be seen from the interpreted seismic lines are represented in the following Figures:

Figure 2.3.1-1	Figure 2.3.1-2	Figure 2.3.1-3	Figure 2.3.1-4	Figure 2.3.1-5
Figure 2.3.1-6	Figure 2.3.1-7	Figure 2.3.1-8	Figure 2.3.1-9	Figure 2.3.1-10
Figure 2.3.1-11	Figure 2.3.1-12	Figure 2.3.1-13	Figure 2.3.1-14	Figure 2.3.1-15
Figure 2.3.1-16	Figure 2.3.1-17	Figure 2.3.1-18	Figure 2.3.1-19	

As depicted in the above-referenced figures, the lateral and vertical continuity of the Injection Zone can be confidently interpreted throughout the AoR and the project area.

2.4.2.2 Upper Confining Zone

The Confining Zone is defined as the zone overlying the Injection Zone that acts as a barrier to fluid movement above an Injection Zone. The Confining Zone must have sufficient rock strength, permeability, areal extent, and thickness to confine injected fluids within the Injection zone.

The Anahuac Formation will serve as the Upper Confining Zone for Project Minerva. The Anahuac Formation conformably overlies the upper Frio Formation (Injection Zone) and acts as a very effective, thick regional seal to many prolific hydrocarbon fields and so can be assumed to be rich in sealing lithologies (Swanson & Karlsen, 2009).

SP, GR, and resistivity log data indicate that the Anahuac Formation is regionally shale-dominated. Available core samples from the Anahuac Formation primarily target high-porosity intervals, resulting in porosity values skewed toward higher averages (Table 2.4.2-2). This bias is influenced by the proximity of the salt dome, where localized diagenetic processes such as fluid flow, recrystallization, and sediment fabric modification can enhance porosity. Therefore, literature and legacy data sources, including Clark (1981), Porter & Newsom (1987), two Core Laboratories reports (1987), and an End-of-Well report (The Dow Company, 2020) for a waste disposal well for the DuPont de Nemours company in

Jefferson County, Texas were used to characterize the petrophysical properties of the Anahuac Formation at Project Minerva.

Porosity estimates were derived from Gulf Coast shale correlations (Porter & Newsom, 1987). The effective shale porosity, which excludes bound water and dead-end pore water, was selected as the most appropriate measure for this analysis. Based on this relationship (Table 2.4.2-5), effective porosity values for the Upper Confining Zone (Anahuac Formation) were assigned as: maximum 0.11, most likely 0.09, and minimum 0.08. A vertical-to-horizontal permeability ratio (Kv/Kh) of 0.1 was applied.

According to Clark (1981), groundwater flow in deep saline aquifers is on the order of ~1 ft/yr, while vertical flow through overlying shales is approximately 1 ft per 10,000 years, confirming the low permeability of Gulf Coastal Plain shale formations. Accordingly, permeability values for the Anahuac Formation were defined as: minimum 1×10^{-6} mD, most likely 1×10^{-4} mD, and maximum 1×10^{-3} mD. These values are weighted toward the lower end of the range, reflecting the predominance of fine-grained, low-permeability intervals observed regionally.

Shale Gouge Ratio (SGR) and Clay Smear Potential (CSP) values of 91% and 94% were computed within the Confining Zone. These high values indicate a shale-rich interval with continuous smear potential and strong sealing efficiency, confirming that the Upper Confining Zone functions as an effective caprock that prevents vertical fluid migration.

GCS does not have core-based mercury injection capillary pressure (MICP) measurements to directly derive capillary entry pressure ($P_{c,\text{entry}}$). As an alternative, empirical/analytical methods SGR and CSP were used to evaluate sealing potential in faults and stratigraphic boundaries. Capillary entry pressure will be determined via core analysis, as described in Section 2.3.3 of the Pre-Operational Testing Program (Attachment C). Within the Project Minerva simulation model, the Confining Zone is characterized using minimum, most-likely, and maximum capillary pressure curves based on the Brooks–Corey formulation (Brooks & Corey, 1964). Additional details are provided in Section 1.5.3.2 (Model Representation) of AoR and Corrective Action Plan (Attachment A). These Pc curves define the caprock's ability to retain CO_2 by representing high entry pressures consistent with fine-grained shale lithologies.

The combined interpretation shows that even where sand-on-shale and shale-on-shale fault juxtapositions may occur, these faults abut a high-Pc caprock. As a result, the modeled pressure behavior indicates that gas-phase CO_2 cannot overcome the capillary entry pressures of the Confining zone. The high SGR/CSP values further substantiate the likelihood that a transmissive pathway is low. Integrating these results with capillary screening overlaying SGR/CSP predictions, caprock Pc curves (or proxies), and modeled CO_2 column heights demonstrate a low risk sealing system with no viable capillary leakage pathway.

Rock compressibility's were estimated by combining data from taken from (Zheng, Sun, & Espinoza, 2019; Zimmerman, 1991; Yale, Nabor, Russell, Pham, & Yousef, 1993). It was assumed that the minimum (min), most likely and maximum (max) formation

compressibility for the Upper Confining Zone were: 3 (min), 6 (most likely) and 10 (max) E-6 pound per square inch $(psi)^{-1}$. A detailed discussion of Rock Compressibility and the methodology, sources, and calculations used to determine the values is provided in Section 1.8.4 (Rock Compressibility) of the AoR and Corrective Action Plan (Attachment A).

At Project Minerva, the Anahuac Formation extends from -6,600 ft TVDSS near Black Bayou Dome to over -9,200 ft TVDSS at the base of a syncline structure located northeast of the AoR (Figure 2.1.2-2, Figure 2.1.2-3, and Figure 2.2.3-1). Depth across the AoR varies from -7,000 ft to -8,400 ft TVDSS. The Anahuac Formation thickens from 800 ft, north of the project area, to over 1,100 ft, south (Figure 2.2.4-1).

The Anahuac Formation forms a syncline structure within the AoR area through the interplay of the regional dip towards the Louisiana Gulf (southeastwards at Project Minerva) with northwards dip off Black Bayou Dome (Figure 2.2.3-1). Areas of increased dip coincide with large-scale normal faults.

Project Minerva proposed injection wells are located >1,000 ft from major faults in areas of low-moderate dip. The Anahuac Formation thickens in a broad wedge geometry, from north to south. Gross thickness varies between 750 ft to >1,200 ft in the main AoR area (spanning).

Figure 2.2.4-1, Figure 2.2.3-1, Figure 2.1.2-2, and Figure 2.1.2-3 clearly demonstrate the lateral continuity of the mapped Upper Confining Zone across the AoR. Log character and interval thickness are demonstrably consistent in cross-section and isopach. At the top of the Anahuac Formation is a seismically complicated reflector, and it is hard to consistently map across the entire 3D seismic dataset. However, due to a good spread of well-to-seismic ties made, GCS has consistently mapped the Anahuac Formation from the interpreted seismic lines in the following Figures:

Figure 2.3.1-1	Figure 2.3.1-2	Figure 2.3.1-3	Figure 2.3.1-4	Figure 2.3.1-5
Figure 2.3.1-6	Figure 2.3.1-7	Figure 2.3.1-8	Figure 2.3.1-9	Figure 2.3.1-10
Figure 2.3.1-11	Figure 2.3.1-12	Figure 2.3.1-13	Figure 2.3.1-14	Figure 2.3.1-15
Figure 2.3.1-16	Figure 2.3.1-17	Figure 2.3.1-18	Figure 2.3.1-19	

The lateral and vertical continuity of the Upper Confining Zone can be confidently interpreted throughout the AoR and the project area.

2.4.2.3 Lateral Extent of the Injection and Confining Zones

The Injection Zone (upper Frio Formation) and the Upper and Lower Confining Zones (Anahuac Formation and shale interval in the upper Frio Formation, respectively) are regionally extensive along the Gulf Coast, Texas and Louisiana. Figure 2.2.4-1, Figure 2.2.4-2, and Figure 2.2.4-3 illustrate the combined gross thickness and mappable large-scale extent. Additionally, Figure 2.1.2-1, Figure 2.1.2-2, and Figure 2.1.2-3 demonstrate the regional continuity of the zones across Project Minerva. Within the AoR, the base of the lowermost USDW, Upper Confining Zone and top/base Injection Zone are clear, consistent picks in the available well log data. The Upper Confining Zone and Injection Zone are

represented by and mapped on well-defined seismic reflectors in 3D seismic data, as depicted in the following Figures:

Figure 2.3.1-1	Figure 2.3.1-2	Figure 2.3.1-3	Figure 2.3.1-4	Figure 2.3.1-5
Figure 2.3.1-6	Figure 2.3.1-7	Figure 2.3.1-8	Figure 2.3.1-9	Figure 2.3.1-10
Figure 2.3.1-11	Figure 2.3.1-12	Figure 2.3.1-13	Figure 2.3.1-14	Figure 2.3.1-15
Figure 2.3.1-16	Figure 2.3.1-17	Figure 2.3.1-18	Figure 2.3.1-19	

The Injection and Upper Confining Zones are demonstrably laterally extensive, exhibiting no evidence of pinchout of sand-rich intervals within the main AoR. Within the Injection Zone, some local variations in interval thickness and extent occur, however these have been factored into the reservoir model, and do not negatively impact the overall behavior of the reservoir in terms of storage capacity, injection rates or safety of the USDW.

The lateral extent of the Injection and Upper Confining zones is demonstrated by the well log data cross-sections, Figure 2.1.2-1, Figure 2.1.2-2, and Figure 2.1.2-3. The extent of the Upper Confining Zone and Injection Zone are demonstrated on isopach maps, Figure 2.2.4-1 and Figure 2.2.4-2; and the well-defined seismic reflectors in 3D seismic data, as depicted in the following Figures:

Figure 2.3.1-1	Figure 2.3.1-2	Figure 2.3.1-3	Figure 2.3.1-4	Figure 2.3.1-5
Figure 2.3.1-6	Figure 2.3.1-7	Figure 2.3.1-8	Figure 2.3.1-9	Figure 2.3.1-10
Figure 2.3.1-11	Figure 2.3.1-12	Figure 2.3.1-13	Figure 2.3.1-14	Figure 2.3.1-15
Figure 2.3.1-16	Figure 2.3.1-17	Figure 2.3.1-18	Figure 2.3.1-19	

2.4.2.4 Lower Confining Zone

The Lower Confining Zone consists of shale interval within the upper Frio Formation, underlying the deepest sands of the Injection Zone. This interval is interpreted as shale-dominated strata that are laterally extensive, with only isolated thin sand layers, and shows no evidence of sand-rich interval pinchouts within the main AoR.

The shale interval is identified at the base of the deepest sand in the upper Frio Formation within the Project Minerva area. The maximum thickness of approximately 149 ft indicates that the unit is sufficiently thick to serve as an effective lower confining layer.

Figure 2.1.2-1 presents the base map of local cross-sections for Project Minerva. Figure 2.1.2-2 shows a north–southwest oriented cross-section (approximately parallel to strike), and Figure 2.1.2-3 displays a west–east oriented cross-section (approximately parallel to dip). GCS has also provided the isopach map of the Lower Confining Zone as Figure 2.2.4-3. As illustrated in these figures, the Lower Confining Zone provides sufficient confinement below the Injection Zone to ensure effective containment.

2.4.2.5 Regional Pressure Sources and Sinks

This section provides clarity on the history-matching methodology employed and quantifies the effect of Phoenix Lake Field production on the horizontal pressure gradient, demonstrating the absence of significant lateral communication with the Project Minerva proposed injection location.

Phoenix Lake Field Production History and Modeling

The Phoenix Lake Field is no longer producing, with production occurring from January 1992 to January 2008. Data for the oil, gas, and water production rates, as well as produced water re-injection rates, were obtained for the Phoenix Lake Field. Historical production data is summarized in Figure 2.4.2-3. To model the effect of this production, the rates were converted into an equivalent reservoir volume of water.

Assumed Formation Volume Factors (FVF) used for conversion were:

- Produced water FVF: 1.0 rb/stb
- Oil FVF: 1.1 rb/stb

The gas-oil ratio was calculated from historical data and assumed to be all dissolved gas (no free gas volume considered), and a single equivalent water production well was placed at the Phoenix Lake Field position within the Project Minerva most likely simulation grid.

History Matching Methodology

The standalone simulation model was executed from January 1990 to January 2150 to assess any residual pressure depletion at the Minerva well locations caused by historical Phoenix Lake Field oil production. The history matching phase of the simulation specifically covered the Phoenix Lake Field production period (January 1990–January 2008), utilizing an equivalent water production profile. The goal of this history-matching segment was to establish a representative pressure baseline prior to the planned Minerva CO_2 injection, which follows the production period in the simulation.

The modeling results on lateral communication, specifically the grid cell pressures at the Minerva CO_2 injection wells, establish that there was no significant effect on Injection Zone pressure at the Project Minerva site associated with the Phoenix Lake Field historical production in 1992–2008. Figure 2.4.2-4 plots the simulated grid cell pressures at the Project Minerva CO_2 injection well sites. The plots show that no pressure decline associated with the historical production is evident from the simulation at the Project Minerva injection well locations.

The pressure impacts were limited to areas closer to the Phoenix Lake Field itself, indicating limited lateral communication across the significant distance to the Project Minerva site.

The history-matched reservoir modeling results establish that there has been no significant effect on upper Frio Formation (Injection Zone) pressures at the Minerva site associated with Phoenix Lake Field historical production in 1992–2008, thus confirming that the horizontal pressure gradient across the distance between the fields was not significantly impacted by

the Phoenix Lake Field production. Pressure gradient will be fully validated via data collected during Pre-Operational Testing.

2.5 GEOMECHANICAL AND PETROPHYSICAL INFORMATION

Geomechanical and petrophysical characterization of the Injection and Upper Confining Zones will be undertaken during construction of injection wells, as outlined in the Pre-Operational Logging and Testing Plan (Attachment C). In the absence of core material from a dedicated stratigraphic well, data has been generated from analogous data and published sources for the Frio Formation.

2.5.1 Geomechanical Information

GCS has conducted an advanced geomechanical literature review to establish the regional stress regime, mechanical properties, and deformation behavior of the Frio Formation. This review provides the conceptual basis for understanding fracture gradients, caprock integrity, and fault-stability. However, because site-specific mechanical data has not yet been collected, these geomechanical parameters are not currently implemented in a fully coupled geomechanical simulation. The current simulation model uses a conservative, decoupled formulation in which rock compressibility is represented only through pore-volume compressibility. Once site-specific measurements become available, GCS will integrate them into a fully coupled flow geomechanical model. Capabilities of the General Enhanced Modular (GEM), a fully compositional reservoir simulation software produced by Computer Modeling Group (CMG) can be found in Section 2.10.5 (Modeling Approach and Simulation).

Geomechanics informs four primary considerations relevant to Project Minerva:

1. Determining the pressure at which new fractures may be initiated,
2. Assessing the mechanical integrity of the Confining Zone,
3. Evaluating the potential for fault reactivation, and
4. Understanding how pore-volume compressibility influences pressure evolution.

These considerations form the basis of the conceptual geomechanical framework. The current simulation configuration can be found in Attachment A.

2.5.1.1 Data Sources

Because site-specific mechanical measurements are not yet available, analogous data were compiled from published studies of the upper and lower Frio Formation (Figure 2.5.1-1):

- **Frio Formation CO_2 injection Pilot Project** (Hovorka, et al., 2005), providing porosity, permeability, grain-size distributions, and elastic properties.
- **Lower Frio in-situ stress testing** (Ramos, Katahara, Keck, & Batzle, 1994), providing stress gradients, elastic moduli, and strength parameters.

These studies constrain the likely stress state and mechanical response of Frio sandstones and shales and establish the uncertainty ranges expected for Project Minerva's fracture-pressure and fault-stability evaluations.

2.5.1.2 Stress

Principle Stress Orientations

Without local stress measurements, orientations of principal horizontal stresses were taken from regional studies (Trevino & Meckel, 2017; Nicholson, 2012; Zoback & Zoback, 1980).

These studies consistently show that the Texas-Louisiana Gulf Coast is characterized by a normal-faulting stress regime, where SHmax trends parallel to the coastline and regional growth-faults systems and SHmin trend perpendicular to those structures. The maximum horizontal stress (SHmax) trends 54.1°, consistent with regional fault-strike trends, and the minimum horizontal stress (SHmin) trends 324.1° (Figure 2.5.1-2).

These orientations are consistent with average fault-strike directions from more than 250 mapped Gulf Coast faults (Trevino & Meckel, 2017; Zoback & Zoback, 1980) and they provide an internally consistent reference frame for slip-tendency and fault-stability assessments in Section 2.3.3 (Fault Stability Analysis).

Vertical and Horizontal Stress Magnitudes

The Gulf Coast stress regime is well described by a near-lithostatic vertical stress and a minimum horizontal stress typically 75-90% of vertical stress (Sv). GCS used published analogs to define the most likely gradients and uncertainty ranges:

Vertical Stress (Sv) Gradient

The overburden stress, Sv, for normal-fault stress regimes is assumed to be an average of 1.0 psi/ft (Nicholson, 2012). This is equivalent to the lithostatic pressure exerted by rock with an average density of 2.3 g/cm3 (Hovorka, Tutton, & Trevino, 2018). (Trevino & Meckel, 2017) assumed a value of 1.0 psi/ft. This data was used for studies of the Lower Miocene in the Texas Gulf of Mexico.

GCS took the most likely total vertical stress gradient to be 1.0 psi/ft.

This compares with a value of 0.9 psi/ft (from the density log) reported by (Ramos, Katahara, Keck, & Batzle, 1994). (Ramos, Katahara, Keck, & Batzle, 1994) derived values for the principal horizontal stress gradients from an unconventional differential strain curve analysis (DSCA). The rock samples were poorly consolidated, and this prevented a conventional DSCA. Based on this data, we estimate the error in the total vertical stress gradient to be approximately ± 0.1 psi/ft.

Minimum Horizontal Stress (SHmin) Gradient

(Nicholson, 2012) assumed a value of 85% of Sv, values consistent with work published by (Engelder, 1974). (Trevino & Meckel, 2017) assumed a value of 0.85 psi/ft (85% of 1 psi/ft for the vertical stress gradient).

GCS expects the most likely value of the minimum horizontal stress gradient to be 0.85 psi/ft.

(Ramos, Katahara, Keck, & Batzle, 1994) reported a value of 0.74 * 0.9 psi/ft = 0.66 psi/ft. Based on this data, we estimate the error in the total minimum horizontal stress gradient to be approximately ± 0.15 psi/ft.

Maximum Horizontal Stress (SHmax) Gradient

GCS took a value equal to the average of the gradients of the total vertical and minimum horizontal stresses, 0.93 psi/ft (to 2 decimal places), with an error of ± 0.07 psi/ft. The estimate of the error is the range between our most likely total vertical and minimum horizontal stress gradients. (Ramos, Katahara, Keck, & Batzle, 1994) reported a value of 0.81 * 0.9 psi/ft = 0.73 psi/ft from six DSCAs, so GCS may be underestimating the error. It is half the error we report for the total minimum horizontal stress. This is because of the extra "information" carried by constraining the expected value to lie between the total vertical and minimum horizontal stress gradients.

Relationship to Fracture Gradient and Fault Stability

These stress magnitudes directly support the AoR fracture-pressure analysis:

- Fracture-gradient range: 0.63–0.90 psi/ft, corresponding to 6,300–9,000 psia at 10,000 ft TVDSS.
- All modeled bottom-hole pressures remain below the lowest credible fracture-pressure estimate.
- Fault-stability evaluations use SHmax, SHmin, friction (μ = 0.72), and cohesion (C = 0) to compute slip tendencies, and results show no faults approach shear failure under any modeled scenario.

Mechanical Properties

Mechanical properties derived from analogs include the Biot Coefficient, Poisson's ratio, Young's modulus, cohesion, coefficient of friction, and poro-elastic, thermo-elastic and linear thermal expansion coefficients, as described below:

Biot Coefficient

(Zheng, Sun, & Espinoza, 2019) reported a value of 0.944 in the effective stress range 3.5 – 7 MPa (500 – 1,000 psi). (Ramos, Katahara, Keck, & Batzle, 1994) assumed a value of 1.0. We assume a value of 1.0. The error is approximately ± 0.06, assumed from (Ramos, Katahara, Keck, & Batzle, 1994).

Poisson's ratio

This is taken from (Zheng, Sun, & Espinoza, 2019), partly reproduced below, GCS took the unloading process values with an average of 0.23 ± 0.04. (Ramos, Katahara, Keck, & Batzle, 1994) reported an average core value of 0.21, based on static tests.

Young's modulus

Young's modulus is taken from (Zheng, Sun, & Espinoza, 2019) (Figure 2.5.1-3). We take the unloading process values with an average of 5.5 ± 0.5 Gpa.

(Ramos, Katahara, Keck, & Batzle, 1994) measured a value of 1.7 Gpa, and with a cohesive (shear) strength of less than 3.4 Mpa (500 psi). It was also noted that the elastic moduli of the sandstones were about twice that of the shale but that the shear strength of the shale was about twice that of the sandstone.

Cohesion, C

Cohesion is assumed to be zero, (Trevino & Meckel, 2017).

Coefficient of friction, μ

(Byerlee, 1978) reports a range of 0.60 – 0.85, (Engelder, 1974) reports a range of 0.68 – 0.72, and (Trevino & Meckel, 2017) reports a value of 0.60. GCS used a Coefficient of Friction value of 0.72 as the midpoint of these published values with an error tolerance of ± 0.10.

These parameters inform the conceptual mechanical response of the Frio Formation even though they are not yet active in the coupled simulation model.

Poro-elastic, thermo-elastic and linear thermal expansion coefficients

The poro-elastic coefficient translates the effect of fluid pressure to the reservoir stress field as $\Delta S \sim \partial S/\partial P * \Delta P$, where ΔS is the change in stress, $\partial S/\partial P$ is the poro-elastic coefficient and ΔP is the change in pressure. The expected value of the poro-elastic coefficient is $6.77E^{-7}$ psi^{-1}.

Current Model Implementation and Future Work

The geomechanical capabilities of the Project Minerva reservoir simulation model are made available through the GEM-GEOMECH module, which is integrated within the CMG compositional simulator. This module is designed to predict stress changes in both the Injection Zone and the Confining Zone, and it can perform geomechanical coupling, which translates the effect of pore pressure and temperature into the reservoir stress field. This functionality is crucial for evaluating caprock integrity and fault activation risk. GEM-GEOMECH enables evaluation of these risks through effective stress and slip-tendency analysis. The module offers the capability to evaluate the stress field as a function of in-situ stress, temperature, pressure, and mechanical properties; however, the fluid flow portion of the model utilizes a corner-point geometry grid to honor stratigraphic dip and fault geometries.

Current Approach (Decoupled Model)

The CMG GEM simulation used for the AoR and Narrative does not activate the GEOMECH module. Accordingly, rock compressibility is represented only as a pore-volume compressibility term. This is appropriate because AoR results show that the bottom-hole pressures remain well below fracture-pressure thresholds, no simulated pressure approaches fault-reactivation criteria, and the Confining Zone is never exposed to tensile or shear failure conditions.

Future Coupling with Site-Specific Data

Once mechanical properties are measured from Project Minerva cores and logs, such as Young's modulus, Poisson's ratio, Biot coefficient, and strength parameters, GCS will activate GEM-GEOMECH to implement:

- Two-way coupling of pore pressure and stress,
- Stress-dependent porosity and permeability,
- Deformation-controlled pore-volume changes, and
- Explicit, mechanically updated fault-stability assessment.

2.5.2 Petrophysical Information

Petrophysical data provides a quantitative description of rock storage and flow properties that underpin the static geomodel, dynamic reservoir simulation, and AoR delineation for Project Minerva. This section serves as the central reference for petrophysical information used throughout the Narrative, summarizing data sources, calibration procedures, derived property ranges, limitations, and planned site-specific validation. Detailed petrophysical processing steps and quality-control procedures are described in Section 2.2.1.3 (Petrophysical Workflow).

Regional analog datasets were used to support petrophysical characterization and provide bounding behavior for property selection. These datasets include published porosity, permeability, capillary pressure, and relative permeability measurements from the upper Frio Formation and Anahuac Formation, as well as CCS-specific laboratory studies and history-matched datasets from the Frio Brine–CO_2 Pilot Project (Hovorka, et al., 2005; Doughty, Freifeld, & Trautz, 2015; Jung & Wheeler, 2017).

Prior to operations at Project Minerva, and consistent with the Pre-Operational Testing Program (Attachment C), logs, fluid samples, and whole core samples will be acquired from the Injection and Upper Confining Zones. The geostatistical and reservoir simulation models will be updated with the newly acquired site-specific data and submitted for review with the Pre-Operations Narrative, Completion Report, and Site Reassessment.

2.5.2.1 Data Sources

Wireline Log Data

Legacy wireline logs from wells within and surrounding the Project Minerva study area form the primary basis for petrophysical interpretation. Available log suites include spontaneous potential (SP), gamma ray (GR), density (RHOB), neutron, and sonic (DT) logs. Log coverage and quality vary by well vintage and location.

Petrophysical interpretations were conducted on 14 wells (Table 2.4.2-1, Figure 2.4.2-1) where high-quality sonic and density logs were available. These wells served as calibration points for defining effective porosity distributions, evaluating lithologic variability within the upper Frio Formation, and supporting development of porosity–permeability relationships. Additional wells with partial log suites were used for facies identification and stratigraphic

correlation, consistent with the workflow described in Section 2.2.1.3 (Petrophysical Workflow).

Core Data

Available core data in the project area is sourced from 24 wells surrounding the Vinton Dome (see Table 2.5.2-1 and Figure 2.4.2-2). All analyzed core samples are percussion side-wall cores (SWC), which present limitations for porosity and permeability analysis due to potential damage incurred during acquisition. Despite this limitation, side-wall core samples have been evaluated for permeability and porosity from the Injection Zone (upper Frio Formation) and from the Upper Confining Zone (Anahuac Formation), as detailed in Table 2.4.2-2. The sidewall core orientation is perpendicular (90°) to the borehole wall.

It should be noted that the samples from the Upper Confining Zone targeted high porosity and permeability intervals, creating a selection bias towards higher values. Site-specific core samples targeting sealing lithologies in the Upper Confining Zone will be collected during preoperational testing to validate/improve this data set (see Preoperational Testing Program, Attachment C). Additionally, analog porosity values from Gulf Coast shales have been incorporated into the porosity/permeability analysis (Table 2.4.2-5).

Proximity to the salt dome can complicate petrophysical evaluations, manifesting as washouts, irregular boreholes, and altered tool responses, potentially skewing porosity and net-to-gross estimates. Salt-related changes in facies, stratigraphic thickening or thinning, and localized cementation or dissolution can further influence porosity-permeability relationships. The utilized core data, sourced from wells near the Vinton Dome remain valid, as they share lithofacies and mineralogical characteristics with the broader regional system. To counteract potential biases related to salt, density-neutron data deemed compromised were excluded, local porosity-permeability transforms were applied, cross-checks with sonic and core data were conducted, and facies mapping with sensitivity analyses helped define residual uncertainties.

2.5.2.2 Porosity Log Calibration

The 24 cored wells were employed to calibrate porosity logs in wells by aligning core-measured porosity with log-derived values within the Injection, Upper, and Lower Confining Zones. The calibration process included depth-matching core and log data, followed by the application of linear regression using density vs. neutron or sonic vs. density correlations to adjust log-derived porosity responses.

The applicable linear regression calibration model follows:

$$\phi_{\text{corrected}} = a\,\phi_{\text{log}} + b \qquad \text{Equation 2.5-1}$$

Where:

$\phi_{\text{corrected}}$= calibrated porosity applied in the model

ϕ_{log}= original log-derived porosity (from density–neutron or sonic–density crossplots)

a= regression slope representing the scaling adjustment

b= regression intercept capturing any systematic log offset

This equation is derived from depth-matched core and log pairs where core measurements are available.

Differences between core porosity points and log-derived porosity are expected due to inherent scale and depth uncertainties associated with sidewall core (SWC) acquisition. SWC measurements are susceptible to depth mismatch, sampling resolution limitations, mechanical disturbance, and poor representativeness in thin-bedded and shale-rich intervals, which may result in artificially elevated porosity values. Variability between core and log measurements is therefore expected, particularly in older percussion sidewall core datasets where sample recovery, depth accuracy, and representativeness may be limited. The core to log interpretation comparison is illustrated in Figure A.1.5.1-2 in Section 1.5.1.1 of the AoR and Corrective Action Plan (Attachment A).

GCS will acquire site-specific whole core, logging, and laboratory data during pre-operational testing to validate and refine the petrophysical interpretation prior to injection activities. Additional details are provided in the Pre-Operational Logging and Testing Plan (Attachment C), Section 2.3.3.

In wells lacking core data, SP logs were normalized and conditioned to facilitate lithology identification and facies definition. Reference intervals were selected to establish clean sand and 100% shale baselines (see Figure 2.2.1-6), typically representing thick, blocky sand in the Injection Zone and shales in the Upper and Lower Confining Zones.

Logs affected by poor data quality, casing interference, or salt dome–related effects such as borehole conditions (e.g., washouts, breakouts, and rugosity) may exhibit anomalous log responses resulting in spurious measurements. These intervals were identified during quality control and excluded from petrophysical interpretation to ensure robustness of the analysis. This quality control and exclusion methodology is applied consistently throughout the GCS petrophysical workflow for the Project Minerva Area of Review (AoR), including wells located near the Black Bayou Dome. GCS will perform pre-operational testing, including the collection of core samples from the injection well, prior to injection as outlined in the Pre-Operational Logging and Testing Plan (Attachment C).

Core data available for this study are limited to porosity and permeability measurements and do not include lithological descriptions or mineralogical analyses required for direct validation of log-derived shale volume (Vshale). Accordingly, the Vshale model is based on petrophysical log interpretation and will be validated upon acquisition of site-specific core and laboratory data during the pre-operational phase, refer to Section 2.5.3.

2.5.2.3 Porosity Characteristics

Injection Zone

Log-derived petrophysical analysis indicates that sand-rich intervals within the upper Frio Formation exhibit effective porosities ranging from approximately 14% to 20%, with an average value of approximately 17% (Table 2.4.2-1; Figure 2.4.2-1). These values are consistent with regional Frio Formation datasets and provide the basis for characterizing reservoir quality across the study area.

Lower porosity shaley and interbedded facies exhibit reduced effective porosity and limited flow capacity and act as baffles to vertical fluid movement while contributing to lateral pressure propagation, as described in Section 1.5 (Parameterization) in the AoR and Corrective Action Plan (Attachment A).

Confining Zone

Petrophysical characterization of the Anahuac Formation, which consists predominantly of shaley–interbedded units, was based on porosity estimates derived from Gulf Coast shale correlations (Porter & Newsom, 1987). Effective shale porosity, which excludes bound water and dead-end pore water, was selected as the most appropriate metric for this analysis. Based on this relationship (Table 2.4.2-5), effective porosity values assigned to the Upper Confining Zone (Anahuac Formation) are a maximum of 0.11, a most-likely value of 0.09, and a minimum of 0.08.

2.5.2.4 Permeability Characteristics

Permeability was computed using a porosity-permeability relationship established from side-wall core sample results (Figure 2.2.1-15). This relationship was formed by binning core measurements into 0.05 porosity intervals and calculating the average porosity with the average log10 permeability for each bin (Figure 2.5.2-1). A 15% porosity cut-off was applied to eliminate spurious values, with trends extrapolated to reflect the lower porosity range. The final porosity-permeability relation applied to the static geomodel is represented in Figure 2.5.2-2.

Injection Zone

Based on this approach, sand-rich intervals within the upper Frio Formation, as identified from sidewall core samples from Vinton Dome (Table 2.4.2-2), exhibit horizontal permeabilities ranging from approximately 61 mD to 1,836 mD, with an average horizontal permeability of approximately 667 mD, consistent with the average values reported for the High-Quality Sandstone facies in the geostatistical model (Table 2.4.2-1). Shaley-interbedded facies exhibit substantially lower horizontal permeabilities, on the order of 0.14 mD, reflecting their higher clay content and reduced pore connectivity.

Vertical permeability was calculated using facies-dependent Kv/Kh ratios derived directly from the same porosity–permeability relationships applied in the geostatistical model described in Section 2.2.1.4 (Geostatistical Model Workflow). For High-Quality Sandstone facies in the upper Frio Formation, a Kv/Kh ratio of approximately 0.62 was applied, reproducing the modeled average horizontal and vertical permeabilities of approximately

392 mD (Kh) and 243 mD (Kv). For shaley-interbedded facies and the Anahuac Formation, a Kv/Kh ratio of approximately 0.10 was applied, consistent with modeled average permeabilities of approximately 0.18 mD (Kh) and 0.018 mD (Kv). These ratios are consistent with depositional anisotropy observed in the Frio Formation and published results from the Frio Brine–CO_2 Pilot Project (Hovorka, et al., 2005).

Permeability values were subsequently upscaled to the simulation grid using NTG-weighted arithmetic averaging for horizontal permeability and geometric averaging for vertical permeability, as described in Section 1.5.1 (Porosity and Permeability) of the AoR and Corrective Action Plan (Attachment A). This approach preserves facies-controlled anisotropy and ensures consistency between the geostatistical model and the dynamic simulation model used for AoR evaluation.

Confining Zone

Permeability was established according to Clark (1981), groundwater flow in deep saline aquifers is on the order of ~1 ft/yr, while vertical flow through overlying shales is approximately 1 ft per 10,000 years, confirming the low permeability of Gulf Coastal Plain shale formations. Accordingly, permeability values for the Anahuac Formation were defined as: minimum 1×10^{-6} mD, most likely 1×10^{-4} mD, and maximum 1×10^{-3} mD. These values are weighted toward the lower end of the range, reflecting the predominance of fine-grained, low-permeability intervals observed regionally. A vertical-to-horizontal permeability ratio (Kv/Kh) of 0.1 was applied.

Wireline logs and core data acquired during pre-operational testing will be used to refine porosity–permeability transforms and permeability distributions prior to the commencement of injection.

2.5.2.5 Formation Fluid Characterization

Twelve wells adjacent to the Project Minerva area were used to estimate salinity via Pickett plots cross-checked with SP-log analysis (Table 2.5.2-2). The average calculated was 115 kppm ± 28 kppm, slightly higher than (Kharaka, Hovorka, Cole, & Gunter, 2006) due to deeper wells and local salt-dome effects; results are consistent within uncertainty. This is described in detail in Sections 1.5.9 and 1.6.4.4 of the AoR and Corrective Action Plan (Attachment A).

The mineralogy and salinity values determined for the upper Frio Formation at the CECOS Project aligns with the constituents identified from literature, nearby analog data and the Frio Brine-CO_2 Pilot Project. For this reason, GCS has elected to utilize the data from the CECOS project (approximately 30 miles northeast of Project Minerva) as a basis for the base case formation matrix and formation fluid. More information is provided in Section 2.8.1 (Geochemical Study) of this document and Section 1.5.9 (Geochemistry) of the AoR and Corrective Action Plan (Attachment A).

Per the Pre-Operational Logging and Testing Plan (Attachment C), GCS will collect formation fluid from the Injection Zone during the drilling of MS CCS 1 and analyze the sample(s) to characterize the chemical properties. Whole cores will be collected from the Confining and

Injection Zones and analyzed to characterize the mineralogy of the formations. The geochemical analysis will be used to validate geochemical compatibility assumptions relating to the formation compatibility with the CO_2 stream.

2.5.2.6 Mineralogical Characterization

Analog mineralogical analyses are available from two samples, near Project Minerva (Tables 2.4.2-3 and 2.4.2-4). Result 1 provides the overall mineral composition, including framework minerals such as quartz and feldspar, carbonates such as calcite, dolomite, aragonite, siderite, sulfides such as pyrite, zeolites such as analcime, and total clay content. This dataset offers a broad overview of the primary mineral phases within the rock, which is essential for reservoir characterization and porosity/injectivity modeling. Result 2 delivers a detailed breakdown of the "Total Clay Minerals" reported in Result 1, identifying specific clay types such as kaolinite, chlorite, illite, smectite, and mixed-layer illite/smectite. This level of detail is critical for evaluating reservoir quality and predicting CO_2 injection behavior, supporting geomechanical modeling, wettability assessments, and reactivity studies.

Due to the limited number of samples, these analyses were used for informational purposes only. However, the results are consistent with mineralogical data from the CECOS Project, located approximately 30 miles northeast of Project Minerva, and the Frio Brine–CO_2 Pilot Project. Based on this alignment, GCS has elected to utilize the CECOS Project data as a basis for the base case formation matrix, as described in Section 2.8.1 (Geochemical Study) of this document and Section 1.5.9 (Geochemistry) of the AoR and Corrective Action Plan (Attachment A).

2.5.3 Planned Pre-Operational Testing and Model Refinement

Site-specific data collection to characterize the petrophysical characteristics of Project Minerva will be undertaken as part of the Pre-Operational Testing and Logging Plan (Attachment C). The pre-operational testing phase involves a comprehensive acquisition of customized log suites, fluid samples, and cores from both the Injection Zone and Upper Confining Zone. Data acquired during pre-operational testing will be used to update the geomechanical workflow, petrophysical workflow, static geomodel, and simulation model and submitted as part of the Pre-Operations Narrative, Completion Report, and Site Reassessment, as required. Vshale estimates are currently derived from petrophysical log analysis. The acquisition of site-specific core, logging, and laboratory data will be used to refine the petrophysical evaluation and support validation and calibration of the Vshale model, as noted in Section 2.5.2.2.

Logging

A Triple-Combo log suite will be utilized for formation evaluation, collecting critical measurements such as gamma ray, density, neutron porosity, and resistivity. These measurements are essential for calculating key petrophysical properties, including total porosity, effective porosity, hydrocarbon saturations, and facies characterization. If required, a Nuclear Magnetic Resonance (NMR) log may also be acquired to enhance formation characterization, particularly if conventional logs are insufficient. The NMR log

will provide detailed insights into pore size distribution, permeability, hydrocarbon attributes, vugs, fractures, and grain size.

Fluid samples will be collected from the Injection Zone as part of the logging and testing program to characterize chemical properties.

Coring and Analysis

GCS plans to implement a core program following well drilling, involving the collection and analysis of whole cores and sidewall cores for calibration purposes. The core samples will undergo routine core analysis to evaluate storage capacity (total and effective porosity), flow units (permeability), and fluid saturation. In addition, LithoScan analyses will be performed to determine key petrophysical and elastic properties, including photoelectric factor (PEF), bulk density, lithology, and compressional and shear wave velocities (Vp–Vs). The results will be used for core-to-log calibration, enabling refinement of the petrophysical model.

Core-derived lithological and mineralogical data will also be integrated with petrophysical log analysis to refine the Vshale model upon acquisition. This will support validation and calibration of log-derived Vshale through core description (visual logging) to identify shale intervals and heterogeneity, X-ray diffraction (XRD) to quantify clay mineral content, thin section and petrographic analysis to evaluate clay distribution and texture, and grain size analysis to distinguish shaley and clean sand intervals.

The resulting datasets will be used to calibrate and optimize site-specific petrophysical workflows for Project Minerva. These calibrated properties will improve the accuracy of petrophysical interpretations and be incorporated into the geostatistical and reservoir simulation models.

Rock Mechanics Testing

Rock mechanics testing will include combined triaxial and ultrasonic tests alongside Mohr-Coulomb borehole stability analysis. Key parameters measured under reservoir stress conditions will encompass Young's modulus, Poisson's ratio, compressive strength, Biot's coefficient, and Brazilian tensile strength.

2.6 SEISMIC HISTORY

2.6.1 Gulf Coast Basin Seismic History

As previously discussed in Section 2.3.1 (Presence of Faults and Fractures), in the area of Project Minerva, the majority of seismic sources in the Gulf Coast Basin involve faulting. The direction of most faulting is parallel to the edge of the Gulf Coast. The faulting is a result of deposition of large quantities of sand and mud along the margins of the Gulf of Mexico resulting in rapid sedimentation creating large normal fault systems near the downdip edge of each sediment wedge within the area of maximum deposition. These faults may exhibit significant growth strata in areas where sedimentation was high, or no growth strata where sedimentation was lower. Regionally, faults may exhibit normal geometry (planar with near-constant dip) or listric geometry (steep dip, flattening with depth, along a detachment

surface/plane). Radial faulting associated with shale or salt piercement structures is also common in the Gulf Coast region.

All faults mapped from surface down to basement in 3D seismic data at the Project Minerva site were determined to be normal, with no significant growth strata in the hanging wall and no listric geometry (see Section 2.3.1 and Figures 2.3.1-1 to 2.3.1-19). Radial faults associated with Black Bayou Dome (2.4 miles east of the injection site) were determined to be normal geometry.

2.6.2 Project Minerva's Seismic History

The Gulf Coast of Texas and Louisiana are historically an area with low probability of hazards from peak ground accelerations (USGS, 2018). Project Minerva is located in an area recognized by the USGS Earthquake Hazards Program having low level of seismic risk in the US (Figure 2.6.2-1).

2.6.2.1 Data Sources

All historical seismic events were sourced from the USGS Earthquake Hazards Program Earthquake Catalog, a part of the program's interactive map in which recorded recent and historic seismic events can be searched with custom parameters for the US and worldwide. Other data of historical seismic events along the Gulf Coast of Texas and Louisiana was sourced from publicly available published literature from the USGS.

Utilizing the USGS Earthquake Hazards Program Earthquake Catalog, parameters were set to search and identify closest proximity seismic events to MS CCS 1 and MS CCS 2 bottom-hole locations. These custom parameters include a min magnitude (Mblg) of 0.5 to a max of 9, and a start date and time of 00:00:00 UTC on January 1st, 1901, to present day (i.e., December 2025) (USGS, 2025). The seismic events identified are discussed in detail below and are listed in Table 2.6.2-1.

2.6.2.2 Historical Seismic Events

At Project Minerva, the likelihood of an earthquake caused by natural forces, fluid injections, and/or oil and gas production is considered exceptionally low. Injection of carbon dioxide is anticipated to be at comparatively low pressures into deep, high porosity and highly permeable formations. These formations are regionally extensive and are not subject to natural earthquakes. Therefore, the probability of an earthquake occurring and negatively impacting Project Minerva's injection capabilities is exceptionally low.

The following subsections outline the recorded historical seismic events that have occurred within 120-mile radius of Project Minerva.

Seismic Events in Louisiana

According to the USGS Earthquake Hazards Program Earthquake Catalog, within a 100-mi radius of MS CCS 1 and MS CCS 2 bottom-hole locations, there is only one recorded earthquake (Figure 2.6.2-2). The earthquake occurred 1 km (0.62 mi) west to northwest of the City of Sulphur in Calcasieu Parish, Louisiana (30° 24' 3" N, 093° 03' 93" W) approximately 14 km (~8.7 mi) deep (Stevenson, 1988) (Stevenson and Agnew, 1988). The

earthquake had a Mblg of 3.8 and had a time of 19:40:50 Universal Time Coordinated (UTC) on October 16th, 1983, (USGS, 2024). Notes from (USGS, 2024) state the earthquake impact was felt at Hackberry, Hayes, Sulphur, Westlake, and in the Lake Charles area.

(Stevenson, 1988) conclude that the earthquake originated from normal basement faulting, striking northeast and dipping to the southeast. While this earthquake occurred approximately 46,000 ft deep, the faults within Project Minera occur less than 12,000 ft deep. Based on a review of seismic images from the project area, the faulting within Project Minerva is not connected to the basement structure, nor are there any major or mappable basement faults sited within Project Minerva.

Seismic Events in Texas

According to the USGS Earthquake Hazards Program Earthquake Catalog, within 115-mi radius of MS CCS 1 and MS CCS 2 bottom-hole locations, and other than the one previously discussed earthquake in Louisiana, there are multiple recorded earthquakes in Texas (Figure 2.6.2-2), and they are described below from latest to earliest:

- The latest earthquake occurred May 2024 at 2:21pm, 5 km west to southwest of Chireno, TX, (31.473°N, 94.398°W) at a depth of approximately 6.4 km (4.0 mi), and a magnitude of 2.6.
- The next most recent event occurred April 2024 at 10:17 pm, 5 km west to southwest of Chireno, TX (31.473°N, 94.404°W) at a depth of approximately 7.6 km (4.7 mi), and a magnitude of 3.0. Table 2.6.2-1 describes the seismic events within the 115-mi radius of MS CCS 1 and MS CCS 2 bottom-hole locations.
- The third most recent event occurred January 2019 at 11:32 pm, 7 km south to southwest of San Augustine, TX (31.470°N, 94.135°W) at a depth of approximately 5 km (3.1 mi), and a magnitude of 3.3.
- The fourth most recent event occurred October 2014 at 4:52 pm, 16 km north to northeast of San Augustine, TX (31.676°N, 94.055°W) at a depth of approximately 5 km (3.1 mi), and a magnitude of 3.1
- The fifth most recent event occurred February 2013 at 6:40 pm, 5 km west of northwest of San Augustine, TX (31.545°N, 94.162°W) at a depth of approximately 5 km (3.1 mi), and a magnitude of 2.1. Notes from (USGS, 2024) state the impact of the earthquake was felt at Garrison and Timpson, Texas.

2.6.3 Project Minerva's Seismic Risk Analysis

A preliminary seismic risk evaluation was conducted for Project Minerva. Project Minerva is located in an area recognized by the USGS Earthquake Hazards Program having low level of seismic risk in the US. The low-level risk is based on the following:

- Low intensity and frequency of seismic events (i.e., natural earthquakes) in the area of Project Minerva, with maximum ground motion on the surface being less than or

equal to an intensity range of Modified Mercalli Intensity (MMI) = V (i.e., Moderate)[1] (USGS, 2024),

- Low population density in Cameron Parish, Louisiana, which limits exposures and impacts, with only about 5,617 total population in the area of Project Minerva,
- Lack of injection-induced seismicity in Underground Injection Control (UIC) Class I hazardous and non-hazardous injection wells operating in Tertiary sediments along the Gulf Coast of Texas and Louisiana, and
- Injection pressures are less than those required to induce slip along pre-existing faults.

Additional information according to Federal Emergency Management Agency (FEMA) Earthquake Hazards Maps, the Gulf Coast of Texas and Louisiana are assigned in the lowest seismic design category (SDC) (Figure 2.6.3-1). In the area of Project Minerva, an SDC, or map color, of A/white is assigned indicating there is a very small probability of experiencing damaging earthquake effects if affected (FEMA, 2024).

2.6.3.1 Model Earthquake at Project Minerva

A “model” earthquake is used to evaluate the potential effects, if any, of natural earthquakes on structures associated with the sequestration project. In general, a source mechanism is required when designing a “model” earthquake. In these cases, it is usual to have a “known” active fault system with a measured strain or stress field. In more active regions of the earth, faults with strain (i.e., movement across the fault without rupture) develop at a rate of up to 5 centimeters (cm)/year, or more (Leeds & Associates, 1989). As a meter or more of strain develops, stress accumulates and eventually the system releases this stored strain energy in the form of elastic waves (i.e., an earthquake).

Although the Gulf Coast of Texas and Louisiana contain several geological features capable of storing and releasing stored energy, all are weak or ineffective in terms of generating even modest ground motion (Leeds & Associates, 1989).

Salt structures develop gravimetrically by the flow of lower density salt through weaker zones of the thick Tertiary sediments. The salt is generally so plastic that it tends to flow rather than develop large fractures. The surrounding sediments are badly faulted by the intrusion of salt and are almost as physically incompetent as the salt, also having low densities, poor cementation, and low shear strength with resulting low shear moduli. It is doubtful that the salt dome as a seismogenic source could develop earthquakes with magnitudes greater than 3.0 and intensity MMI>IV (Leeds & Associates, 1989). These events could be felt locally but are unlikely to propagate damaging ground motions. The events might be perceptible, but the level of shaking could not be considered damaging.

[1] According to Modified Mercalli Intensity Scale (MMI) by the USGS Earthquake Hazards Program, a V (i.e., Moderate) is described as “Felt by nearly everyone; many awakened. Some dishes, windows broken. Unstable objects overturned. Pendulum clocks may stop (USGS, 2024).

Growth faults have also developed along the Texas/Louisiana Gulf Coast which may be responsible for seismic activity. Considering the Gulf Coast as a whole, a level of Mb=4.2 is considered an upper level for this kind of source in this area (Leeds & Associates, 1989). The several low magnitude events within about 50 miles of the coastline are probably attributable to this mechanism.

The possibility that growth faults may be triggered by faults in the basement is suggested by Stevenson and Agnew (1988) in their discussion of the Lake Charles Earthquake. Details of the event were developed from recordings of Department of Energy (DOE) supported microseismic networks deployed for monitoring geothermal experiments (withdrawal and injection) in southern Louisiana. The interpreted depths ≥14+ km for these events are deeper than have previously been reported and well beneath anticipated injection depths for the sequestration project. Additionally, none of the events were attributable to the geothermal extraction/reinjection operations (Stevenson (pers comm.), in (Leeds & Associates, 1989).

Design Earthquake for Seismic Risk Analysis

In the evaluation of the potential effect of seismicity on a Class I Injection Well Facility located near the western margins of Project Minerva, (Leeds & Associates, 1989) used a modeled seismic event with a body-wave magnitude, Mb of 4.2 ±0.2 as a conservative working model for the design earthquake and presumed that the source area for the event would be along one of the nearby coast parallel growth faults.

The maximum ground motion on the surface generated by the design earthquake would be within the intensity range of MMI=V. This intensity equates to a horizontal surface acceleration of 0.05 grams (g) (Leeds & Associates, 1989). This is the same value used as an “Operating Basis Earthquake” (OBE) for Gulf Coast nuclear power plant electric generating stations. The Nuclear Regulatory Commission (NRC) estimates the risk each year of an earthquake intense enough to cause core damage to the reactor at River Bend (north of Baton Rouge) was 1 in 40,000, according to an NRC study published in August 2010 (Hiland, 2010). The empirical correlation between intensity and acceleration has a wide spread of data, with recordings varying from horizontal accelerations of 0.025 g to 0.15 g for intensity MMI=V event.

The design earthquake for seismic risk analysis at Project Minerva is based on the empirical data of normal shallow focus (<12 miles) earthquakes on soft sites (Leeds & Associates, 1989). (Leeds & Associates, 1989) assumes that in the Gulf coastal seismic environment, the release of energy from less competent materials than usual, would result in longer surface rise times; therefore, the ground motion would be biased to longer periods with lower frequencies and result in low accelerations, large displacements, and long durations.

Studies over the years of the effect of depth on seismic ground motion have all noted the attenuation that is realized with depth. Observations in deep mines and boreholes have confirmed this phenomenon. The data strongly indicates dampening of amplitude with depth and are an average of one-half, or less, of the ground motion. The motion may be as low as one-fifth and for small motions, where the materials remain completely elastic, the diminution of amplitude may be as small as much one-tenth (Leeds & Associates, 1989).

The effect of ground motion on saturated granular soils is the buildup in pore water pressure. If the water table is located near the surface (within about 15 ft to 20 ft), if the sands are reasonably well sorted and clean (free of clay), and if ground accelerations exceed about 0.25 g, a type of soil failure known as liquefaction can occur (Leeds & Associates, 1989). Liquefaction causes a loss of shear strength of the soil and may result in ejection of sand and water to the surface (sand boils), and collapse of the foundations of structures supported by soils. In extreme cases, multistory buildings have rolled over (Niigata, Japan Earthquake in 1964) and buried tanks have "floated" to the surface (Leeds & Associates, 1989). Following liquefaction, there is settlement and ensuing densification of the soil. Project Minerva does not meet the conditions expected to trigger liquefaction since the acceleration levels (0.05g) are only about one-fifth that required (Leeds & Associates, 1989).

As depth increases there is attenuation and reduction of motion. While pore pressures could increase, the soils framework is not used as support the lithostatic sediment column. Additionally, within the short duration of shaking, there is insufficient time or place for the fluid to go to. Thus, it remains incompressible. (Leeds & Associates, 1989) concludes that possible interactions between sedimentary horizons due to casings penetration and cement are minimal since there are only minor differential movements as the seismic wave passes through the matrix. They conclude that there might be only several centimeters of displacement over the wavelength of the seismic waves and that the normal elasticity of well casing and tubing is sufficient to accommodate the strain (Leeds & Associates, 1989). It is only in extreme cases, such as in Kern County, California, where surface accelerations can reach 0.5 g and there are many miles of surface rupture, that existing wells may be affected. The 1952 event, approximately 2% of the wells in the area had some surface damage due to settlement of surficial soils (Leeds & Associates, 1989). This event caused some subsurface damage including collapsed tubing near the surface due to the sharp rise in causing pressure accompanied the shock. However, all wells returned to normal status within 2-to-3 weeks of the event (Leeds & Associates, 1989).

2.6.4 Induced Seismicity

Seismicity related to fluid injections normally results from activity involving high pressures and large volumes, such as those associated with high-pressure water flood projects for enhanced oil recovery. The seismicity caused by increased pore pressure, which reduces frictional resistance, allows the rock to fail. Fluid withdrawals has caused land subsidence and earthquakes due to dewatering and differential compaction of the sediments. Earthquakes of a magnitude, ml of 3.4 to 4.3 on the Richter scale appear to have been caused by fluid withdrawal near some oil fields in east Texas (Davis, Pennington, & Carlson, 1989).

Since 2010, the occurrence of earthquakes with a magnitude, ml of ≥3.0 have increased from 20 events/year (from 1967-2000) to ≥100 events/year (2010-2013) in the central and eastern US regions (Ellsworth, 2013). The increased rate of occurrence in previously inactive seismic areas has been correlated with the increased use of injection wells located near faults. Fluid injections induced by earthquakes are mostly caused by the increased pore pressure from injection operations which have reduced effective stress of faults leading to

failure. This mechanism has been used to explain the best-known cases of injection-induced seismicity which was first studied in the Rocky Mountain Arsenal near Denver, Colorado. New case studies have increased the use of wastewater injection wells associated with hydraulic fracking. In many sites, smaller seismic occurrences have been shown to be precursors to larger events. More data has become available since the Rocky Mountain study in the 1960's, leading to a better understanding of factors and processes associated with induced seismicity.

One of the most notable regional cases of induced seismicity associated with injection wells occurred in Youngstown, Ohio. In 2011, a ml of 12 low-magnitude seismic events occurred along a previously unknown fault line (ODNR, 2012). These events occurred less than a mile from Class II injection well, Northstar I. Previously, the area was seismically inactive, with earthquakes beginning a few months after the injection of wastewater. The injectable pressure at Northstar I increased twice over 6 months (ODNR, 2012) and may have reduced the effective stress on a fault. After the well was shut down by the ODNR, the seismic activity declined. As a result of this case, seismic monitoring prior to injection and after injection has become common in Class II sites.

A case study in the Dallas-Fort Worth area tied small seismic events to a Class II injection well. There are 11 hypocenters in which have been observed at a focal depth of 4.4 km and 0.5 km from a deep saltwater disposal (SWD) well (Frohlich, Potter, Hayward, & Stump, 2010). Injection at this well began 8 weeks prior to the first recorded seismic event. A northeast trending fault is located approximately at the same location as the DFW focus (Frohlich, Potter, Hayward, & Stump, 2010). As a result of fluid injection into the disposal well, the stress upon the fault had been reduced and thus reactivated the fault (Frohlich, Potter, Hayward, & Stump, 2010). All the seismic events associated with the DFW focus are small magnitude events (less than 3.3) and occur very shortly after initial injection.

In Oklahoma, one of the largest earthquakes in the state's history may have been a result of wastewater injection at a Class II disposal site. In 2011, Prague, Oklahoma was the location of a 5.7 magnitude earthquake that was followed by thousands of smaller aftershocks. Wastewater had been pumped continuously into an old oil well for 17 years. As the pore spaces filled, the wellhead pressure increased to continually inject the wastewater. This reduced the effective stress upon the Wilzetta fault located 650 meters from the well (Keranen et al., 2013). The fluid was injected into the same sedimentary strata at which 83% of the aftershocks originated (Keranen et al., 2013). In this case, the seismic event occurred years after the initial injection phase. Since the area was considered low risk seismically, there is no data on smaller earthquakes that may have proceeded with the event in 2011.

In north-central Arkansas, multiple earthquakes have been triggered because of a Class II injection well. Since the operation of the disposal well in 2009, the site has experienced an increase from two events in 2008 to 157 events in 2011 (Horton, 2012). It was also tied to the discovery of a new vertical fault. 98% of earthquakes within this area occurred within 6 km of one of three waste disposal sites (Horton, 2012). The depth of the earthquake foci occurred between 6.7 and 7.6 km. Injection of fluid occurred at a depth of 2.6 km. At this disposal site, E-W trending (Enders Fault) cut into the aquifer in which the fluid was injected

and then acted as a conduit to the new fault at the depth of 6.7 to 7.6 km (Horton, 2012). The disposal wells were shut down in 2011 by the Arkansas Oil and Gas Commission. The rate and size of the earthquakes steadily decreased following the shutdown of the wells (Horton, 2012).

In Texas there are at least two known examples of previously seismically inactive areas becoming seismically active after major injection programs began. One site is located in the Central Basin Platform, near Kermit, and the other is in the Midland Basin near Snyder. In both cases, large scale, high pressure, oil field related, water flooding projects were under way, and earthquakes with a magnitude of over 4.0 on the Richter.

2.7 HYDROLOGIC AND HYDROGEOLOGIC INFORMATION

2.7.1 Data Sources

All hydrologic and hydrogeologic data was sourced from the C&E, Strategic Online Natural Resources Information System (SONRIS), TWDB Submitted Drillers Reports Database (SDRD), and publicly available published literature from the TWDB and USGS.

The SONRIS database was used to source all water well data for the state of Louisiana and the TWBD SDRD was used to source all water well data for the state of Texas. Well log data was used to construct maps using the well locations and depths as control points and calculate formation fluid salinity by determining the resistivity of the formation fluid (R_w). See Section 2.7.2 (USDW within the AoR) for a detailed discussion. All publicly available published literature was sourced for published cross-sectional maps, isopach and structural maps, graphs and charts regarding thickness and depth, and/or research regarding characteristics and properties of hydrogeologic units.

2.7.1.1 Water Wells and Data Sets

Water well data was sourced from the C&E SONRIS database. The SONRIS database includes the best available sources of well data for the state of Louisiana. Water well data is current through August 2024.

All water wells were searched and identified within Project Minerva's AoR and are represented on Figure 2.7.1-1. Table 2.7.1-1 includes data for water wells within the AoR as well as water wells within a conservative 2-mile radius from Project Minerva's AoR.

Within the AoR, there is only one water well (58911Z) (Figure 2.7.1-1 and Table 2.7.1-1). Water well 5891Z is an active well completed at 400 ft below ground level and withdraws from the Chicot aquifer, with the "200-foot sand" as the main water supply. Water is not withdrawn from the deeper Evangeline aquifer for public use within Project Minerva's AoR.

2.7.2 USDW within the AoR

The base of the lowermost USDW is identified across Project Minerva based upon 91 publicly available well log data. Figure 2.7.2-1 shows the locations of well log data used to determine the lowermost USDW and the structural interpretation of the lowermost USDW at Project Minerva. Figure 2.7.2-2 and Figure 2.7.2-3 show the lateral extent of the lowermost USDW across Project Minerva's AoR.

The nearest well to MS CCS 1 and MS CCS 2 that logs the base of the lowermost USDW is Watkins Well No. 80 (Map ID 5, SN 46471) (Figure 2.7.2-1). Based on SONRIS, the lowermost USDW was identified on the log at approximately -1,020 ft KB, however the base of the sand unit that contains the USDW is interpreted at approximately -1,090 ft KB (Figure 2.7.2-3).

This interpretation is consistent with C&E's guidance for estimating the lowermost USDW. Their methodology utilizes the deep induction curve of an open-hole log and uses the following resistivity (ohm) threshold at various depths to define the USDW:

- Ground surface to -1,000 ft: 3.0 ohms or greater is considered USDW,
- -1,000 ft to -2,000 ft: 2.5 ohms or greater is considered USDW, and/or
- -2,000 ft and deeper: 2.0 ohms or greater is considered USDW.

The lowermost USDW must be selected at the base of the sand unit (with an underlying isolating shale) that contains the resistivity values defined as USDW. At Project Minerva, the USDW is identified at a depth range of approximately -1,110 ft to -1,200 ft KB, based on the C&E methodology.

The lowermost USDW is consistent with the base of the "700-foot sand" in the Chicot Aquifer at Project Minerva. The base of the lowermost USDW does not follow the stratigraphic formations and the units above the lowermost USDW are hydraulically connected. Therefore, the lowermost USDW varies from the upper portion of the Evangeline aquifer into the base of the "700-foot sand" of the Chicot aquifer based upon the conservative 2-ohm resistivity cutoff.

The position and depth of the lowermost USDW is influenced by the proximity of well log data to the adjacent Black Bayou Dome. Near the Black Bayou Dome, the lowermost USDW deepens slightly from approximately -1,000 ft to approximately -1,250 ft MSL. The lowermost USDW is located approximately at the base of the Chicot aquifer's 700-Foot Sand (Figure 2.1.2-4 and Figure 2.1.2-5). However, the sands of the aquifers are mostly saline groundwater at Project Minerva and are not usable groundwater sources in Cameron Parish, Louisiana.

The top of salt at Black Bayou Dome is deep, and saline influence from the salt dome on the overlying aquifers is prevented due to a thick caprock covering the dome. However, as the strata dips towards the Louisiana Gulf Coast, evidence of saltwater encroachment into the deeper aquifers, such as the Evangeline aquifer and Jasper aquifer exist in the southernmost portion of Calcasieu Parish and in Cameron Parish, Louisiana due to pumping operations. The Chicot Aquifer though less impacted by the increase in groundwater withdrawals and saltwater encroachment.

2.8 GEOCHEMISTRY

2.8.1 Geochemical Study

GCS conducted a geochemical study for Project Minerva, focusing on the interactions between the injected CO_2 stream, formation fluids, and surrounding geological solids. The study aimed to identify factors influencing the AoR over time and to ensure stability.

Additionally, GCS examined key processes affecting CO_2 dissolution, the potential for mineralization, and reactions that could increase environmental risks.

In the absence of site-specific data, GCS used the analogous data from the CECOS Project as a basis for assessing potential geochemical reactions that impact injectivity and storage. The CECOS Project is a Class I Injection Well project at the CECOS Waste Disposal Facility in Calcasieu Parish, Louisiana, approximately 30 miles northeast of Project Minerva. The CECOS well, WDW Well No. 004 (WDW-4), SN 975888, was completed in the upper Frio Formation at a total depth of 7,900 ft Kelly Bushing (KB). The completion report for WDW-4, which includes formation fluid laboratory analysis from the Frio Formation and an x-ray diffraction report for the cores from the Anahuac (Confining Zone) and upper Frio (Injection Zone) Formations, is included as Appendix VII-1. A summary of the laboratory analysis of the formation fluid from the Frio Formation is provided as Table 2.8.1-1, and a summary of mineralogy from the Anahuac and Frio Formations based on the X-ray diffraction analysis is presented in Table 2.8.1-2.

Per the Pre-Operational Logging and Testing Plan (Attachment C), GCS will collect whole cores from the Confining and Injection Zones and formation fluid from the Injection Zone during the drilling of MS CCS 1. The formation fluid samples will be analyzed to characterize their chemical and physical properties, validating assumptions about the compatibility of formation water with the CO_2 stream. The whole cores from the Confining and Injection Zones will be analyzed for their mineralogy, further supporting the assessment of geochemical compatibility related to these formations and the CO_2 stream.

The following sections outline the study of the constituents of the proposed CO_2 stream, the formation fluid, and the formation solids; the potential geochemical reactions in a CCS system; and recommendations for preliminary geochemical modeling.

2.8.1.1 Physical and Chemical properties

CO_2 Stream

The concentrations of various constituents in the proposed CO_2 stream for Project Minerva are presented in Table 2.8.1-3, along with a description of its behavior in geological formations and the potential environmental impacts.

Nitrogen (N_2) and methane (CH_4) form significant constituents of the CO_2 stream. N_2 and CH_4 particularly affect the density, viscosity, and compressibility of the CO_2 mixture and thus require integration into the simulation model. The interactions and behaviors of these gases in the CO_2 stream are essential for optimizing operational strategies and ensuring safe, effective long-term carbon storage, and defining the AoR.

Nitrogen

In the context of reservoir simulation, N_2 significantly impacts:

- Density (reduced)
- Compressibility (increased)
- Joule-Thomson cooling effect during expansion

- Phase envelope (changes critical point)

Omission of Nitrogen in the simulation modeling can lead to inaccurate predictions of pressure, temperature, and flow dynamics.

Methane

In the context of reservoir simulation, CH_4 significantly impacts:

- Density (reduces)
- Compressibility (increased)
- Phase envelope (changes critical point and two-phase regions)
- Storage in the reservoir via competitive interactions between CO_2 and methane

Omission of methane in the simulation modeling can lead to inaccurate predictions of pressure, temperature, and flow dynamics.

Formation Fluid

GCS utilized the nearest offset data from the CECOS Project to establish a baseline profile of the formation fluid for Project Minerva. A summary of the formation fluid laboratory analysis is provided as Table 2.8.1-1.

The formation fluid exhibits the following key physical characteristics:

- pH: 6.96 (slightly acidic)
- Temperature: 67.8 °F (20 °C)
- Density: 1.0782 g/cm3 (relatively high, indicating a significant amount of dissolved solids)
- Conductivity: 15,2700 uS/cm (high, confirming high salinity)
- Resistivity: 7 ohm*cm (low, consistent with high conductivity)
- TDS: 97,728 mg/L (very high, indicating a highly saline brine)

The key chemical characteristics include:

- Chloride (Cl): 69,383.9 mg/L
- Sodium (Na): 30,745.89 mg/L
- Calcium (Ca): 2,460.64 mg/L
- Magnesium (Mg): 770.47 mg/L
- Barium (Ba): 15.57 mg/L
- Strontium (Sr): 137.66 mg/L
- Iron (Fe): 40.18 mg/L
- Sulfate (SO4): 51.37 mg/L
- Silicon (Si): 9.7 mg/L

Mineralogy

In absence of core analysis from the proposed site, GCS utilized the nearest offset core analysis of the Anahuac Formation (Confining Zone) and upper Frio Formation (Injection Zone) from the CECOS project. A summary of the mineralogy from the x-ray diffraction is provided as Table 2.8.1-2.

Confining Zone

Based on the mineralogy identified in the core sample of the Anahuac Formation (Table 2.8.1-2), the Confining Zone is dominated by illite and quartz, with lesser amounts of smectite or illite/smectite mixed-layer clays, and minor proportions of kaolinite. Calcite and dolomite are present as separate fragments in cuttings, likely representing bioclastic fragments as well as diagenetic cements (possibly concretions). Minor amounts of pyrite are also present.

The high content of total clay (52.2% to 64.8%) suggests that the Anahuac Formation is predominantly a shale or claystone formation. Such formations are known for their low permeability and are effective as confining layers, capable of preventing fluid migration.

Injection Zone

Based on the mineralogy identified in the core sample of the Frio Formation (Table 2.8.1-2), the core samples from the proposed Injection Zone were dominated by quartz grains. With quartz content ranging from 61.6% to 66.4%, the upper Frio Formation appears to be a sandstone formation. High quartz content is characteristic of sandstones, making these formations generally more permeable than shales. K-Feldspar content ranges from 11.8% to 17.6%, providing a robust framework for fluid movement. The presence of K-feldspar also supports the classification as sandstone since feldspars are common in clastic, sandy environments.

In contrast to the Anahuac Formation, the total clay content in the Frio Formation is significantly lower, ranging from 4.0% to 11.4%, which contributes to enhanced permeability and facilitates the injection process. Additionally, the calcite content is minimal, at just 0.3%, but its dissolution and secondary precipitation can serve an effective mineral trapping mechanism for CO_2. Other present minerals include plagioclase and pyrite, which further contribute to the geochemical diversity of the formation.

2.8.1.2 Geochemical Reactions

CO_2 Stream Reactions

CO_2 is highly soluble in brine, forming carbonic acid, influencing pH and impacting the reservoir simulation via geochemical reactions (e.g., lowers pH and promotes mineral dissolution/precipitation). N_2 and CH_4 have very low solubility in saline water compared to CO_2:

- N_2 solubility: ~0.02 mol/kg at reservoir conditions.
- CH_4 solubility: slightly higher than N_2 but still much lower than CO_2 (Sørensen, 2002).

The majority of injected N_2 and CH_4 is predicted to remain in the gas phase and will not dissolve in the Injection Zone fluid. Additionally, they are inert. Consequently, N_2 and CH_4 do not react significantly with brine or minerals. Their presence mainly affects physical trapping, not chemical trapping. This is represented in the simulation model and resulting AoR.

For the above reasons, the geochemical discussion focuses on CO_2 interactions with the formation fluids and minerals in the proposed reservoir.

Aqueous Reactions

CO_2 Dissolution

Supercritical CO_2 is dense and highly soluble in saline water under reservoir conditions (Rosenbauer, 2005). Diffusion occurs due to the concentration gradient, where CO_2 moves from regions of higher concentration (the CO_2 plume) to regions of lower concentration in the surrounding brine. As CO_2 dissolves, it reacts with water to form carbonic acid:

$$(H_2CO_3): CO_2\,(g) + H_2O\,(l) \rightleftharpoons H_2CO_3\,(aq) \qquad \text{Equation 2.8-1}$$

Only a small fraction of the dissolved CO_2 exists as the acid H_2CO_3, the equilibrium constant being equal to 1.3 E-3 typically. The time scale to form H_2CO_3 is of the order of seconds. Though, carbonic acid is a weak acid that can dissociate into bicarbonate (HCO_3^-) and hydrogen ions (H^+) in an equilibrium reaction:

$$H_2CO_3\,(aq) \rightleftharpoons HCO_3^-\,(aq) + H^+\,(aq) \qquad \text{Equation 2.8-2}$$

This reaction introduces acidity into the brine, which can influence the solubility of minerals and the overall chemical environment. The bicarbonate (HCO_3^-) can further dissociate into carbonate (CO_3^{2-}) and hydrogen ions (H^+) in an equilibrium reaction:

$$HCO_3^-\,(aq) \rightleftharpoons H^+\,(aq) + CO_3^{2-} \qquad \text{Equation 2.8-3}$$

The reactions establish a chemical equilibrium determined by the pH of the brine and its ionic composition. The presence of dissolved salts in brine can influence the degree of dissociation of carbonic acid and the resulting pH. The dissolution of CO_2 increases the density and acidity of the brine, which may affect the solubility of minerals and other elements within the formation. This can lead to a reduction in the mobility of CO_2 back into the gas phase as it becomes more integrated into the aqueous solution.

Salinity

The salinity of formation waters affects the solubility of CO_2. Higher salinity, indicated by high TDS values, can enhance the density of the brine, which may improve CO_2 solubility due to increased ionic strength, leading to different geochemical reactions compared to freshwater systems (Sørensen, 2002). Increased salinity typically increases the density and viscosity of the formation water. This can affect the mobility of CO_2 during injection, as denser brine may restrict the upward movement of CO_2, potentially improving the stability of the stored CO_2. Saline water can modify capillary pressure relations within the formation, which in turn may impact the phase distribution of CO_2 and brine, affecting the effectiveness of capillary trapping mechanisms.

GCS conducted a salinity study (Section 2.5.2.5) of 12 wells in the immediate area of Project Minerva to estimate salinity using Pickett plots cross-checked with SP-log analysis (Table 2.5.2-2). The average salinity is 115 kppm ± 28 kppm, slightly high due to deeper wells and local salt-dome effects. The CECOS formation fluid analysis noted a TDS value of 97,728

mg/L (ppm), which falls within the standard deviation of the most-likely salinity value of 115 kppm. For permitting, the model used 115 kppm (most likely), 80 kppm (minimum), 150 kppm (maximum). The sensitivity study presented in Section 5.1 (Sensitivity Analysis) of the AoR and Corrective Action Plan (Attachment A) examines the system's sensitivity to salinity and its impact on dissolution and phase distribution.

pH, Temperature and Pressure

The pH of the brine affects the formation of carbonic acid (H_2CO_3) when CO_2 dissolves in water. A lower pH (higher acidity) can enhance CO_2 dissolution, as more CO_2 can be converted into H_2CO_3, leading to further dissociation into bicarbonate (HCO_3^-) and carbonate (CO_3^{2-}), which facilitate more CO_2 retention (Rosenbauer, 2005). Temperature and pressure of the formation fluid play a crucial role in determining the solubility of CO_2. Generally, higher pressures favor gas dissolution, while temperature can affect kinetic dynamics and solubility limits.

Mineral Reactions

Carbonates

When CO_2 is injected into a geological formation, it first forms carbonic acid, which can react with available ions to produce carbonates such as calcite (Ca^{2+}) or dolomite (Mg^{2+}). The equilibrium between carbonate species in the brine shifts with changes in pH: at lower pH levels, bicarbonate ions (HCO_3^-) dominate, while at higher pH levels, carbonate ions (CO_3^{2-}) become more prevalent. The availability of carbonate ions facilitates the precipitation of calcite, particularly at pH levels above approximately 6.5, with significant precipitation commonly occurring between pH 7.5 and 9.0. This reaction can be represented as follows:

$$Ca^{2+} + CO_3^{2-} \rightleftharpoons CaCO_3\,(s) \qquad \text{Equation 2.8-4}$$

Research highlights the crucial role of calcium in mineralization during CO_2 sequestration (Cygan, 1991).

In addition to calcite, other carbonate minerals like magnesite and dolomite can precipitate under certain conditions. The presence of magnesium can enhance the precipitation of magnesium carbonate, particularly when pH increases:

$$Mg^{2+} + CO_3^{2-} \rightleftharpoons MgCO_3\,(s) \qquad \text{Equation 2.8-5}$$

Similarly, dolomite can form when carbonic acid reacts with minerals such as calcite, releasing calcium and magnesium ions into the brine, which can then precipitate as dolomite:

$$Ca^{2+} + Mg^{2+} + 2CO_3^{2-} \rightleftharpoons CaMg(CO_3)_2 \qquad \text{Equation 2.8-6}$$

As CO_2 dissolves further, the system may re-equilibrate, leading to a gradual increase in pH and causing the brine to become supersaturated with respect to carbonate minerals. Among these reactions, calcite precipitation is particularly relevant to CO_2 injection projects due to its stability and the critical role it plays in long-term carbon storage.

Silicates

Silicates, such as quartz (SiO_2), plagioclase ($NaAlSi_3O_8$), and potassium feldspar ($KAlSi_3O_8$), are present in the mineralogy of the upper Frio Formation.

Quartz (SiO_2) is chemically inert, meaning it typically does not react directly with CO_2 or carbonic acid under normal reservoir conditions. However, it can influence the surrounding chemistry by affecting fluid flow and mineral interactions.

Plagioclase ($NaAlSi_3O_8$) can undergo hydrolysis, particularly in acidic conditions created by the presence of carbonic acid. This reaction leads to the release of sodium ions (Na^+) and silica (SiO_2) in the form of silicic acid:

$$NaAlSi_3O_8 + 2H_2CO_3 + 9H_2O \rightarrow Al_2Si_2O_5(OH)_4 + 2Na^+ + 4H_4SiO_4 + 2HCO_3^- \quad \text{Equation 2.8-7}$$

This reaction can increase the concentrations of sodium and silicic acid in the surrounding pore water. Hydrolysis of potassium feldspar ($KAlSi_3O_8$) under acidic conditions can occur, leading to clay mineral formation and the release of potassium (K^+) and silica (SiO_2): this reaction releases potassium ions and silicic acid into the formation water, potentially leading to the formation of secondary clay minerals.

Clays

Illite, a type of clay mineral, can also undergo similar reactions as smectite. In an acidic environment, components such as potassium ions (K^+) can be released, and the mineral may stabilize or alter:

$$\text{Illite-}K^+ + HCO_3^- \rightleftharpoons \text{Illite-}HCO_3^- + K^+ \quad \text{Equation 2.8-8}$$

Smectite is another type of clay mineral characterized by its capacity for cation exchange and swelling. The presence of CO_2 leads to the formation of carbonic acid, which can enhance the capacity of cation exchange. The general reaction for cation exchange can be expressed as:

$$\text{Smectite-}Na^+ + H^+ \rightleftharpoons \text{Smectite-}H^+ + Na^+ \quad \text{Equation 2.8-9}$$

If the pH decreases due to the acidic conditions generated by the injection of CO_2, smectite may lead to the release of exchangeable cations (like Na^+, Ca^{2+}, K^+), altering its mineral structure and promoting mineral transformations.

Secondary Mineral Formation

Cation exchange from clays like smectite, particularly with the release of calcium (Ca^{2+}), can lead to the precipitation of secondary carbonate minerals such as calcite ($CaCO_3$) when equilibrium conditions shift:

$$Ca^{2+} + 2HCO_3^- \rightleftharpoons CaCO_3\,(s) + H_2CO_3 \quad \text{Equation 2.8-10}$$

If calcite precipitates and reduces the concentration of Ca^{2+}, or if sodium from dissolved plagioclase becomes available, the brine can become supersaturated with respect to plagioclase ($NaAlSi_3O_8$):

$$Na^+ + Al_2O_3 + 3SiO_2 + H_2O \rightleftharpoons NaAlSi_3O_8\,(s) \quad \text{Equation 2.8-11}$$

Smectite clays can also facilitate the release of sodium ions into the solution through cation exchange:

$$\text{Smectite-Na}^+ + \text{H}_2\text{O} \rightleftharpoons \text{Smectite-H}_2\text{O} + \text{Na}^+ \qquad \text{Equation 2.8-12}$$

These released sodium ions contribute to the saturation necessary for plagioclase precipitation if silicate species, such as SiO_2, are present.

Near Wellbore Scaling

In CO_2 injection environments, various precipitates can form near the wellbore, presenting challenges for injectivity and flow. High concentrations of iron (Fe) can lead to significant iron scaling, as iron reacts with carbonate ions to form iron carbonate (FeCO3):

$$\text{Fe}^{2+} + \text{CO}_3^{2-} \rightleftharpoons \text{FeCO}_3(s) \qquad \text{Equation 2.8-13}$$

If oxygen is present, iron oxides may also form, which contributes to further precipitation issues.

Barite scaling can occur when barium (Ba) and sulfate (SO4) combine to produce barium sulfate (BaSO4), especially with changes in pressure or temperature:

$$\text{Ba}^{2+} + \text{SO}_4^{2-} \rightleftharpoons \text{BaSO}_4(s) \qquad \text{Equation 2.8-14}$$

This precipitation phenomenon is difficult to remove and can significantly impair well injectivity.

Additionally, the injection of CO_2 may induce halite precipitation from highly saline pore waters adjacent to the injection well, resulting from water vaporization into CO_2. Although this is characteristic of very saline formation fluids, the moderate salinity of the Injection Zone at Project Minerva makes significant halite precipitation unlikely. Nonetheless, if dissolved salts (Na^+ and Cl^-) become overly concentrated, halite (NaCl) may precipitate:

$$\text{Na}^+ + \text{Cl}^- \rightleftharpoons \text{NaCl}(s) \qquad \text{Equation 2.8-15}$$

Overall, the potential for iron scaling, barite formation, and halite precipitation poses operational challenges that must be managed to maintain effective CO_2 injection and storage.

Trace Metals

The formation of metal-hydroxide complexes and the coordination of metal ions with dissolved species can occur, influencing trace metal mobility and retention in the formation.

Iron is primarily sourced from the oxidation of pyrite (FeS_2), a common mineral that can release ferrous ions (Fe^{2+}) under acidic conditions following CO_2 injection. Pyrite oxidation can be represented as:

$$\text{FeS}_2 + \text{O}_2 + 4\text{H}_2\text{O} \rightarrow 2\text{Fe}^{2+} + 2\text{SO}_4^{2-} + 4\text{H}^+ \qquad \text{Equation 2.8-16}$$

This reaction highlights how CO_2-induced acidification can mobilize iron into the formation water.

The oxidation of pyrite and the subsequent release of iron would be diminished in a higher pH environment. The reaction for pyrite oxidation, which is facilitated by acidic conditions, would be suppressed. Therefore, significant amounts of ferrous iron would not be released into the formation water.

With a pH above 5, metal-hydroxides (e.g., ferric hydroxide) may begin to precipitate rather than remain in solution, further reducing the mobilization of metals like iron. This precipitation can also lead to the retention of other trace metals that could have been released in a more acidic context, limiting their potential environmental hazard (Worden, 2003).

Trace metals in clays and other minerals rely on acidic conditions for optimal solubility and mobilization. A higher pH would reduce the solubility of many metal ions and thereby limit the complexation reactions that typically enhance metal mobility. For example, zinc, lead, and cadmium may not be as readily released from clay minerals due to decreased ion exchange processes when pH is above 5.

2.8.1.3 Conclusion and Recommendations

In summary, the interactions between CO_2 and geological materials in carbon capture and storage (CCS) systems lead to a complex series of aqueous and mineral reactions that significantly influence geochemical environments. The dissolution of supercritical CO_2 in saline water forms carbonic acid, which enhances the brine's acidity and alters the solubility of minerals. This process is influenced by various factors, including salinity, pH, temperature, and pressure, each of which plays a critical role in determining the extent of CO_2 retention and mineral reactions.

The formation of carbonates, such as calcite and dolomite, illustrates how changes in pH can enhance carbonate precipitation, thus aiding in CO_2 sequestration via mineral trapping. Additionally, the hydrolysis of silicate minerals, like albite and feldspar, releases ions (sodium, potassium, and silicic acid) into the solution, potentially contributing to the precipitation of secondary minerals. However, acidic conditions also promote cation exchange processes in clay minerals, which can facilitate trace metal release and mobility.

Challenges arise from possible near-wellbore scaling due to iron carbonate formation and barite precipitation, both of which can impede injection efficacy. Moreover, the mobilization of trace metals, such as iron, zinc, and lead, can be affected by pH, with higher pH environments reducing the solubility and mobility of these metals. Overall, understanding these geochemical reactions is essential for optimizing CO_2 injection strategies, ensuring effective long-term storage, and minimizing environmental risks associated with CCS operations.

Based on this study, GCS identified the following components and processes to model geochemical reactions, examine the interactions, and evaluate changes in formation water chemistry, as well as mineral precipitation and dissolution, and their potential impact on formation permeability:

- **CO_2 dissolution in brine:** Modeled at most-likely pH, temperature, pressure, and salinity
- **Carbonates:** Calcite was selected due to its mineral trapping effect and the presence of Ca in the formation fluid and Calcite presence in the Injection Zone rock matrix
- **Silicates:** Plagioclase (albite) and potassium feldspar (K-feldspar) were selected since quartz is inert and does not directly react with CO_2 or carbonic acid
- **Clays:** Illite and smectite were selected due to their abundance in the Injection and Confining Zones and to understand the impact of possible ion exchange on the potential secondary precipitation
- **Near wellbore scaling:** Halite was selected as the most-likely constituent that would impact wellbore injectivity
- **Trace Metals:** Pyrite was selected based on its presence in the Injection Zone and its potential for mobility

The modeling results are presented in in the following section, along with the final parameters included in the final base case.

2.8.2 Preliminary Geochemistry Modeling

Geochemical modeling was utilized to simulate the potential interactions identified in the previous sections and predict potential outcomes, including the risk of trace element release into the environment. Together, these analyses provide a holistic view of the geochemical processes at play in Project Minerva, informing risk management and ensuring environmentally responsible sequestration of carbon dioxide.

2.8.2.1 Modeling Software

The reservoir simulations for Project Minerva were conducted using GEM, a fully compositional reservoir simulation software produced by CMG. A full description of CMG, the software's capabilities, and utilization for Project Minerva's simulations is provided in Section 2.10.5 (Modeling Approach and Simulation).

Within GEM, geochemical coupling is available through the GEM-GEOCHEM module. This module was activated for Project Minerva to model aqueous phase CO_2 dissolution, associated aqueous speciation, and mineral reaction. The model used a combination of equilibrium aqueous reactions that govern pH evolution and Transition State Theory (TST) kinetic reactions to capture mineral dissolution and precipitation rates where required.

CMG incorporates three primary CO_2 trapping mechanisms to accurately predict the long-term fate of the injected plume, as illustrated in the model setup:

1. **Solubility Trapping (CO_2 Solubility in Water)**: This mechanism occurs immediately upon injection as CO_2 dissolves into the saline formation water (brine), forming carbonic acid (H_2CO_3). This is the first line of chemical defense and is always selected in the model.

2. **Mineral Trapping (Rock Dissolution and Mineral Trapping)**: This long-term mechanism involves the slow chemical reaction of the acidic, CO_2-saturated brine with the reservoir rock matrix. This is a crucial component of permanent, irreversible storage and long-term pH buffering.
3. **Residual Trapping (Relative Permeability Hysteresis)**: This physical trapping mechanism occurs as the supercritical CO_2 plume migrates through the porous rock. As the plume passes, a fraction of the CO_2 is immobilized as isolated, immobile bubbles or ganglia trapped by capillary forces in the pore spaces. This is a highly effective, fast-acting physical trapping method.

To ensure geochemical accuracy given the high salinity of the formation water, the Pitzer activity model was selected for CCS options, as recommended for high-salinity brines.

2.8.2.2 Geochemical Modeling Results

The GEM-GEOCHEM model allows users to select the geochemical reactions associated with desired aqueous and mineral reactions. Users can initiate the "Input Geochemistry Data" portal which contains the Wolery Database thermodynamic data files for modeling geochemical reactions. Default reaction type, reactive surface area, activation energy and $\log^{10}$ of reaction rate values were applied in lieu of not having site-specific data.

Results Based on Initial Parameters

As discussed in Section 2.8.1.3 (Conclusion and Recommendations), the GCS geochemical study recommended the inclusion of:

- Standard aqueous reactions necessary to describe the CO_2-water system,
- Minerals that are representative of expected mineral reactions: calcite, plagioclase (albite), potassium feldspar (K-feldspar), illite, smectite, halite, and pyrite.

The geochemical reactions associated with these aqueous and mineral reactions were selected from the Worley Database reactions, as depicted in Figure 2.8.2-1.

The initial brine and aqueous compositions and mineral volume fractions were derived from the CECOS data discussed in Section 2.8.1 (Geochemical Study). Representative values were entered into the "Initial Data for Geochemistry" portal, as depicted in Figure 2.8.2-2.

Initial tests confirmed that the majority of minerals showed negligible molar change. Figure 2.8.2-3 shows that calcite, plagioclase (albite), and smectite exhibit the most significant molar change, while quartz, K-feldspar, pyrite and illite indicate very little molar change. While halite showed an increase in molar mass, the change is associated with near wellbore precipitation and does not impact the injectivity of the formation significantly.

Although quartz makes up the majority of the reservoir rock (~60% volume fraction), its kinetic dissolution rate is extremely slow (log k ~ -12.0). Over the 475-year simulation window, the molar change from Quartz dissolution is effectively zero. Including it would only increase computational time without contributing to pH buffering or permanent CO_2 storage.

K-feldspar (~ 14% volume fraction) is a silicate mineral with geochemical behavior similar to plagioclase (albite). However, its kinetic rate is slightly lower than that of plagioclase (albite) (log k for K-feldspar is typically around -10.0, compared to -8.8 for plagioclase (albite)). Therefore, plagioclase (albite) (~11% volume fraction) should be included as a conservative, kinetically representative proxy for all reactive silicate dissolution, ensuring the long-term buffering capacity is fully captured without redundancy.

Despite its very low volume fraction (0.27%), calcite is mandatory due to its extremely fast reaction rate (log k = -5.81). It is the primary, rapid-acting carbonate buffer that immediately stabilizes the pH of the acidified brine, preventing potential formation damage from highly acidic water.

The simulation was thus optimized to include only calcite, plagioclase (albite), and smectite, which dominate the geochemical kinetics and provide the necessary pH stability and long-term permanent storage, as shown in the base case model results.

Results Based on Final Parameters

The three mineral components—calcite, plagioclase (albite), and smectite—were specifically chosen because they represent the minerals with the highest chemical reactivity rather than purely volume fraction.

The geochemical reactions associated with the limited aqueous and mineral reactions were selected from the Wolery Database reactions, as depicted in Figure 2.8.2-4. Representative values for the aqueous and mineral parameters were entered into the "Initial Data for Geochemistry" portal, as depicted in Figure 2.8.2-5.

Figure 2.8.2-6 shows that calcite, plagioclase (albite), and smectite exhibit the most significant molar change, confirming they are the most chemically active minerals relevant CO_2 trapping and buffering.

2.8.2.3 Mass Balance Reflecting Geochemical Inputs

After incorporating the final parameters into the reservoir-geochemical simulation, the long-term fate and stability of the injected CO_2 over the 475-years of simulation period was analyzed. The CO_2 mass balance plot illustrates how the total injected mass of CO_2 is distributed among the four primary trapping phases over the simulation period.

Figure 2.8.2-7 displays the mass of CO_2 stored in different forms, measured in pounds (lb), over the simulation history. The graph illustrates the distribution and progression of CO_2 mass for Project Minerva over time. Initially, total CO_2 gas peaks rapidly, with a significant portion as free CO_2. Over time, the free CO_2 decreases as CO_2 becomes dynamically trapped and dissolves. The mass of CO_2 dynamically trapped stabilizes, indicating effective long-term storage, while dissolved CO_2 and mineralized CO_2 gradually increase, reflecting ongoing chemical interactions and mineralization. Aqueous Ion CO_2 remains relatively low, suggesting limited impact on ionic concentration. Overall, the project demonstrates a successful transition from mobile gas to stable forms, ensuring effective sequestration.

2.9 OTHER INFORMATION

2.9.1 Magnetometer Survey

To preform due diligence on Project Minerva, GCS hired a third-party vendor to conduct an extensive search to identify any potential undocumented artificial penetrations. The main objective was to locate potential leak points that could provide pathways for fluids to vertically migrate outside of the proposed Injection Zone. The search covered an area of interest that encompasses approximately 10,400 acres and incorporates drone-based aerial surveys to efficiently and non-invasively cover the large area. The Figure on page 3 of Appendix VIII-1 (Magnetometer Survey Strategy) depicts the search area encompassing the Project Minerva AoR plus an additional 6,837 acres, including the 0.25-mile boundary buffer established within the AoR and Corrective Action Plan (Attachment A).

One drone conducts a magnetometer survey, with flight lines spaced at 50m with 500m spaced tie lines. During flight, the magnetometer continuously records the magnetic field at 10 Hz intervals. A base station magnetometer was deployed to account for background magnetic variability. A second drone captured Red, Blue, and Green (RGB) Imagery, which provides a 5 cm resolution image. GCS included this add-on imagery map to rule out obvious cultural features, such as metallic infrastructures or hurricane debris. All aerial data was processed to remove noise and correct for any diurnal variations and maneuver errors. A magnetic interpretation expert reviewed the Total Magnetic Intensity (TMI) data and RGB image together to map and identify any magnetic anomalies. The combination of these two data types provides a location accuracy of 5 m to 30 m.

The final interpretation report is provided in Appendix VIII-2 (Magnetometer Survey Results). GCS assessed and identified all magnetic anomalies listed by the interpretation expert. Ground truthing efforts were deployed for flagged anomalies that could not be confidently identified. See the AoR and Corrective Action Plan (Attachment A) for specifics.

2.10 SITE SUITABILITY

2.10.1 Lithological Distribution

The intervals of interest at Project Minerva are the Oligocene and Miocene deposits of the Gulf Coastal Plain. The Oligocene and Miocene deposits are characterized by rapid subsidence in areas of high sediment loading through multiple cyclic depositional episodes. The Oligocene and Miocene deposits are subdivided according to depositional cycles and paleontological zones (Foote, 1984; Swanson, Karlsen, & Valentine, 2013). Figure 2.1.1-5 represents the depositional cycles of the subdivisions listed below, in ascending order:

- Vicksburg Group (early Oligocene). Represents a transgressive phase (mainly shale and some sandstone lenses),
- Frio Formation (middle Oligocene). Split into the lower, middle, and upper Frio Formation. Represents a dominantly regressive phase. The upper Frio comprises a mixture of marginal marine and deltaic sandstones and shales, with localized deep marine shales. The lower and middle Frio are dominated by deep marine shales and

turbidite sandstones. Downdip equivalent of the continental Catahoula Formation (Swanson, Karlsen, & Valentine, 2013). The Injection Zone is located in upper Frio Formation, and the Lower Confining Zone is defined as a shale interval near the base of the upper Frio Formation.

- Anahuac Formation (late Oligocene). Represents transgression (marine shales and thin sandstones). This formation is the Upper Confining Zone at Project Minerva, and
- Fleming Formation (Miocene). Represents a very high number of alternating regressive and transgressive phases (progradational sandstones and retrogradational shales). This formation serves a potential containment interval should fluids unexpectedly migrate outside of the Upper Confining Zone.

The Upper Confining Zones, Injection Zone, injection intervals, and Lower Confining Zone have been chosen based on each of the reservoir's permeability, porosity, thickness, and lateral continuity to accept and contain injected material. The massive fluvial-deltaic sandstones of the upper Frio Formation provide effective injection reservoirs in terms of their lateral extent, mineralogical composition, and petrophysical characteristics. The overlying aquiclude layers in the upper Frio Formation are sufficiently thick, impermeable, and laterally continuous to contain the injected fluids in the Injection Zone. Shales of the overlying Anahuac Formation possess the necessary Confining Zone criteria to be effective barriers for potential upward migration. The thick Anahuac Formation shales extend laterally across the region and are well over 1,000 times less permeable than the underlying injection reservoirs. Additionally, more than 5,000 ft of overlying, shale-rich Miocene section provides a containment interval to capture and retain any fluids that might migrate vertically through an undetected potential breach in the Injection Zone and Upper Confining Zone. The existence of multiple sand/shale layers between the top of the Injection Zone and the base of the lowermost USDW ensures additional protection from the contamination of a USDW.

Lateral and vertical continuity of the Confining Zones, Injection Zone, and injection intervals can be confidently interpreted throughout the AoR. Figure 2.1.2-1, Figure 2.1.2-2, and Figure 2.1.2-3 demonstrate the mapped intervals of interest across the AoR.

2.10.2 Confinement

Project Minerva benefits from the characteristics noted below to form a robust framework for effective CO_2 containment. The interplay of physical barriers, chemical processes, and geological features ensures that injected CO_2 will not migrate from the designated storage formation, thus contributing significantly to the overall effectiveness of carbon capture and storage strategies.

- A Confining Zone with high enough capillary entry pressure to prevent vertical CO_2 migration.
- Shale Gouge Ratio (SGR) and Clay Smear Potential (CSP) values of 91% and 94%.
- Sufficient areal extent and integrity to contain CO_2 stream and potential displaced formation fluids.

- Buoyancy trapping against the Upper Confining Zone.
- Relative permeability hysteresis trapping.
- Dissolution of gaseous phase CO_2 into the formation's aqueous phase.
- Mineralization trapping of CO_2.

2.10.3 CO_2 Stream Compatibility

Table 2.10.3-1 provides the proposed CO_2 stream specification for Project Minerva. This specification is designed to ensure safe operation of the project work and ensure no-endangerment of USDWs. Project Minerva will utilize CO_2 from multiple sources, all capable of meeting or exceeding the specified requirements, which the reservoir simulation model has fully accounted and explored.

The proposed CO_2 stream is compatible with the mineralogy, petrology, and pore waters of the Injection Zone and the Confining Zone. As previously discussed in Section 2.8 (Geochemistry), GCS studied the effect of CO_2 injection at reservoir conditions. Geochemical interaction between the injected CO_2 and the subsurface formations, beyond the dissolution of some gaseous CO_2 into the formation fluids, are not expected to negatively impact injection or potentially endanger the USDW at Project Minerva.

Appendix IX (CO_2 Stream Compatibility) provides an overview of the study set up, analysis and results of the material section analysis for Project Minerva. Appendix IX-1 presents material selection analysis conducted by Nippon Steel Corporation which was based on the proposed GCS CO_2 stream composition and well conditions. The analysis recommended Super Duplex Stainless Steel (SM25CRW) as the best CO_2 compatible option for expected conditions. GCS' inclusion of SM25CRW in the well design is discussed in detail in Section 5.3.3 (Borehole and Casing Size and Grade).

The primary cement used in the long string within the Injection and Confining Zones will be a specialized CO_2 compatible cement. Although final vendor selection has not been made, Appendix IX-2 provides specifications for PermaSet™ System Cement, a proprietary blend developed by Baker Hughes. GCS will ensure that final cement selection is equally compatible with the proposed injection environment. The complete cementing program is presented in Section 5.4 (Cementing Program).

2.10.4 Storage Capacity

The Injection Zone is a laterally extensive, high net-to-gross interval with significant storage capacity, as evidenced by the region's extensive history of oil and gas development. Within Project Minerva, some local variations in pay sand thickness and lateral extent are observed in the facies models, but the overall interval remains geologically robust.

Facies were interpreted using SP logs, applying a PHIE ≥ 10% cut-off to define sand packages. These packages represent the sand to shale sequence, reflecting the high net -to-gross interval and are illustrated in Figure 2.2.1-10.

2.10.5 Modeling Approach and Simulation

The reservoir simulation model for Project Minerva was developed using the CMG software suite, an industry-standard platform for CO_2 storage modeling. CMG provides a comprehensive set of physics, numerical solvers, and coupled modules that enable detailed simulation of multiphase flow, compositional behavior, geochemistry, thermal processes, and geomechanical responses. All geological, petrophysical, and fluid-property data assembled for the project were incorporated into this modeling environment to construct the dynamic reservoir simulation model referenced throughout the permit application and supporting documents.

2.10.5.1 CMG Modeling Platform and Full Capabilities

CMG Version 25.30 includes several advanced modules relevant to CO_2 storage. GEM simulator forms the core of the Project Minerva model. GEM is a fully compositional, three-dimensional reservoir simulator capable of representing aqueous, gaseous, and oil phases, although only the aqueous brine and CO_2-rich gaseous/supercritical phases are used in this project. GEM's full component mass-balance formulation captures multiphase flow driven by viscous, capillary, and buoyancy forces. Fluid behavior is modeled using the Peng–Robinson Equation of State (EOS) through WINPROP (Peng and Robinson, 1976), allowing CO_2 density, viscosity, and phase behavior to depend on pressure, temperature, and composition.

CMG provides several advanced physics options that can be activated as needed. The GEM-THERMAL module supports full energy balance calculations, including conductive and convective heat transfer, temperature-dependent phase behavior, and Joule–Thomson effects. The GEM-GEOMECH module provides two-way coupling between pore pressure, temperature, and mechanical deformation, enabling simulation of effective-stress changes, pore-volume strain, permeability evolution, caprock integrity, and fault slip tendency. The GEM-GEOCHEM module supports reactive transport, aqueous speciation, mineral–fluid reactions, and pH evolution. CMG also integrates with WINPROP for fluid characterization, Builder for model construction and grid generation, and CMOST-AI for optimization and uncertainty analysis.

Together, these capabilities provide a complete reservoir simulation environment suitable for detailed evaluation of CO_2 injection, plume migration, long-term stabilization, and mechanical integrity.

2.10.5.2 Capabilities Activated in the Project Minerva Model

For Project Minerva, the reservoir model activates those CMG capabilities necessary to simulate the dominant physical processes governing CO_2 storage in the Frio Formation. The simulation employs GEM's full compositional flow formulation, including pressure-, saturation-, and composition-dependent fluid properties. The injected CO_2 stream is represented using a simplified three-component mixture of 97 mol% CO_2, 1.5 mol% CH_4, and 1.5 mol% N_2. Table 2.10.3-1 details the CO_2 composition planned for Project Minerva. Henry's Law based dissolution is applied to represent CO_2 partitioning into the aqueous

phase, enabling solubility trapping. Relative permeability and capillary pressure functions include hysteresis to represent drainage and imbibition cycles and residual trapping.

The GEM-GEOCHEM module is fully activated in the model. Reactive transport is solved concurrently with compositional flow, enabling simulation of aqueous-phase speciation, dissolved CO_2 chemistry, mineral dissolution and precipitation kinetics, brine density evolution, and pH changes.

The model uses a fully implicit finite-difference solver with adaptive timestep control, and the computational grid uses corner-point geometry to honor stratigraphic dip, reservoir structure, and fault offsets.

Although GEM includes full thermal and geomechanical coupling capabilities, these modules are not activated in the current simulation. The model is run under isothermal conditions, as temperature changes associated with CO_2 injection are expected to be small relative to multiphase flow effects and would not materially influence plume migration or pressure evolution for AoR delineation.

Similarly, GEM-GEOMECH is not activated because site-specific mechanical property data (e.g., Young's modulus, Poisson's ratio, Biot coefficient, cohesive strength) have not yet been collected from the Project Minerva wells. Geomechanical behavior is instead evaluated analytically and conceptually, as described in Section 2.5.1 (Geomechanical Information) of this document and the AoR and Corrective Action Plan (Attachment A), using fracture-pressure analysis and fault-stability screening. Excluding thermal and geomechanical coupling yields a conservative model configuration, ensuring that simulated pressures and plumes do not underestimate potential reservoir response.

2.10.5.3 Simulation Grid and Model Domain

The simulation grid was constructed in Petrel and exported to CMG using the RESQML/RESCUE format. The final structured corner-point grid consists of 125 grid cells in the X-direction, 87 cells in the Y-direction, and 63 cells in the Z-direction, totaling 685,125 cells, of which 476,812 are active. Horizontal coordinates are expressed in feet, and temperatures are expressed in degrees Fahrenheit.

The model domain spans approximately 58,080 ft (11 miles) in the X-direction and 42,240 ft (8 miles) in the Y-direction. A uniform horizontal discretization of 500 × 500 ft was selected to ensure consistent lateral resolution of the CO_2 plume and pressure front while maintaining numerical stability and computational efficiency. Vertical discretization consists of stratigraphically proportional layers, which preserve gross geological thickness and heterogeneity. This approach provides the highest vertical resolution within the Injection Zone, where accurate representation of buoyancy, saturation changes, and dissolution is required. Coarser vertical resolution is used in the Confining Zone, where fewer hydraulic changes occur and less detail is necessary.

2.10.5.4 Physical Processes Represented in the Model

The Project Minerva GEM model simulates CO_2 injection under isothermal conditions, resolving the multiphase flow of CO_2 and brine during both injection and long-term post-

injection periods. CO_2 is injected at fixed rates in its supercritical state, and GEM captures the resulting evolution of pressure, saturation, and fluid properties. Buoyancy-driven vertical migration is explicitly resolved, and solubility trapping is represented through dissolution of CO_2 into formation brine. Hysteretic relative permeability enables residual trapping, while reactive transport through GEOCHEM allows mineral–fluid interactions and pH changes to influence fluid behavior. No thermal effects, stress coupling, salt precipitation, or water evaporation into the CO_2 phase are included. These exclusions produce a conservative representation of reservoir performance.

3 AOR AND CORRECTIVE ACTION

3.1 PROJECT PLAN

The Area of Review (AoR) and Corrective Action Plan is provided as Attachment A of this Narrative. The AoR and Corrective Action Plan Report satisfies the requirements of LAC 43:XVII §3607.C.2.l, §3615.B.2, and §3615.B.3.

The report covers in detail the computational modeling approach to the delineation of the AoR, the Corrective Action Plan relating to existing well penetrations within the AoR, and the Reevaluation Schedule for AoR delineation once operations commence. A thorough review of the hydrogeology is also supplied, along with a comprehensive bibliography of references utilized during the AoR modeling execution and reporting phase.

3.2 SUBMISSION

The AoR and Corrective Action Plan Report (Attachment A) has been submitted to C&E for review and approval. In accordance with LAC 43:XVII §3629.A.5, the AoR and Corrective Action Plan Report (Attachment A) will be submitted to the USEPA.

4 FINANCIAL RESPONSIBILITY DEMONSTRATION

4.1 FINANCIAL RESPONSIBILITY DEMONSTRATION REPORT

The Financial Responsibility Demonstration Report is provided as Attachment B of this Narrative. The Financial Responsibility Demonstration Report satisfies the requirements of LAC 43:XVII §3607.C.2.m.

4.2 SUBMISSION

The Financial Responsibility Demonstration Report (Attachment B) has been submitted to C&E for review and approval. In accordance with LAC 43:XVII §3629.A.5, the Financial Responsibility Demonstration Report will be submitted to the USEPA.

5 INJECTION WELL CONSTRUCTION

GCS proposes to drill and complete two Class VI injection wells, MS CCS 1 and MS CCS 2, in compliance with LAC 43:XVII §3617, Well Construction and Completion requirements. GCS will ensure that all phases of Class VI well construction will be supervised by people who are knowledgeable and experienced in practical drilling engineering and are familiar with the special conditions and requirements of injection well construction.

Class VI injection wells are designed to ensure the permanent sequestration of CO_2 and prevent its movement into Underground Sources of Drinking Water (USDWs). The injection wells are constructed and operated to prevent fluid migration into or between USDWs, as well as into any non-approved zones. The design allows for the effective use of testing devices and workover tools and supports continuous monitoring of the annulus between the injection tubing and long-string casing.

Key factors considered in the well design include the expected injection volume, rate, chemical composition, and physical properties of the injectate, including its potential corrosiveness and interactions with wellbore materials. Appendix XII (Operating Plans) provides detailed operational parameters and CO_2 injection composition.

MS CCS 1 and MS CCS 2 will be constructed and operated to effectively manage pore space utilization in the reservoir, contain CO_2 within the authorized Injection Zone, and comply with LAC 43:XVII §3617.

Figures 5-1 and 5-2 provide wellbore schematics for MS CCS 1 and MS CCS 2, respectively. MS CCS 1 is planned as a vertical well, while MS CCS 2 is planned to be drilled directionally. The proposed directional drilling plans are provided in Appendix X (Drilling Plans)

The surface wellhead design will be consistent for both injection wells. The proposed wellhead schematic is provided in Figure 5-3.

5.1 WELL CONSTRUCTION PLANS

The well construction plans for proposed injection wells MS CCS 1 and MS CCS 2 have been designed to prevent fluid movement from the Injection Zone into overlying formations. Each injection well will have six permanent barriers between USDW and the injection activities in the well interior: three casing strings with cement circulated to surface within each of the three annuli. Additionally, two further barriers will separate injection fluids from the USDW: a tubing wall and pressurized fluid in the tubing-casing annulus. In total, there will be eight man-made barriers and one natural barrier (the Anahuac Formation Upper Confining Zone) to prevent fluids from migrating to the USDW.

5.2 CONSTRUCTION REQUIREMENTS

5.2.1 Prevention of Vertical Fluid Migration

The construction plans described in this section detail the steps required to drill and construct MS CCS 1 and MS CCS 2. These steps include drilling through the USDW and a substantial impermeable formation that confines fluids to the underlying Injection Zone.

The plan specifies drilling through the USDW to a depth that ensures sufficient formation strength to support the installation of 20 inch casing. The casing will be cemented with a sufficient volume of cement to circulate cement from the casing shoe to surface, providing complete coverage of the USDW with a bonded layer of steel and hardened cement.

Drilling will continue through the Upper Confining Zone to approximately 150 ft (TVD) above the top of the Injection Zone. At this point, 13 ⅜ inch casing will be installed and cemented to surface, providing further isolation and protection of the USDW.

After drilling to the Injection Zone, logging and sampling will be conducted in accordance with LAC 43§3617.4.b requirements. Details can be found in the Pre-Operational Logging and Testing Program (Attachment C). Then, the 9 ⅝ inch casing will be installed and cemented in two stages. Stage 1 will consist of specialized CO_2 compatible cement, specifically formulated to ensure long-term integrity, placed across the Injection and Confining Zones. Stage 2 will include adding ~330 feet of the specialized CO_2 compatible cement followed by Class H (with additives) cemented to surface. Corrosion-resistant alloy (CRA) materials will be used across the Injection and Confining Zones to ensure sufficient corrosion resistance for CO_2 injection. This long-string casing provides an additional layer of steel and cement between the injection operations and the USDW.

A 4 ½ inch tubing string and packer will be placed within the long-string casing. CO_2 will be injected down the tubing and through perforations in the long-string below the packer. The annular space between the tubing and long string will be filled with 9.3 ppg $CaCl_2$ inhibited brine with corrosion control (98% Magnesium Oxide), pressurized, and continuously monitored, enabling prompt action if any leaks are detected.

The injection well designs will meet or exceed the following American Petroleum Institute (API) standards:

- API Specification 5CT
- API RP 5C1
- API RP 10D-2
- API Specification 11D1

All well materials to be used, including casing, cement, tubing, and packer, are compatible with the fluids they are expected to contact and will meet or exceed standards established by the American Petroleum Institute or comparable organizations.

In total, the wells will have eight permanent barriers installed between the USDW and the injection operations: three steel casing strings, three cement sheaths, the tubing wall, and the pressurized annular fluid. Additionally, the Upper Confining Zone (Anahuac Formation) acts as a natural barrier to prevent fluid migration out of the Injection Zone.

5.2.2 Drilling Practices and Contingencies

Class VI well construction will be supervised by personnel knowledgeable and experienced in practical drilling engineering, with specific familiarity in injection well construction and its unique requirements. Standard drilling practices will be employed to drill the well to total depth (TD), reaching the geologically favored target location.

The surface hole will be drilled vertically, with surveys conducted every 500 ft to accurately determine the well's subsurface position at -3,000 ft TVD. The remainder of the well will be drilled using directional drilling bottom-hole assemblies (BHAs), that incorporate a bent-housing mud motor and a measurement-while-drilling (MWD) tool. The MWD tool has accelerometers and magnetometers to determine the downhole position (surveys) in reference to the surface location (the center of the rotary table on the rig floor). Surveys will be taken at intervals of at least 95 ft to calculate the wellbore position, allowing for any necessary adjustments to be made using the mud motor to steer the bit back on the desired path.

All drilling tools (e.g. mud motors, stabilizers, drill collars, drill pipe) will undergo inspection before entering the wellbore. The integrity of the tool body and the threaded connections between tools will meet the standards of DS-1, Category 3. Any tools that do not meet body, thread, and shoulder specifications will be rejected, ensuring only reliable tools are used in the well. In the event that a downhole tool fails, the operable portion of the drill string will be pulled out of the hole, leaving a "fish" in the well. Accurate measurements of each tool's top are taken prior to entry, allowing an appropriately sized fishing tool to be used to latch onto the top of the failed component and recover it, if needed.

The well has been designed to set surface casing at a depth that extends into a confining bed—such as a shale—below the base of the deepest formation containing a USDW. This ensures that the formation strength, specifically resistance to fracturing, is sufficient to safely drill the remainder of the well to total depth.

Per LAC 43:XVII§3617.A.3.a, and A.3.a.i, after cementing each casing string but before drilling out the respective casing shoe, all casings shall be hydrostatically tested to verify casing integrity and the absence of leaks.

In accordance with LAC 43:XVII§3617.A.3.b, and A.3.b.i, after drilling out the casing shoe, the casing seat and cement of any intermediate and injection casings (i.e., long-string casing) will be hydrostatically tested. At least 10 ft of formation below the respective casing shoes shall be drilled before the test, test pressures shall never exceed the known or calculated fracture gradient of the appropriate subsurface formation.

Once drilling is complete, the long-string casing will be run and cemented, with cement densities and volumes specifically designed to avoid formation fractures at any depth. The long-string casings in both wells are planned to include a stage tool so that the casings can be cemented in stages. After pumping the first stage of cement, GCS will wait on the cement to properly cure before initiating the second stage of cement. This will ensure that cement loss is not induced by high hydrostatic loading conditions. Lost circulation due to imposed drilling or cementing forces is not expected. While lost circulation is not anticipated, plans are in place to address it if it does occur. If lost circulation occurs, lost circulation material (LCM) will be added to the mud to plug/block/seal the intervals downhole where fluid loss is occurring. LCM will be available on-site throughout drilling operations.

All practices described above are standard oilfield best practices, allowing for safe and efficient drilling of MS CCS 1 and MS CCS 2.

5.2.3 Testing and Monitoring Devices Within the Borehole and Annulus

The long-string casing for MS CCS 1 and MS CCS 2 will have a 9 ⅝ inch outer diameter and an inside diameter of 8.535 inches. The injection tubing will have an outer diameter of 4 ½ inch, which comfortably fits inside the long-string casing, leaving an annular space of approximately 2 inches. Distributed temperature sensing/distributed acoustic sensing (DTS/DAS) fiber optic cables will be clamped to the outside of the long-string casing from the surface to TD. An additional backup fiber optic cable will be installed from the surface to the depth of the intermediate casing shoe.

Annular measurements will also be taken at depth using downhole-deployed gauges fit with ¼ inch control lines, which are connected across the multiple tubing joints via clamps. Surface measurements of annular pressure will be collected with gauges installed on the wellhead, as illustrated in the cut-away schematic shown in Figure 5-3. These monitoring practices are essential to ensure well integrity and detect potential issues in real-time.

5.3 CASING PROGRAM

5.3.1 Injection Zone Depth

The Injection Zone for Project Minerva is the upper Frio Formation. The projected depths to the top and base of the Injection Zone in MS CCS 1 and MS CCS 2 are provided in Table 5.3.1-1.

5.3.2 Lithology of Injection and Confining Zones

The Upper Confining Zone is the shale-rich Anahuac Formation, which conformably overlies the upper Frio Formation (Injection Zone). The Lower Confining Zone consists of shale intervals within the upper Frio Formation underlying the deepest sands of the Injection Zone. Offset resistivity, spontaneous potential, and gamma ray logs confirm that both the Upper and Lower Confining Zones exhibit regionally high shale content. The upper Frio Formation itself comprises stacked shoreline sandstones interbedded with shales. Detailed descriptions of both the Injection Zone and the Confining Zones are provided in Section 2 (Site Characterization) of the Narrative.

5.3.3 Borehole and Casing Size and Grade

5.3.3.1 Borehole Sizes

MS CCS 1 and MS CCS 2 are each designed with a 26 inch hole for the surface casing, a 17 ½ inch hole for the intermediate casing, and a 12 ¼ inch hole for the long-string casing, as depicted in Figures 5-1 and 5-2.

5.3.3.2 Casing Size and Grade

From surface to below the base of the USDW, the surface casing will be composed of a 20 inch, 133 lb/ft, L80 grade casing.

The intermediate casing string, extending from surface to significantly into the Upper Confining Zone, will be composed of 13 ⅜ inch, 68 lb/ft, L80 casing. L80 casing is a

commonly used oilfield casing grade that offers sufficient minimum yield and tensile strength for drilling operations.

The long-string casing will extend from the surface– through the Upper Confining Zone, Injection Zone, and Lower Confining Zone– to total depth and will be composed of 9 ⅝ inch, 53.5 lb/ft casing. From the surface to above the Upper Confining Zone, L80 casing with a premium connection (VAM-21 or equivalent) will be installed. From above the Upper Confining Zone to total depth, corrosion resistant alloy casing (Super Duplex 25 Chrome casing, grade: 25CRW-125, specifically Nippon's SM25CRW-125®) will be tied into the 80 casing with the same premium connection (VAM-21 or equivalent). Super Duplex 25 Chrome is a cold-hardened duplex stainless steel intended for corrosion resistance in sweet (CO_2) and mildly sour (H_2S) environments with high chloride content, requiring high strength up to 450°F. It has a high pitting resistance equivalence (PREN) greater than or equal to 40.

The size, grade, and depths of the surface casings, intermediate casings, and long-string casings are provided in Table 5.3.3-1 and depicted in Figures 5-1 and 5-2. The need for a galvanic cross-over in the long-string will be evaluated and incorporated if deemed technically necessary to properly manage the transition between carbon steel and CRA.

5.3.3.3 Casing and Tubing Strength

Table 5.3.3-2 provides casing details including the tensile, burst, and collapse strength for MS CCS 1 and MS CCS 2. The casing has been designed to withstand expected forces, incorporating a substantial factor of safety, during injection operations. For example, each casing will be cemented with a sufficient volume of cement to circulate cement from the casing shoe to surface, with cement bond logs run to confirm proper bonding to both the casing and the formation.

Casing strength can be degraded if the wall thickness is reduced by corrosion or erosion. A baseline inside diameter of each long-string casing will be measured with a casing caliper log during pre-operational testing. This log can be repeated during the life of the well whenever the tubing is pulled. The critical section of the long-string casing is the packer setting area, which must retain sufficient wall thickness to maintain structural integrity, particularly hoop stress, throughout the injection activities' operational life. For this reason, corrosion-resistant (CRA) casing has been specified for this interval.

Expected loads on the surface casing, intermediate casing, long-string, and injection tubing were found to be within equipment specifications. Modeled loads (downhole stresses) with design limits and equipment specifications limits can be found in the following Figures:

- 20 inch Surface Casing, MS CCS 1 (Figure 5.3.3-1)
- 20 inch Surface Casing, MS CCS 2 (Figure 5.3.3-2)
- 13 ⅜ inch Intermediate Casing, MS CCS 1 (Figure 5.3.3-3)
- 13 ⅜ inch Intermediate Casing, MS CCS 2 (Figure 5.3.3-4)
- 9 ⅝ inch Long String Casing (Stage 2), MS CCS 1 (Figure 5.3.3-5)
- 9 ⅝ inch Long String Casing (Stage 2), MS CCS 2 (Figure 5.3.3-6)
- 9 ⅝ inch Long String Casing (Stage 1), MS CCS 1 (Figure 5.3.3-7)

- 9 ⅝ inch Long String Casing (Stage 1), MS CCS 2 (Figure 5.3.3-8)
- 4 ½ inch Tubing, MS CCS 1 (Figure 5.3.3-9)
- 4 ½ inch Tubing, MS CCS 1 (Figure 5.3.3-10)

5.3.4 Downhole Temperature

The expected temperature at total depth is 216°F for MS CCS 1 and 214°F for MS CCS 2, which is not expected to adversely impact the cement, casing, packer element, or downhole gauges. The cement reaches a value close to its maximum compressive strength within days and gradually becomes more competent with time and bottomhole temperature.

Similarly, the crystalline structure of casing steel is not significantly affected at this temperature. The thermal effect at < 216°F is minimal since it takes temperatures around 1,500°F to alter the crystalline structure of steel. Therefore, the casing will not experience detrimental effects from the anticipated downhole temperature.

5.4 CEMENTING PROGRAM

Centralizer placement will be designed utilizing the final cementing vendor's software and actual deviation surveys. Centralizers will be placed in all casings, as per the design, to aid in the centering of the casing in the open hole and optimize uniform cement placement behind pipe. Complete cement details have been provided in Table 5.4-1.

5.4.1 Circulation of Cement

In all cases, multi-arm caliper logs will be run prior to running casing. Cement volumes will be calculated based on the recorded hole caliper, with an excess volume factored in to ensure the complete circulation of cement to the surface. All cement returns to the surface will be recorded in daily drilling reports.

5.4.2 Cement and Cement Additives

Additives used to achieve the desired properties of the cement slurry include defoamers, accelerators, and retarders. Table 5.4.2-1 lists the proposed additives for each cement slurry utilized in the well designs. The primary cement used in the long string within the Injection and Confining Zones will be a specialized CO_2 compatible cement, such as PermaSet™ System Cement, which is a proprietary blend developed by Baker Hughes. For more details, refer to Appendix IX-2. The proprietary blend replaces calcium hydroxide [$Ca(OH)_2$] with calcium (alumino)silicate hydrate (C-(A-)S-H) phases to enhance resistance to acid-induced corrosion.

The secondary cement used in the well designs is Class H cement with the following additives to improve compatibility with CO_2: tricalcium silicate (C_3S), dicalcium silicate (C_2S), tricalcium aluminate (C_3A), tetra calcium aluminoferrite (C_4AF).

5.5 TUBING AND PACKER

LAC 43:XVII§3617.A.4 requires that the tubing and packer must be compatible with the fluids they contact and meet or exceed recognized industry standards. Considering the potential formation of carbonic acid from a mixture of water and CO_2, the injection tubing for Project

Minerva is specified as 4 ½ inch, 25 CR-rated steel. The added chrome content in the steel replaces iron, reducing the amount of ionic activity available to react with carbonic acid. The 4 ½ inch outside diameter (OD) tubing size was selected by considering the total proposed injection volume of CO_2 during the project life. Additionally, premium tubing connections using gas-tight sealing surfaces (VAM-21 or equivalent) will ensure the integrity of the tubing string and mitigate weakness at the connections.

The packer will be comprised of CRA materials and installed inside the 53.5 lb/ft, 9 ⅝ inch long-string casing across an interval confirmed to be cemented near the top of the Injection Zone. The packer anchors the tubing string, provides structural stability, and isolates the overlying annular space from the Injection Zone, allowing the annulus to be monitored for potential tubing and packer leaks. The CRA retrievable injection packer will be manufactured using carbon dioxide-compatible elastomer materials and will be rated to withstand the pressure differentials during installation, workovers, and the injection phase, including an additional safety factor.

The following parameters are the basis of design for the tubing and packer:

- **Completion Intervals:** Will be executed in a bottoms-up sequence, starting with the deepest interval and progressing upward as scheduled. Final depths will be confirmed from logging data, and perforations established across the targeted reservoir interval after tubing and packer installation.
- **Setting depth:** Approximately 9,000 ft TVD, or within 150 ft of the top perforations in the Upper Frio Formation. The setting depths for each well will be slightly different due to formation tops and geometry of the directional well; 9,000 ft is used as a generalization knowing that precise depths will be confirmed upon drilling and logging.
- **CO_2 stream specification:** Expected to be within specs shown in Table 2.10.3-1.
- **Maximum proposed injection pressure:** Approximately 3,200 psig at the surface during the injection period. This equates to downhole pressures of 4,907 psig and 4,826 psig in MS CCS 1 and MS CCS 2, respectively.
- **Annular pressure requirements:** In accordance with Class VI requirements, the annular pressure (between the tubing and long-string casing) will be maintained greater than the fluctuating daily injection pressure, which will vary due to ambient temperature changes.
- **Injection wells planned:** Two injection wells are planned for Project Minerva. Proposed injection rates and volumes are shown in Table 5.5-1.

The International Organization for Standardization (ISO) and the American Petroleum Institute (API) have created standards (ISO 14310:2001 E and API Specification 11D1) to guide packer selection. Project Minerva specifies packer validation level Q1, which provides maximum trace documentation, and a standard design-validation grade of V1.

Tubing and packer details are provided in Tables 5.5-2 and 5.5-3.

5.6 MECHANICAL INTEGRITY

Per LAC 43:XVII §3627A.1, a Class VI well has mechanical integrity if there are no significant leaks in the casing, tubing, or packer (internal integrity) and there is no significant fluid movement into the USDW through channels adjacent to the injection wellbore (external integrity). Additional information about the internal and external mechanical integrity testing performed prior to operations can be found in the Pre-Operational Testing Program (Attachment C). The Testing and Monitoring Plan (Attachment D) covers specifics about internal and external mechanical integrity testing that will be performed over the operational life of the wells.

5.6.1 Internal Integrity

To demonstrate internal integrity, GCS will perform an annulus pressure test after initial well construction (LAC 43:XVII §3617.B.1.d.i) and once operational, at least once every 12 months and after performing any remedial work that involved unseating the tubing or packer (LAC 43:XVII §3627.A.2.a). GCS will ensure annulus pressure tests are witnessed by an Louisiana Department of Conservation and Energy (C&E) Enforcement Agent.

Additionally, GCS will continuously monitor injection pressure, rate, and volume; downhole pressure monitoring of the tubing-casing annulus; and annulus fluid volume (LAC 43:XVII §3627.A.2.b). Continuous monitoring will allow GCS to identify any potential internal integrity issues between annual testing events and allow immediate response to potential integrity issues.

5.6.2 External Integrity

To demonstrate external integrity prior to operating the wells, GCS will perform a temperature log and a casing inspection log (LAC 43:XVII §3617.B.1.d.ii-iv). Each of these logs will provide a baseline for future testing/logging throughout the operational life of the wells.

Once the wells are operational, GCS will perform a DTS MIT and a temperature log at least once every 12 months to confirm external mechanical integrity (LAC 43:XVII §3627.A.3). After the DTS MIT data has been sufficiently corroborated via temperature logging data, GCS will submit a request to the C&E Secretary to utilize DTS MIT as the primary form of external MIT (LAC 43:XVII §3627.A.5). Upon request by the C&E Secretary, GCS will perform a casing inspection log to determine the presence or absence of corrosion in the long-string casing (LAC 43:XVII §3627.A.4).

6 PRE-OPERATIONAL LOGGING AND TESTING

6.1 PROJECT PLAN

The Pre-Operational Logging and Testing Plan is provided as Attachment C of this Narrative. The Pre-Operational Logging and Testing Plan satisfies the requirements of LAC 43:XVII §3607.C.2.g.

6.2 SUBMISSION

The Pre-Operational Testing Plan (Attachment C) has been submitted to C&E for review and approval. In accordance with LAC 43:XVII §3629.A.5, the Pre-Operational Testing Plan will be submitted to the USEPA.

7 WELL OPERATION

7.1 OPERATIONAL PROCEDURES

The Operating Plans for proposed MS CCS 1 and MS CCS 2 are provided in Appendix XII (Operating Plans).

GCS has defined the following key objectives for operation:

- Maintain and achieve a safe, reliable, and efficient sequestration system.
- Ensure operations remain within safe parameters.
- Maximize continuous injection of CO_2 and minimize cycling of the injection wells.

Per LAC 43:XVII§3617.A.2, GCS will prevent injection into the wellbore annulus of any casing protecting the USDWs.

Table 7-1 shows the operational parameters for injection well MS CCS 1 and MS CCS 2. Please see Section 1.6 (Model Boundary and Initial Conditions) and Section 1.7 (Injection Schedule and Operating Parameters) of the Area of Review and Corrective Action Plan (Attachment A) for further discussion on the use of Computer Modeling Group (CMG) Version 25.30 for well simulation and operational parameter details.

GCS will implement a comprehensive testing and monitoring plan for Project Minerva, satisfying the well operation planning requirements outlined in LAC 43:XVII §3621.A, §3625.A, and §3627.A. Please refer to Appendix XII (Operating Plans) for operational parameters specific to each injection well and the Injection Zone. The Testing and Monitoring Plan (Attachment D) covers specifics about external mechanical integrity testing and the overall testing and monitoring approach for MS CCS 1 and MS CCS 2.

7.1.1 Injection Rate

Project Minerva will utilize a sequential completion strategy, starting with the bottom interval and progressing upwards. Targeted injection rates are set at 17 MMSCF/D in MS CCS 1 and 16.5 MMSCF/D in MS CCS 2 for the bottom interval (Interval 1) for 17 years and 23 MMSCF/D into the intermediate interval (Interval 2) of MS CCS 1 and MS CCS 2 for 13 years. The project will inject a combined average range of 0.547- 0.746 metric tons (MMT) of CO_2 per year over its 30-year lifespan, split between the two injection wells, as defined in Table 7-1.

An upside scenario has been demonstrated to prove additional storage potential in a discrete reservoir interval (Interval 3), which targets injection rates of 12 MMSCF/D in both MS CCS 1 and MS CCS 2 for the top interval (Interval 3) for 6 years, this upside scenario would extend the total injection period from 30 to 36 years.

7.1.2 Injection Pressure

7.1.2.1 Bottom-Hole Injection Pressure

Injection induced pressure will not exceed 90% of the fracture pressure of the zone. The bottom-hole pressures are significantly smaller than the estimated fracture pressure and

induced seismicity pressure. The initial formation pressure is based on the most-likely initial formation pressure gradient of 0.457 psi/ft.

The most-likely value of the minimum horizontal stress gradient is assumed to be 0.85 psi/ft, as provided in Section 2.5.1.2 (Total Minimum Horizontal Stress) of the Project Minerva Narrative.

The depth of the deepest completion interval in MS CCS 1 is approximately 9,996 ft TVD, which calculates to a minimum horizontal stress of approximately 8,496 psia. The depth of the deepest completion interval in MS CCS 2 is approximately 9,870 ft TVD, which calculates to a minimum horizontal stress of approximately 8,390 psia.

Assuming a safety factor of 90%, this gives an estimate of the formation fracturing pressure to be approximately 7,647 psia at 9,996 ft TVD in MS CCS 1 and 7,551 psia at 9,870 ft TVD in MS CCS 2. This is a conservative estimate as it assumes no cohesion in the formation, i.e. the formation parts as soon as the effective minimum horizontal stress is less than zero. The induced seismicity pressure is estimated to be 9,996 psia at a depth of 9,996 ft TVD in MS CCS 1 and 9,870 psia at a depth of 9,870 ft TVD in MS CCS 2, at the pressure gradient of 1 psi/ft.

7.1.2.2 Surface Injection Pressure

The surface injection pressure required to inject CO_2 into the formation is a function of the bottom-hole pressure and the hydrostatic pressure (pressure due to the weight of the CO_2 column at the depth of the upper perforation). The maximum surface injection pressure is the difference between the maximum bottom-hole pressure and the hydrostatic pressure minus atmospheric pressure:

$$P_{Smax} = P_{BH} - (SGCO_2 \times P_w \times \text{shallowest depth of injection}) - atm \qquad \textit{Equation 7.1-1}$$

where,

P_{Smax} = maximum surface injection pressure (psig)
P_{BHmax} = maximum bottom-hole injection pressure (psi)
$SGCO_2$ = specific gravity of CO_2 (0.675, assumed average)
Pw = hydrostatic water pressure gradient (0.4333 psi/ft)
atm = atmospheric pressure (14.7 psi).

Using the calculated bottom-hole pressure of 7,647 psia for MS CCS 1 and an injection depth of 9,996 ft TVD, the maximum surface injection pressure calculates to 4,709 psi.

$$4{,}709 \text{ psig} = 7{,}647 \text{ psi} - (0.675 \times 0.4333 \text{ psi/fti} \times 9{,}996 \text{ ft TVD}) - 14.7 \text{ psi}$$

Using the calculated bottom-hole pressure of 7,551 psi for MS CCS 2 and an injection depth of 9,870 ft TVD, the maximum surface injection pressure calculates to 4,650 psi.

$$4{,}650 \text{ psig} = 7{,}551 \text{ psi} - (0.675 \times 0.4333 \text{ psi/ft} \times 9{,}870 \text{ ft TVD}) - 14.7 \text{ psi})$$

7.1.3 Stimulation Program

All stimulation activities will be approved by the C&E Secretary prior to conducting the stimulation. GCS will carry out the stimulation program in accordance with Appendix XI of this application.

7.1.4 CO_2 Mass

Project Minerva is designed to permanently store a total mass of 19.0 MMT, in the base case. This mass will be achieved by injecting at an average rate ranging from 0.547-0.746 MMT/yr for 30 years (Table 7-1).

7.2 PROPOSED CARBON DIOXIDE STREAM

The emissions that are anticipated for Project Minerva in the near term are likely to be high purity CO_2. Examples of high purity CO_2 anticipated to be economically capturable include natural gas processing and other natural gas derived processes including blue H_2 and LNG. The Gulf Coast region of Southeast Texas and Southwest Louisiana have a variety of currently operating or planned facilities for natural gas processing. Such applications can meet the CO_2 specification that GCS has proposed. Further, such specification of CO_2 is consistent with the existing CO_2 pipeline infrastructure in the Gulf Coast region.

Table 2.10.3-1 provides the proposed CO_2 stream specification for Project Minerva. This specification is designed to ensure safe operation of the project work and ensure no-endangerment of USDWs. Component concentrations were defined based on recommended impurity limits for different applications, including carbon steel pipelines, EOR, CO_2 saline storage and CO_2+H_2S saline storage. (Shirley & Myles, 2019) provides recommendations based on review of 55 different specifications from literature.

The logic of proposed component concentrations is as follows:

- Limited primarily by reservoir considerations include:
  - Total non-condensable gases affect CO_2 phase behavior and migration of the CO_2 plume in the subsurface. Value chosen to limit effects on plume migration and pressure propagation in the Injection Zone.
  - Oxygen (O_2) and H_2S are primarily limited for other reasons, but partly to limit possible reactions with minor mineral components in the Injection Zone and Confining Zones.
- Limited primarily for operational performance include:
  - O_2 contributes to total non-condensable gases and is further limited to reducing the potential for corrosion of metallic facilities components in the presence of H_2O, sulfate (SO_4^{2-}) and/or nitrogen dioxide (NO_2). It is also limited to reduce potential reactivity with minor minerals in the reservoir and caprock.
  - CH_4 contributes to total non-condensable gases and is further limited to reduce energy requirements for compression and pumping.
  - Dense-phase CO_2 may carry considerable amounts of H_2O in vapor phase,

which is not problematic. Total H_2O is limited to ensure there is no condensation of liquid H_2O anywhere within the facilities under the anticipated full range of operating conditions. CO_2 and other minor components (e.g., O_2, H_2S) form corrosive agents in the presence of liquid H_2O.

- H_2S is limited primarily for health and safety, but partly to limit the formation of corrosive compounds in the presence of liquid H_2O and/or O_2.

— Limited primarily to protect human health and safety and the environment include:

- H_2S, which carries significant risk (including toxicity) to humans and other organisms if introduced to the environment.
- Hg, which is associated with long-term health risks and environmental degradation if introduced to the environment.

Under the proposed operational conditions (e.g., down-hole P/T) for the lifetime of the injection project, the proposed CO_2 stream specification is compatible with the mineralogy, petrology, and pore waters of the Injection Zone and the Upper Confining Zone. Geochemical interactions between the injected CO_2 and the subsurface formations and formation fluid are studied in Section 2.8 (Geochemistry). As previously discussed in Section 2.8.1.3 (Conclusions and Recommendations), formation fluid salinity impacts the dissolution rate of CO_2 and formation mineralogy can facilitate precipitation and mineralization. Any interactions are highly unlikely to negatively affect CO_2 injection operations or CO_2 storage integrity.

Although small-scale, localized mineral reactions may occur, these interactions are highly unlikely to affect CO_2 injection operations or CO_2 storage integrity. All well materials in contact with CO_2 will be CO_2 compatible (i.e. cement and long-string casing from the top of the Upper Confining Zone through total depth) or replaceable (i.e. tubing) throughout the life of the project. Nippon Steel Corporation conducted a material selection analysis based on the provided CO_2 stream composition and well conditions. Super Duplex Stainless Steel (SM25CRW) is recommended as the best corrosive resistant option for expected conditions. Appendix IX, CO_2 Stream Compatibility (IX-1 Nippon Steel Material Recommendation), outlines the study setup, analysis, and results of the material section review for Project Minerva. The well material selections are discussed in detail in Section 5 (Injection Well Construction).

8 TESTING AND MONITORING

8.1 PROJECT PLAN

The Testing and Monitoring Plan is provided as Attachment D of this Narrative. The Testing and Monitoring Plan Report satisfies the requirements of LAC 43:XVII §3607.C.2.n and §3625.A.

The plan covers in detail the overall strategy and approach for testing and monitoring, carbon dioxide stream analysis, continuous recording of operational parameters, corrosion monitoring, Above Confining Zone monitoring, external mechanical integrity testing, pressure fall off testing, carbon dioxide plume and pressure front tracking, and sampling/analytical procedures.

A Quality Assurance and Surveillance Plan (QASP) is submitted as an appendix to the Testing and Monitoring Plan, and includes additional information related to project management, data generation and acquisition, assessment and oversight and data validation and usability.

8.2 SUBMISSION

The Testing and Monitoring Plan (Attachment D) has been submitted to C&E for review and approval. In accordance with LAC 43:XVII §3629.A.5, the Testing and Monitoring Plan will be submitted to the USEPA.

9 INJECTION WELL PLUGGING PLAN

9.1 PROJECT PLAN

The Injection Well Plugging Plan is provided as Attachment E of this Narrative. The Injection Well Plugging Plan satisfies the requirements of LAC 43:XVII §3607.C.2.o and §3631.A.3.

The plan covers in detail the proposed tests and measurements to determine the bottom-hole reservoir pressure; planned external mechanical integrity tests; information on the proposed plugs; methods used for volume calculations; required notifications, permits and inspections; plugging procedures; and contingency procedures/measures.

9.2 SUBMISSION

The Injection Well Plugging Plan (Attachment E) has been submitted to C&E for review and approval. In accordance with LAC 43:XVII §3629.A.5, the Injection Well Plugging Plan will be submitted to the USEPA.

10 POST INJECTION SITE CARE AND SITE CLOSURE

10.1 PROJECT PLAN

The Post-Injection Site Care (PISC) and Site Closure Plan is provided as Attachment F of this Narrative. The Post Injection Site Care and Site Closure Plan satisfies the requirements of LAC 43:XVII §3607.C.2.p and §3633.A.1.

10.2 SUBMISSION

The Post-Injection Site Care (PISC) and Site Closure Plan (Attachment F) has been submitted to C&E for review and approval. In accordance with LAC 43:XVII §3629.A.5, the PISC will be submitted to the USEPA.

11 EMERGENCY AND REMEDIAL RESPONSE PLAN

11.1 PROJECT PLAN

The Emergency and Remedial Response Plan (ERRP) is provided as Attachment G of this Narrative. The Emergency and Remedial Response Plan Report satisfies the requirements of LAC 43:XVII §3607.C.2.r and §3623.A.1.

The plan covers in detail the local resources and infrastructure, potential risk scenarios, response personnel and equipment, emergency communications plan, plan review, staff training, and exercise procedures.

11.2 SUBMISSION

The Emergency and Remedial Response Plan(ERRP) (Attachment G) has been submitted to C&E for review and approval. In accordance with LAC 43:XVII §3629.A.5, the ERRP will be submitted to the USEPA.

12 REFERENCES

Anderson, R.E, Eargle, D.G, & Davis, B. (1973). *Geologic and hydrologic summary of salt domes in Gulf Coast region of Texas, Louisiana, Mississippi, and Alabama*. U.S. Geological Survey.

Baker Jr, E. T. (1978). *Stratigraphic and Hydrogeologic Framework of Part of the Coastal Plain of Texas*. Austin: USGS, Texas Water Development Board.

Baker Jr, E. T. (1986). *Hydrology of the Jasper Aquifer in the Southeast Texas Coastal Plain*. Texas Water Development Board. Austin: U.S. Geological Survey.

Baria, L. R., Stoudt, D. L., Harris, P. M., & Crevello, P. D. (1982). Upper Jurassic reefs of the Smackover Formation, United States Gulf Coast. *AAPG Bulletin, 66*(10), 1449–1482. https://doi.org/10.1306/03B5A96C-16D1-11D7-8645000102C1865D

Beckman, J. D., & Williamson, A. K. (1990). *Salt-Dome Locations in the Gulf Coastal Plain, South-Central United States*. Austin: US Geological Survey.

Bethke, C. M., Altaner, S. P., Harrison, W. J., & Upson, C. (1988). Supercomputer Analysis of Sedimentary Basins. *Science, 239*(4837), 261-267. doi:10.1126/science.239.4837.261

Byerlee, J. (1978). Friction of rocks. In J. D. Byerlee & M. Wyss (Eds.), *Rock friction and earthquake prediction* (Contributions to Current Research in Geophysics, Vol. 6, Birkhäuser.

Chowdhury, A. H., & Turco, M. J. (2006). Chapter 2. Geology of the Gulf Coast Aquifer, Texas. In T. W. Board, *Aquifers of the Gulf Coast of Texas* (pp. 23-50). Austin: Texas Water Development Board.

Clark, J. E. (1981). Groundwater Flow in Deep Saline Aquifers.

Clark, J. E., Papadeas, P. W., Sparks, D. K., & McGowen, R. R. (1991). *DuPont borehole closure test well demonstration, Orange County, Texas*. Beaumont: E. I. du Pont de Nemours & Co., Inc.

Coleman, J., & Galloway, W. E. (1990). *Petroleum geology of the Vicksburg Formation, Texas* (pp. 17-19). Gulf Coast Association of Geological Societies and Gulf Coast Section of Society of Economics, Paleontologists, and Mineralogist *(SEPM)* (pp. 17-19). Lafayette, Louisiana: AAPG Bulletin.

Collier, A. L., & Sargent, B. P. (2018). *Water Use in Louisiana, 2015*. Louisiana Department of Transportation and Development. Baton Rouge: U.S. Geological Survey.

Core Laboratories. (1987, June 3). *Petrographic study of selected sidewall core samples from a Beaumont disposal well for DuPont Chemicals, Inc.* Beaumont, Texas, United States of America: Litton Core Lab.

Core Laboratories. (1987, June 1). *Special core analysis study for E.I. duPont De Nemours & Company, Inc., Waste Disposal Tests*. Beaumont, Texas, United States of America: Western Atlas International.

Cygan, R. E. (1991). The solubility of gases in NaCl brine and a critical evaluation of available data. *SPE Reservoir Engineering*, 223-230.

Davis, S. D., Pennington, W. D., & Carlson, S. M. (1989). *A compendium of earthquake activity in Texas*. Geological Circular 89-3, 1-219.

Delaney, P. J. (1963). Stratigraphy of the Vicksburg Equivalent of Louisiana: ABSTRACT. *AAPG Bulletin, 47*(2), 355. doi:10.1306/BC7439B5-16BE-11D7-8645000102C1865D

Department of Environmental Quality of Louisiana. (2009). *Appendix 4 to the 2009 Triennial Summary Report: Evangeline Aquifer Summary, 2007*. Aquifer Sampling and Assessment Program.

Department of Environmental Quality of Louisiana. (2017). *Appendix 10 to the 2018 Triennial Summary Report*. Aquifer Sampling and Assessment Program.

Dewhurst, D. N., Cartwright, J. A., & Lonergan, L. (1999). The development of polygonal fault systems by syneresis of collodial sediments. *Marine and Petroleum Geology, 16*, 793-810.

Dvory, N.Z., & Zoback, M.D. (2025). Assessing Fault Slip Potential in a Continuously Varying Stress Field: Application in the Delaware Basin. In Proceedings of the 55th U.S. Rock Mechanics/Geomechanics Symposium American Rock Mechanics Association

Downey, M. W. (1984). Evaluating Seals for Hydrocarbon Accumulations. *AAPG Bulletin*, 1752-1763.

Eaton, B. A. (1969). Fracture gradient prediction and its application in oilfield operations. *Journal of Petroleum Technology Transactions, 246*.

Ellsworth, W. L. (2013). Injection-Induced Earthquakes. *Science, 341*. doi:DOI: 10.1126/science.1225942

Engelder, J. T. (1974). Coefficients of friction for sandstone sliding on quartz gouge. In *Advances in rock mechanics: Proceedings of the Third Congress International Society for Rock Mechanics (Part A*, p. 499).

Federal Emergency Management Agency. (2024, May 13). *Earthquake hazard Maps*. Retrieved from FEMA; Earthquake Risk: https://www.fema.gov/emergency-managers/risk-management/earthquake/hazard-maps

Foote, R. Q. (1984). *Summary report on the regional geology, petroleum potential, environmental consideration for development, and estimates of undiscovered recoverable O&G resources of the US Gulf of Mexico Continental Margin in the area of proposed O&G Lease Sales 81 and 84*. U.S. Geological Survey and U.S. Minerals Management Service. doi:10.3133/ofr84339

Frohlich, C., Potter, E., Hayward, C., & Stump, B. (2010). Dallas-Fort Worth earthquakes coincident with activity associated with natural gas production. *The Leading Edge*, 270-275. doi:10.1190/1.3353720

Galloway, W. E. (1985). Depositional framework of the Lower Miocene (Fleming) episode, northwest Gulf Coast Basin. *AAPG Bulletin, 69*(9), 1421. doi:10.1306/AD462CDB-16F7-11D7-8645000102C1865D

Galloway, W. E., Henry, C. D., & Smith, G. E. (1982). *Depositional framework, hydrostratigraphy, and uranium mineralization of the Oakville Sandstone (Miocene), Texas Coastal Plain*. (Report of Investigations No. 113). doi:10.23867/RI0113D

Galloway, W. E., Hobday, D. K., & Magara, K. (1982). Frio Formation of Texas Gulf Coastal Plain: Depositional Systems, Structural Framework, and Hydrocarbon Distribution. *AAPG Bulletin, 66*(6), 649-688. doi:10.1306/03B5A2F5-16D1-11D7-8645000102C1865D

Gray, G. R., Darley, H., & Rogers, W. F. (1980). *Composition and Properties of Oil Well Drilling Fluids*. Gulf Publishing Company .

Gregory, J. L. (1966). Lower Oligocene Delta in subsurface of southeastern Texas: Abstract. *AAPG Bulletin, 50*(10), 2323. doi:10.1306/5D25B745-16C1-11D7-8645000102C1865D

Griffith, J. M. (2003). *Hydrogeologic framework of southeastern Louisiana*. Louisiana Department of Transportation and Development & U.S. Geologic Survey.

Harder, A. H. (1960). *The geology and ground-water resources of Calcasieu Parish Louisiana*. United States Department of Interior. Washington, D.C.: U.S. Geological Survey.

Haskell, N., Nissen, S., & Hughes, M. (1999). Delineation of geologic drilling hazards using 3-D seismic attributes. *The Leading Edge, 18*(3), 373-382.

Hennings, P. H., Lund Snee, J., Osmond, J. L., DeShon, H. R., Dommisse, R., Horne, E., et al. (2019). Injection-induced seismicity and fault-slip potential in the Fort Worth Basin, Texas. *Bulletin of the Seismological Society of America, 109, 1615–1634*. https://doi.org/10.1785/0120190017

Hennings, P.H, Nicot, J.P., Gao, R.S., DeShon, H. R., Lund Snee, J.E., Morris, A.P., Brudzinski, M.R., Horne, E.A., & Breton, C. (2021). Pore pressure Threshold and Fault Slip Potential for Induced Earthquakes in the Dallas-Fort Worth Area of North Central Texas. *Geophysical Research Letters, 48*. doi: 10.1029/2021GL093564

Hiland, P. (2010). *Memorandum: Safety/risk assessment results for generic issue 199, "Implications of updated probabilistic seismic hazard estimates in central and eastern united states on existing plants"*.

Houser, B. B., & Ryan, G. S. (1983). *Mineral resource potential map of the Four Notch Roadless Area, Sam Houston National Forest, Walker County, Texas*. (Miscellaneous Field Studies Map MF-1549). U.S. Geological Survey.

Hovorka, S. D., Collins, D., Bensen, S., Myer, L., Byrer, C., & Cohen, K. (2005). Update on the Frio brine pilot: Eight months after injection. In Proceedings of the *Fourth Annual Conference On Carbon Capture And Sequestration*. U.S. Department of Energy / National Energy Technology Laboratory.

Hovorka, S., Tutton, P., & Trevino, R. H. (2018). *Feasibility study of CO_2 storage in saline formations in the region of the planned Lake Charles Methanol Plant*. Gulf Coast Carbon Center Bureau of Economic Geology.

Intera Incorporated. (2020). *The delineation of the Burkeville Confining Unit and the base of the Chicot Aquifer to support the development of the Gulf 2023 groundwater model*. Texas Water Development Board. https://hgsubsidence.org/wp-content/uploads/2021/06/Final_HGSD_FBSD_Burkeville_Report_final.pdf

Intera Incorporated, Frontera-Exploration, Hamlin, S., & Baker, E. (2012). *Final report: updating the hydrogeologic framework for the northern portion of the Gulf Coast Aquifer*. Austin: Texas Water Development Board. https://texashistory.unt.edu/ark:/67531/metapth542209/m2/1/high_res_d/txcs-0715.pdf

Jackson, M. P., & Galloway, W. E. (1984). *Structural and depositional styles of Gulf Coast Tertiary continental margins: Application to hydrocarbon exploration*. American Association of Petroleum Geologists.

Johnston, O., & Greene, C. J. (1979). *Investigation of artificial penetrations in the vicinity of subsurface disposal wells*. Texas Department of Water Resources.

Jolley, S. J., Dijk, H., Lamens, J. H., Fisher, Q. J., Manzocchi, T., Eikmans, H., & Huang, Y. (2007). Faulting and fault sealing in production simulation models: Brent Province, northern North Sea. *Petroleum Geoscience, 13*, 321-340.

Jones, P. H., Turcan Jr, A. N., & Skibitzke, H. E. (1954). Geology and ground-water resources of southwestern Louisiana. (*Geological Bulletin No. 30)*, 285.

Knipe, R. J. (1989). Faulting processes and faul seal. In R. M. Larsen, H. Brekke, B. T. Larsen, & E. Talleraas, *Structural and Tectonic Modelling and its Application to Petroleum Geology* (pp. 325-342). Department of Earth Sciences, The University of Leeds.

Knipe, R. J. (1997). Juxtaposition and seal diagrams to help analyze fault seals in hydrocarbon reservoirs. *AAPG Bulletin, 81*(2), 187-195.

Kreitler, C. W., Collins, E. W., Davidson Jr., E. D., Dix, O. R., Donaldson, G. A., Dutton, S. P., ... Wuerch, H. V. (1981). *Geology and geohydrology of the East Texas Basin*. US Department of Energy.

Krevor, S. C., Pini, R., Zuo, L., & Benson, S. M. (2012). Relative permeability and trapping of CO_2 and water in sandstone rocks at reservoir conditions. *Water Resources Research, 48, W02532*. doi:10.1029/2011WR010859

Kumar, A., Ozah, R., Noh, M., Pope, G. A., Bryant, S., Sepehrnoori, K., & Lake, L. W. (2005). Reservoir simulation of CO_2 storage in deep saline aquifers. In *Proceedings of the Society of Petroleum Engineers* (pp. 336-348).

Leeds, D. J., & Associates. (1989). *Consultants in engineering seismology, geology, geophysics*. Leeds and Associates.

Lehner, F. & Pilaar, W.F., (1997). The emplacement of clay smears in synsedimentary normal faults: Inferences from field observations near Frechen, Germany. In *Hydrocarbon Seals: Importance for exploration and production* (pp. 39-50)

Lindaman, M. A. (2023). *Hydrogeologic framework of southwestern Louisiana*. (Scientific Investigations Report 2023-5004) U.S. Geological Survey. https://doi.org/10.3133/sir20235004

Lindsay, N. M.-W. (1993). Outcrop studies of shale smear on fault surfaces. *International Association of Sedimentologists Special Publication 15*, 113-123.

Loucks, R. G., Dodge, M. M., & Galloway, W. E. (1986). *Controls on porosity and permeability of hydrocarbon reservoirs in lower tertiary sandstones along the Texas Gulf Coast*. The University of Texas at Austin, Bureau of Economic Geology. doi:10.23867/RI0149D

Louisiana Geological Survey. (2000). Folio Series No. 8: Stratigraphic Charts of Louisiana 2000. *Folio Series No. 8: Stratigraphic Charts of Louisiana 2000*.

Lovelace, J. K., Fontenot, J. W., & Frederick, C. P. (2004). *Withdrawals, water levels, and specific conductance in the Chicot aquifer system in southwestern Louisiana*. U.S. Geological Survey.

Lundstern, J.-E., & Zoback, M. D. (2020, April 23). Multiscale variations of the crustal stress field throughout North America. *Nature Communications,* 11, Article 195. https://doi.org/10.1038/s41467-020-15841-5

Mancini, E. A., Mink, R. M., Bearden, B. L., & Wilkerson, R. P. (1985). Norphlet Formation (Upper Jurassic) of southwestern and offshore Alabama: Environments of deposition and petroleum geology. *AAPG Bulletin, 69*(6), 881-898. doi:10.1306/AD462B14-16F7-11D7-8645000102C1865D

Mason, C. C. (1963). *Availability of ground water from the goliad sand in the alice area, Texas*. Texas Water Commission: USGS.

Milner, L. R., & Fish, C. (2009). *Geological characterization of the Chicot/Atchafalaya aquifer region: Southwest Louisiana*. (Water Resources Series No. 4) Louisiana Geological Survey.

National Ocean and Atmospheric Administration. (1985). *Gulf of Mexico atlas*: National Centers for Environmental Information. https://www.ncei.noaa.gov/maps/gulf-data-atlas/atlas.htm

Nicholson, A. (2012). *Empirical analysis of fault seal capacity for CO_2 sequestration, Lower Miocene, Texas Gulf Coast.* (GCCC Digital Publication Series No.12-29). Gulf Coast Carbon Center

Nicol, A., Seebeck, H., McNamara, D., & Field, B. (2016). *Fault Permeability.* IEA Environmental Projects Ltd. (IEAGHG).

Nyman, D. J. (1984). *The occurence of high concentrations of chloride in the Chicot aquifer system of southwestern Louisiana*. U.S. Geological Survey & Louisiana Department of Transportation of Development

Ohio Department of Natural Resources. (2012). *Preliminary report on the Northstar 1 Class II injection well and the seismic events in the Youngstown, Ohio, Area*.

Parkhurst, D. L., & Appelo, C. A. J. (2024). *Description of input and examples for PHREEQC, version 3: A computer program for speciation, batch-reaction, one-dimensional transport, and inverse geochemical calculations*. U.S. Geological Survey https://water.usgs.gov/water-resources/software/PHREEQC/documentation/phreeqc3-html/phreeqc3-2.htm

Peng, D.-Y., & Robinson, D. B. (1976, February). A new two-constant equation of state. *Industrial & Engineering Chemistry Fundamentals, 15*(1). doi:10.1021/i160057a011

Porter, W. M., & Newsom, S. W. (1987). *Shale porosity and permeability*.

Purpera, D. G. (2020). *Louisiana's Management of Water Resources*. Baton Rouge: Louisiana Legislative Auditor.

Rainwater, E. H. (1968). Geological history and oil and gas potential of central Gulf Coast: Abstract. *AAPG Bulletin, 52*(9), 1826. doi:10.1306/5D25C4DF-16C1-11D7-8645000102C1865D

Ramos, G., Katahara, K., Keck, R., & Batzle, M. (1994). In-situ stress predictions and measurements in an unconsolidated sandstone formation, the Lower Frio, East Texas. *ARCO Exploration and Production Technology*, 361-368.

Rosenbauer, R. E. (2005). Experimental investigation of CO_2-brine-rock interactions at conditions relevant to geologic carbon sequestration. *Chemical Geology, 217(1-2)*, 1-15.

Secor, D. T. Jr. (1965). Role of fluid pressure in jointing. *American Journal of Science*, 633-646.

Shirley, P., & Myles, P. (2019). *Quality guidelines for energy systems studies: CO_2 impurity design parameters*. (NETL-PUB-22529) National Energy Technology Laboratory.

Sibson, R. (2000). Fluid involvement in normal faulting. *Journal of Geodynamics*, *29*, 469-499.

Simpson, R.W. (1997). Quantifying Anderson's fault types. *Journal of Geophysical Research: Solid Earth, 102(B8), 17,909-17,919*. doi: 10.1029/97JB01274

Smith, D. A. (1966). Theoretical considerations of sealing and non-sealing faults. *AAPG Bulletin, 50*, 363-374.

Smith, D. A. (1980). Sealing and nonsealing faults in Louisiana Gulf Coast salt basin. *AAPG Bulletin, 64*(2), 145-172.

Smoot, C. W. (1988). *Louisiana hydrologic atlas map no. 3: Altitude of the base of freshwater in Louisiana*. Baton Rouge: USGS. doi:10.3133/wri864314

Sørensen, H. E. (2002). Modeling of gas solubility in brine. *Organic Geochemistry, 33(6)*, 635-642.

Sperrevik, S. G. (2002). Empirical estimation of fault rock properties. *Hydrocarbon Seal Quantification (Norwegian Petroleum Society Special Publication)*, 113-133.

Stevenson, D. (1988). Lake Charles Louisiana, earthquake of 16 October 1983. *Bulletin of the Seismological Society of America*, 1463-1474.

Swanson, S. M., & Karlsen, A. W. (2009). *U.S. Geological Survey assessment of undiscovered oil and gas resources for the Oligocene Frio and Anahuac Formations, onshore Gulf of Mexico Basin*, USA. American Association of Petroleum Geologists Annual Convention

Swanson, S. M., Karlsen, A. W., & J, V. B. (2013). *Geologic assessment of undiscovered oil and gas resources—Oligocene Frio and Anahuac Formations, United States Gulf of Mexico coastal plain and State waters*. (Open-File Report 2013-1257). U.S. Geological Survey. doi:10.3133/ofr20131257.

Teeple, A. P., Becher, K. D., Walton-Day, K., Humberson, D. G., & Gallegos, T. J. (2022). Development and description of a composite hydrogeologic framework for inclusion in a geoenvironmental assessment of undiscovered uranium resources in Pliocene- to Pleistocene-Age Geologic Units of the Texas Coastal Plain. *Minerals*, *12(4)* 420. doi:10.3390/min12040420

The Dow Chemical Company. (2020, May 12). Well Test Interpretation for The Dow Company Injection Well No. 3 - 2020 Falloff. Jefferson County, Texas, United States of America.

Todd, R. G., & Mitchum, R. M. (1977). Seismic stratigraphy and global changes of sea level, part 8: Identification of Upper Triassic, Jurassic, and Lower Cretaceous seismic sequences in Gulf of Mexico and offshore West Africa. In C. E. Payton, *Seismic Stratigraphy — Applications to Hydrocarbon Exploration* (AAPG Memoir 26). American Association of Petroleum Geologists. doi:10.1306/M26490C10

Trevino, R. H., & Meckel, T. A. (2017). *Geological CO_2 sequestration atlas of Miocene strata, offshore Texas State Waters*. Bureau of Economic Geology.

U.S. Department of Energy (1978). *Final environmental impact statement: Strategic Petroleum Reserve Texoma Group salt dome*. (Vol. 1 of 5). Retrieved from https://www.energy.gov/sites/prod/files/2015/06/f23/EIS-0029-FEIS-volume1.pdf

U.S. Energy Information Administration (2020, October 5). *The economic impact of the oil and natural gas industry in Louisiana*: https://www.eia.gov/state/seds/sep_prod/pdf/P4.pdf

U.S. Environmental Protection Agency. (2023, August 18). *EPA FLIGHT*: *Greenhouse Gas Reporting Program*. https://ghgdata.epa.gov/ghgp/

U.S. Geological Survey. (2018). *2018 long-term national seismic hazard map*. https://www.usgs.gov/media/images/2018-long-term-national-seismic-hazard-map

U.S. Geological Survey (2021, December 5). *PHREEQC version 3*. https://www.usgs.gov/software/phreeqc-version-3

U.S. Geological Survey. (2025, November 7). *Earthquake hazards program*. https://earthquake.usgs.gov/earthquakes/map/?extent=7.88515,-147.74414&extent=59.933,-42.27539

U.S. Geological Survey. (2024, May 13). *Modified Mercalli intensity scale*. https://www.usgs.gov/media/images/modified-mercalli-intensity-scale

U.S. Geological Survey. (2024). *USGS earthquake hazards program: Interactive U.S. fault map*.https://usgs.maps.arcgis.com/apps/webappviewer/index.html?id=5a6038b3a1684561a9b0aadf88412fcf

Vail, P. R., Mitchum, R. M., & Thompson, S., III. (1977). Seismic stratigraphy and global changes of sea level, part 4: Global cycles of relative changes of sea level. In C. E. Payton (Ed.), *Seismic stratigraphy—Applications to hydrocarbon exploration* (AAPG Memoir 26). American Association of Petroleum Geologists. https://doi.org/10.1306/M26490

Walsh, F. R., & Zoback, M. D. (2016). Probabilistic assessment of potential fault slip related to injection induced earthquakes: Application to north-central Oklahoma, USA. *Geology, 44(12), 991–994*. https://doi.org/10.1130/G38275.1

Walsh, R., Zoback, M., Lele, S., Pais, D., Weingarten, M., & Tyrrell, T. (2016-2018). *FSP 2.0: A program for probabilistic estimation of fault slip potential resulting from fluid injection*. Retrieved from Bureau of Economic Geology: https://www.beg.utexas.edu/texnet-cisr/fsp

Warner, D. L. (1988). Abandoned oil and gas industry wells and their environmental implications. In *Proceedings of the American Petroleum Institute Conference* (pp. 69–89). American Petroleum Institute.

Warner, D. L., & Syed, T. (1986). *Confining layer study: Supplemental report (Chapter 9)*. Engineering Enterprises, Inc.

Wesselman, J. B., & Aronow, S. (1971). *Ground-water resources of Chambers and Jefferson Counties, Texas*. Texas Water Development Board.

White, V. E., & Griffith, J. M. (2020). *Potentiometric surfaces, 2011–12, and water-level differences between 1995 and 2011–12, in wells of the "200-foot," "500-foot," and "700-foot" sands of the Lake Charles area, southwestern Louisiana*. Reston: U.S. Geological Survey.

Woessner, W. W., & Poeter, E. P. (2020). 4.2 Hydraulic head. In W. W. Woessner, & E. P. Poeter, *Hydrogeologic properties of earth materials and principles of groundwater flow* (Section 4.2, p. 205). The Groundwater Project.

Worden, R. &. (2003). Sandstone diagenesis: the evolution of sand to stone. In R. H. Worden & S. Morad (Eds.), *Sandstone diagenesis: Recent and ancient* (pp. 3-44). Blackwell Publishing.

Yale, D. P., Nabor, G. W., Russell, J. A., Pham, D., & Yousef, M. (1993). Application of variable formation compressibility for improved reservoir analysis. *In Proceedings of the SPE Annual Technical Conference and Exhibition* (pp. 435-450). Society of Petroleum Engineers

Yielding, G. (2002). Shale gouge ratio-Calibration by geohistory. In *Hydrocarbon seal quantification* (Norwegian Petroleum Society Special Publications). Elsevier

Young, S. C., Ewing, T., Hamlin, S., Baker, E., & Lupton, D. (2012). *Final report: Updating the hydrogeologic framework for the northern portion of the Gulf Coast Aquifer*. Texas Water Development Board.

Young, S. C., Knox, P. R., Budge, T., Kelley, V., Deeds, N., Galloway, W. E., & Baker, E. T. (2006). Stratigraphic, lithology, and hydraulic properties of the Chicot and Evangeline aquifers in the LSWP study area, central Texas Coast. In Texas Water Development Board (Ed.), *Aquifers of the Gulf Coast of Texas* (pp. 129-138). Texas Water Development Board.

Zheng, X., Sun, Z., & Espinoza, N. D. (2019). Uniaxial strain unloading compressibility of Frio Sand: Measurements and Implications on Reservoir Pressure Management for CO_2 storage. *In Proceedings of the American Rock Mechanics Association Conference*. American Rock Mechanics Association.

Zhu, J. G. & Gong, Y. (2016). Quantitative evaluation of fault lateral sealing. *IOSR Journal of Engineering*, 29-33.

Zimmerman, R. W. (1991). *Compressibility of Sandstones*. Berkley: Elsevier.

Zoback, M. L., & Zoback, M. (1980). State of stress in the conterminous United States. *Journal of Geophysical Research, 85*(B11), 6113-6156.